Optimization of DEM simulation time of Monopile penetration through scour rock layer using Scaling

ME54010

Anil Kumar Vaddi

Delft University of Technology

TU Delft

Optimization of DEM simulation time of Monopile penetration through scour rock layer using Scaling

by

Anil Kumar Vaddi

Master Thesis

in partial fulfilment of the requirements for the degree of

Master of Science
in Mechanical Engineering

at the Department of Maritime and Transport Technology of the Faculty of Mechanical Engineering of Delft University of Technology
To be defended on Monday, January 2025, at 14:30

Student Number : 5491436
MSc Track : Multi Machine Engineering
Report Number : 2024.MME.9023

Supervisors: Dr. Hao Shi
Committee Chair: Prof. Dingena Schott
Date: 20-01-2025

TU Delft

Summary

This thesis investigates the optimization of simulation time for monopile penetration through a scour rock layer in offshore wind turbine installations using scaling techniques in the Discrete Element Method (DEM). The study focuses on the penetration phase, analyzing the effects of various parameters on penetration resistance and work. Three scaling approaches are evaluated: exact scaling with Froude similarity, coarse graining, and a novel hybrid approach combining both techniques.

The research establishes a robust numerical model and systematically evaluates the accuracy and efficiency of each scaling approach. Findings show that exact scaling with Froude scaling principles accurately represents monopile-rock interaction at full scale, preserving gravitational and dynamic effects. Coarse graining allows for efficient simulation of large sand volumes, while hybrid scaling combines the benefits of both techniques for a computationally feasible and physically accurate simulation of the entire monopile installation process.

Contents

List of Figures

List of Tables

Nomenclature

Abbreviations

Abbreviation	Definition
FEM	Finite Element Method
DEM	Discrete Element Method
MPM	Material Point Method
CFD	Computational Fluid Dynamics
KPI	Key Performance Indicator
ILT	Integrated Lifting Tool
FDM	Finite Difference Method
OEPP	Open-Ended Pipe Piles
AR	Advancement Ratio
CPT	Cone Penetration Test
NPG	Number of Particles per Grain
SF	Scale Factor

1

Introduction

Energy derived from offshore sources, like oil and gas reserves, as well as wind and wave power, is known as offshore energy. Offshore wind turbines play a crucial role in the mix of renewable energy by converting the force of the wind into electricity. These turbines are commonly positioned on foundations that are connected to the seabed. In the last decade, the offshore wind industry has grown seamlessly [1]. The main advantage of offshore over its twin brother onshore is that wind resources are higher in the sea than in the coastal and other onshore areas. To erect these wind turbines on the surface of the sea, different foundations are used (Figure 1.1), considering the depth of the seabed, local conditions, and marine climate throughout the evolution of these wind turbines [2].

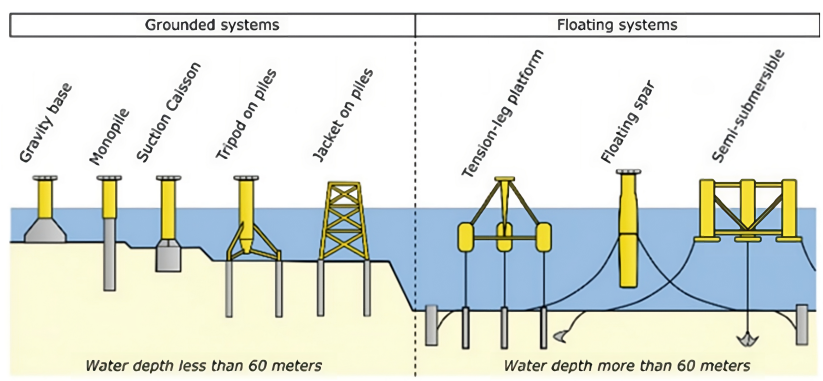

Figure 1.1: Type of offshore wind turbine foundations [3].

Among these monopiles are the most commonly used foundation in shallow waters up to around 30 - 50 meters depth for offshore wind turbines. These are made of thick steel and have a cylindrical geometry (Figure 1.2) [4]. By 2018 more than half of the offshore turbines in the world were installed on a monopile foundation [2]. Monopile foundations offer a compelling combination of cost-effectiveness, proven reliability, and ease of installation, making them the preferred choice for many offshore wind projects, particularly in shallower waters. Along with offshore wind turbines foundations, monopiles were also used as foundations of

Figure 1.2: Monopile foundation for an offshore wind turbine [5]

oil and gas platforms.

1.1. Upcoming Challenges

Over the years, the installation of wind turbines has been moving further offshore to take advantage of stronger wind gusts. This trend favors the use of more stable foundations, such as jackets and tripods, which are better suited for greater depths. However, in most parts of the world the installation still has not crossed the intermediate depths (20-40m). Table 1.1 shows the trend towards deeper offshore installations favoring jackets and tripods despite that XXL monopiles that exceed 7 m in diameter and 65 m in length are being suggested as a potential replacement for jacket and tripod structures in deeper waters [5]. The appeal of monopiles lies in their relative simplicity and cost-effectiveness compared to complex jacket and tripod structures.

Wind Farm	Location	Year Completed	Capacity (MW)	Average Water Depth (m)	Foundation Type
Hollandse Kust Zuid	Netherlands	2023	1500	18	Monopile
Dogger Bank A	UK	2023	1200	29	Monopile
Seagreen	UK	2023	1100	50-55	Jacket
Vineyard Wind 1	USA	2023	800	26	Monopile
Parkwind Arcadis Ost 1	Germany	2023	257	40	Monopile
Saint-Brieuc	France	2023	496	16-33	Jacket
Changfang and Xidao	Taiwan	2022	589	35-55	Jacket
Triton Knoll	UK	2022	857	16-24	Monopile
Moray East	UK	2022	950	28-57	Jacket
Yunlin	Taiwan	2021	640	8-50	Monopile/Jacket

Table 1.1: Recently installed offshore wind farms and foundation used to install the turbines.

The reason for the increasing size of wind turbines and their installation in deeper waters is driven by the pursuit of higher energy yields, cost efficiency, technological advancements, and environmental considerations. Larger turbines with longer blades can capture more wind energy, particularly in deeper waters with stronger and more consistent winds. Although larger turbines require a higher initial investment, they offer long-term cost savings through reduced installation, maintenance, and operating costs. Technological advancements have enabled the construction of larger and more efficient turbines that can withstand harsh offshore conditions. Additionally, deeper water installations minimize visual impact and potential con-

Year	Power Installed (MW)	Turbines Installed	Average Turbine Power, Pn (MW)	Average Diameter, Ø (m)	Average Length, L (m)	Average Depth, d (m)	Average Distance to Coast, DC (Km)
2009	457	127	3.6	4.85	37.8	7.6	5.7
2010	862	311	2.8	4.26	40.4	11.7	20.2
2011	232	72	3.2	5	43	19.3	15
2012	184	51	3.6	6	55	27	22
2013	2149	599	3.6	5.13	47.8	13.1	15.7
2014	1063	317	3.4	5.48	58.8	19.2	24.4
2015	2072	564	3.7	5.47	55.4	17.9	27.8
2016	698	191	3.7	5.68	62.2	9.5	16.5
2017	3144	609	5.2	6.83	69	23.6	46.1
2018	3598	608	5.9	7.26	69.1	22.4	27.4

Table 1.2: Evolution of Offshore Wind Turbine Technology and Deployment (2009-2018) [2]

flicts with other marine activities, contributing to a more sustainable energy solution. This combination of factors has fueled the trend towards larger wind turbines and deeper water installations, with XXL monopiles emerging as a potential alternative to traditional jacket and tripod structures. The sheer size and weight of bigger monopiles, coupled with the complex soil conditions and harsh environmental factors encountered in deeper waters [6], necessitate specialized equipment and innovative installation techniques. This complexity often translates to longer installation times, potentially leading to project delays and increased costs [7]. Moreover, the dynamic interaction between the monopile, soil, and environmental forces during installation is not fully understood, further complicating the prediction and optimization of installation procedures.

As discussed above the monopile installation is a time consuming and expensive process. To conduct the installation process seamlessly, the soil behavior needs to be understood. Apart from soil behavior, micro-mechanical properties like particle crushing, stress distribution, force distribution, and penetration resistance also have to be studied. Although the experimental results are good enough to study the soil behavior, the cost and time of these experiments are relatively high [8].

After installation, monopiles remain susceptible to scour, a phenomenon where the seabed around the foundation is eroded by currents and waves (Figure 1.3a). Scour can undermine the structural integrity of the monopile and compromise the stability of the wind turbine.

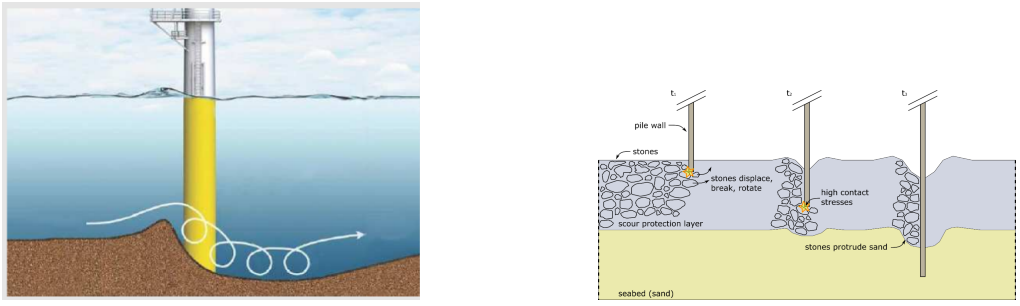

(a) **(b)**

Figure 1.3: Pictorial representation of : (a) scouring around monopile [9], (b) penetration through scour layer [10].

To mitigate this risk, scour protection measures are implemented around the base of the monopile. These typically involve placing a layer of rock or other erosion-resistant material around the foundation to protect the seabed from the erosive forces of currents and waves

(Figure 1.3b). The design of scour protection systems is complex and involves considering factors such as local hydrodynamic conditions, soil properties, and the expected life expectancy of the wind farm. Understanding the interaction between the monopile, scour protection layer, and the surrounding soil is crucial for designing effective scour protection systems.

1.2. Aim

Understanding the behavior of monopile foundations during installation in deep waters, particularly through scour protection layers, is crucial for the design and optimization of offshore wind farms. Experimental studies are essential for validating theoretical models, identifying potential risks, and optimizing installation procedures. Experimental studies provide valuable information on the complex interactions between the monopile, the scour protection layer, and the underlying soil. However, conducting full-scale experimental studies of monopile penetration in deep waters is practically impossible due to several challenges. The immense size and weight of monopiles, coupled with the vast depths involved, make it logistically and financially infeasible to create realistic full-scale experimental models. In addition, harsh environmental conditions in deep waters, such as strong currents, waves, and varying soil properties, further complicate the experimental setup.
Although reduced-scale experimental models offer a more practical alternative, they also come with limitations. Scaling down the dimensions of the monopile and scour protection layer can introduce scaling effects that may not accurately represent the behavior of full-scale structures. Moreover, the cost of constructing and operating even reduced-scale experimental models can be significant, limiting the number of tests that can be performed.
Given the challenges and limitations of experimental studies, numerical simulations provide a valuable alternative for investigating monopile penetration through scour layers. There are several numeri cal methods that can simulate the monopile installation like Finite Element Method (FEM), Discrete Element Method (DEM), Material Point Method (MPM) and Computational Fluid Dynamics (CFD), etc. FEM is more suitable for simulating continuous bodies, whereas the DEM is more suitable for simulating problems at the particle scale. CFD is employed to analyse the hydrodynamic loads that are experienced by monopiles during wave breaking [11]. MPM and DEM have quite similar applications, but MPM models the soil as a continuum and avoids handling contact between fine particles, whereas DEM captures the contact characteristics of particles and simulates large-deformation events [12]. The major set back that DEM has is the simulation time which leads to higher computational cost. The simulation time increases as the number of particles increases; even simulating laboratory systems might be difficult as trillions of particles would be cumbersome even if a supercomputer is deployed.
To counter this problem the concept of scaling technique has been introduced in DEM. This allows us to scale the system by preserving the system's physical properties and behaviors while adjusting it's size.

1.3. Research Questions

The current research focuses on the use of scaling techniques to simulate monopile installation in a reasonable time by reducing the number of particles. This leads us to the main

research question and sub research questions:

" ***Which scaling techniques can be applied to model offshore wind turbine monopile installation and represent real field scenarios?***"

(RQ1): *What is the current state of the art research on the application of Discrete Element method in monopile installation procedure and scaling techniques ?*

(RQ2): *What are the optimal model parameters and numerical settings for accurately and efficiently simulating monopile penetration through scour layers using DEM?*

(RQ3): *What kind of scaling technique and scaling laws can be used specifically to upscale the simulation of monopile penetration in DEM ?*

(RQ4): *How reliable and accurate are the scaled DEM simulations ?*

(RQ5): *What are the remaining gaps that can be studied further to address future challenges in offshore wind turbine installation, such as larger turbines or different seabed conditions ?*

1.4. Structure of Report

The thesis opens by introducing the growing challenges in offshore wind turbine installation, particularly focusing on monopile foundations - the most common foundation type for offshore wind turbines in shallow waters. It explains how the increasing size of wind turbines and their installation in deeper waters has created new complexities in understanding the penetration mechanics of monopiles through scour protection layers. The introduction establishes the need for advanced simulation techniques, specifically the Discrete Element Method (DEM), while highlighting the computational challenges that arise when modeling such large-scale systems.
Chapter 2 provides a comprehensive examination of previous research in monopile installation and DEM simulation techniques. It traces the evolution of DEM applications in geotechnical engineering, from simple 2D circular particle models to sophisticated 3D simulations using complex particle shapes. The chapter critically analyzes various scaling techniques that researchers have developed to address computational limitations, setting the foundation for the study's innovative approach to scaling DEM simulations.
Chapter 3 details the meticulous development of a reference numerical model for simulating monopile penetration. Through systematic investigation of parameters including contact models, timestep selection, domain dimensions, and particle properties, the chapter establishes optimal settings that balance computational efficiency with physical accuracy. This foundational work creates a robust baseline for evaluating different scaling approaches in subsequent chapters.
Chapter 4 introduces the theoretical framework for three distinct scaling approaches: exact scaling, coarse graining, and a novel hybrid scaling technique. It develops the mathematical relationships and scaling laws that govern each method, with particular attention to preserving critical physical behaviors while reducing computational demands. The chapter demonstrates how Froude scaling principles can be effectively combined with particle upscaling to create a practical simulation framework for industrial-scale applications.

Chapter 5 The results and discussion chapter presents a comprehensive evaluation of the three scaling approaches through a series of carefully designed numerical simulations. It compares the Key Performance Indicators of each scaling technique for evaluation, revealing the strengths and limitations of different scaling strategies. The chapter demonstrates that while exact scaling provides modelling of scour layer, coarse grain offers optimizing the particle number for sand bed and the hybrid approach combines the both techniques to model a monopile penetration simultion through scour layer.
The conclusion synthesizes the key findings and contributions of the research, highlighting how the developed scaling methodologies enable practical simulation of industrial-scale monopile installations while maintaining essential physical accuracy. It also discusses the promising directions for future research, including the potential for experimental validation and the application of these techniques to different seabed conditions.

2

Literature Review

2.1. Monopile installation

Monopiles are extensively used as the main type of foundation for offshore wind turbines. These structures are composed of a single steel tube with substantial diameter that is inserted forcefully into the seabed utilizing impact hammers. The purpose of a monopile is to secure the tower, along with the nacelle of the offshore wind turbine, firmly to the ground. In most instances, the tower is connected to the monopile by means of a transition piece. The installation of monopile foundations for offshore wind turbines entails various essential specifications. Firstly, the diameter typically ranges from 4 to 6 meters, although it can extend to 10 meters for the subsequent generation of XXL monopiles [5]. Furthermore, the length of these foundations varies between 60 and 120 meters, with the newer XXL monopiles reaching lengths greater than 150 meters [13]. The wall thickness measures around 60 to 120 mm [14]. It is generally recommended that the penetration depth of these foundations into the seabed ranges from 30 to 50 meters [15]. In terms of hammer energy, it is crucial to utilize up to 3000 kJ to effectively drive the piles into the seabed. Lastly, cranes with lifting capacities of up to 5000 tonnes are employed to undertake the installation process [16]. Monopile installation takes place in a sequence and could be defined in six steps:

1. Initially, the monopile is transported from the production facility to the installation site. This can be accomplished through various methods. By utilizing end caps, the monopile can be made buoyant and towed to the site by a tugboat. Alternatively, the monopile can be positioned on a barge or on the deck of the installation vessel.
2. The monopile is transported in a horizontal orientation, necessitating the up-ending of the monopile prior to installation. The up-ending process is facilitated by a crane situated on the installation vessel. During this procedure, the crane (and vessel) is subjected to both horizontal and vertical loads.
3. Following the up-ending process, the monopile is suspended vertically from the crane. Subsequently, it is lowered through the splash zone and placed onto the seabed. The

monopile experiences first-order wave forces while descending through the splash zone, and the motion of the vessel (specifically the roll and pitch motions) introduces significant tip motions to the crane. As a result, the monopile exhibits motion.

4. Once the monopile is set on the seabed, the precise position of the monopile's bottom end, concerning the Earth's fixed location, is determined. Due to its own weight, the monopile partially self-penetrates the seabed or rock armour layer if the scour protection is applicable to a depth equivalent to half its diameter. The degree of self-penetration depends on the soil properties. The crane wire remains attached to the monopile, resulting in the application of forces from both crane tip motions and wave forces. However, the interaction between the soil and the monopile counteracts these forces. Additionally, a gripper frame is affixed to the monopile.
5. The crane's Integrated Lifting Tool (ILT), which is connected to the monopile, is detached. Subsequently, a hydro hammer is retrieved from the deck of the vessel and positioned on top of the monopile to drive it into the soil. Due to the limited interaction between the monopile and the soil, the monopile behaves as an unstable inverted pendulum. To maintain the upright position of the monopile, the pile gripper frame is crucial. During this installation phase, the monopile is hammered into the soil until it reaches a penetration depth that allows for stable monopile-soil interaction. The gripper frame is then disconnected, the inclination is measured and adjusted to meet the installation requirements, and the monopile is hammered into the soil until it reaches its final penetration depth.
6. The monopile ultimately reaches its final penetration depth, at which point the gripper frame has already released it. The hydro hammer is subsequently recovered onto the vessel's deck [15].

Steps 4 and 5 represent monopile penetration on a seabed; this plays a crucial role in ensuring that the installation is seamless. The seamlessness of the penetration depends on applying the right force to overcome the resistance of the soil. To study these steps, DEM is employed.

2.2. DEM Simulation of Pile Penetration

2.2.1. Circular particle shape (2D)

Esposito et al. conducted a sensitivity analysis using DEM to investigate the effects of installing a single pile in granular soil [17]. Their study highlighted the influence of installation method (displacement vs. bored piles) and particle rotation on the stress, porosity changes, and contact orientations around the pile. They found that inhibiting particle rotation increased tip resistance but did not affect skin friction, suggesting the need for alternative approaches to accurately model pile-soil interface behavior. This study demonstrates the power of DEM in simulating and analyzing pile installation processes. It highlights the importance of considering various factors, such as the installation method and particle rotation, to predict the behavior of piles in granular media.

Liu et al. employed DEM to investigate the installation responses of open-ended piles in granular soil [18]. The study focused on the micro-mechanics of soil plugging, shear band

development, and stress distribution during pile installation. The simulations revealed that soil plug resistance is concentrated within a zone 2-3 times the diameter of the pile above the base of the pile, and that the unit external friction decreases with pile installation at specific depths. The study also found that pile installation increases the average stresses surrounding the pile, with the major influence zone concentrated within six times the diameter of the pile. These findings provide valuable insights into the complex behavior of open-ended piles during installation and can inform the design and optimization of pile foundations.

Li et al. used the DEM to examine the mechanisms behind soil plug behavior inside open-ended piles during installation [19]. Their simulations showed that plugging is more common in jacked piles than dynamically installed piles, and that factors such as larger penetration, smaller pile diameter, and higher soil density promote plug formation. The study also found significant stress concentration at the lower part of the soil plug and highlighted the impact of installation methods on resistance, with jacking producing the largest resistance compared to dynamic installation methods.

Zhong et al used DEM to model the installation of a series of bio-inspired piles [20]. The piles were inspired by snake skin, with a series of scales of varying heights and lengths along the shaft of the pile. They found that the bio-inspired piles had greater shaft resistance than the reference pile, and that the shaft resistance increased with increasing scale height and decreasing scale length. The authors concluded that the increased shaft resistance and soil disturbance of the bio-inspired piles were due to the passive resistance of the scales against the soil.

Duan et al. used DEM to model the installation of a closed-ended displacement pile in sand [8]. The sand was modeled as uncrushable discs, and the pile was modeled as a rigid clump of overlapped discs. The authors investigated the micro-mechanical behavior of the sand around the pile during installation, including changes in stress, strain, and volume. The simulation results showed that the sand along the pile shaft experienced volume reduction as the pile passed by, followed by dilation as the pile moved further down. This process provides insights into the degradation of shaft friction at a given sand horizon, which is a critical factor in pile design. The authors concluded that the DEM model could effectively capture the micro-mechanical behavior of sand during pile installation and provide valuable insights into the friction degradation phenomenon.

2.2.2. Spherical particle (3D)

Zhou et al. used a coupled discrete-continuum model to simulate pile driving in sand [21]. DEM was used to model the sand near the pile, while a finite difference method (FDM) was used to model the sand farther away from the pile. The FDM is a numerical method that can be used to solve differential equations. The authors used a self-developed non-circular particle numerical simulation program to model the sand near the pile. The sand away from the pile was simulated as a continuous medium exhibiting linear elastic behaviors. The domain analyzed was divided into two zones. Contact forces at the interface between the two zones were obtained from a discrete zone and applied to the continuum boundaries as nodal forces, while the interface velocities were obtained from the continuum zone and applied to the discrete boundaries. The authors found that the coupled discrete-continuum simulation

can give a microscopic description of the pile penetration process without losing the discrete nature of the zone concerned, and may significantly improve computational efficiency.

Komodromos et al. used DEM to model the installation of open-ended pipe piles (OEPP) in granular soils [22]. They studied the influence of rolling resistance on the soil response during pile installation. The authors found that the DEM model was able to reproduce several key features of OEPP installation observed in the field, including the formation of a soil plug inside the pile and the development of stress and strain fields in the soil around the pile. The study also showed that rolling resistance plays an important role in the behavior of the soil during pile installation. In particular, the presence of rolling resistance was found to increase the resistance of the soil to pile penetration and to reduce the interaction between the pile and the soil particles. These findings have important implications for the design and installation of OEPP in granular soils.

Zhang and Fatahi used DEM to study the load transfer mechanism of open-ended tubular piles driven into rocks [23]. They investigated internal and external shaft friction, base resistance, and stress distribution in the surrounding rock. The authors calibrated the rock behavior against triaxial test results for a pyroclastic weak rock. A 30 degree segment of a true-scale model was simulated using DEM. The results showed that the external shaft resistance of the pile with an inner pile shoe increased linearly with penetration depth. The internal shaft friction was notably less than the external shaft friction for both piles with and without a shoe. Plugging was observed for both piles, with the inner pile shoe allowing partial plugging to occur at shallower penetration depths. The study provides insights into the load transfer mechanism of open-ended tubular piles and the effect of pile shoes on axial capacity in rocks.

Sharif et al. used the DEM to investigate the effect of the advancement ratio (AR) on the installation requirements and axial performance of screw piles in sand [24]. The advancement ratio is defined as the ratio between the vertical displacement per rotation to the geometric pitch of the screw pile helix. The authors modeled the installation of a single screw pile geometry in sand with varying relative densities (30%, 52%, and 83%) and AR values (0.5, 0.8, 1.0, and 1.2). The results showed that over-flighting the pile (AR < 1) significantly reduced the required installation force and torque compared to pitch-matched installation (AR = 1). While over-flighting decreased the compressive capacity of the pile, it substantially increased the tensile capacity, particularly in loose sand. The authors attributed this increase to a change in the soil failure mechanism during uplift, from a flow-around mechanism in pitch-matched piles to a conical wedge failure in over-flighted piles. Additionally, the study found that the empirical torque-capacity correlation factors commonly used for screw piles are not universally applicable and can be significantly influenced by the installation method, soil density, and relative embedment depth. The authors concluded that over-flighting could be a beneficial installation strategy for screw piles, especially in offshore applications where tensile capacity is critical.

Hunt et al. investigated the effect of the cone apex angle on the penetration resistance in coarse-grained soils using numerical and experimental methods [25]. Discrete element modeling (DEM) simulations were performed in unconfined and confined specimens to model shallow and deep penetration conditions, respectively. Centrifuge penetration tests were also

performed. The numerical and experimental results indicated that at shallow depths, sharper tips (i.e., those with smaller apex angles) mobilize smaller penetration resistances. In deep penetration conditions, the changes in penetration resistance with tip apex angle are less pronounced. The authors proposed a relationship characterizing the functional form between tip apex angle and normalized penetration resistance. A mesoscale analysis of the DEM simulation results showed that the zone where large particle displacements and stress changes occur is large and located below the tip for penetration with blunt tips, whereas the zone is smaller and located both laterally and below the tip for sharp tips.

Gezgin et al.(2022) used DEM to simulate pile installation in dry, cohesionless soils [26]. Because DEM models can be computationally expensive, the authors explored the effect of various soil parameters on model outcomes to help future researchers optimize their models. They varied one soil parameter at a time (e.g., particle stiffness, void ratio, interparticle friction, particle size, particle size distribution, particle shape, and rolling friction) while holding other parameters constant. They found that some parameters (particle stiffness, void ratio, interparticle friction, particle size, particle size distribution, and particle shape) affected pile penetration resistance, while the results of models with rolling friction are compared with the results of models with non-spherical particles, it is noticed that rolling friction cannot properly mimic the shape effect in the case of penetration problems. They concluded by providing recommendations for model optimization.

Author	Number of Particles	Domain /w	Contact Model	Penetration Velocity	Particle Shape	Software
Esposito et al. (2018) [17]	114036	61	Elasto-plastic	10 cm/s	Circular	PFC2D
Liu et al. (2019) [18]	35357	26.6	NS	NS	Circular	PFC2D
Li et al. (2021) [19]	356976	22.2	Linear	2 m/s	Circular	PFC2D
Zhu et al. (2021) [27]	70675	53.3	Linear	NS	Circular	PFC2D
Zhong et al. (2021) [20]	40128	20	Linear	25 mm/s	Circular	PFC2D
Duan et al.(2021) [8]	80640	53.3	Linear spring	NS	Circular	PFC2D
Zhou et al. (2012) [21]	26700	25	Elasto-plastic	NS	Elliptical (Two-sphere)	PFC2D
Komodromos et al. (2021) [22]	12800	4	Linear	NS	Sphere	NS
Zhang and Fatahi (2021) [23]	557000	15	Bonded-Particle	NS	Sphere	PFC3D
Sharif et al. (2021) [24]	270000	22.7	Linear	0.1 m/s	Sphere	PFC3D
Hunt et al. (2023) [25]	120000	15.9	Linear	0.2 m/s	Sphere	PFC3D
Gezgin et al.(2022) [26]	111624	16.6	Hertz-Mindlin	35 mm/s	Clump (2 spheres)	EDEM
Peng et al. (2022) [28]	NS	20	Bonded-Particle	0.1 mm/min	Clumped (4 spheres)	NS

w - Width of the pile
NS - Not specified

Table 2.1: Overview of DEM simulations of penetration through granular medium

Section 2.2 demonstrates the versatility of DEM in simulating pile penetration, considering various factors like particle shape, installation methods, and soil properties. It highlights the importance of understanding micro-mechanical behavior and optimizing model parameters for accurate and efficient simulations.

Table 2.1 provides a concise overview of various DEM simulations of pile penetration in granular media, highlighting key aspects of their methodologies and findings.

1. Particle Shape: Most studies employed either circular (2D) or spherical (3D) particles, with limited use of elliptical or clumped particles. This suggests a need for further exploration of the impact of particle shape on penetration behavior.
2. Contact Models: The choice of contact models varied across studies, with Hertz-Mindlin,

linear, and bonded-particle models being the most common. This indicates that the selection of an appropriate contact model depends on the specific research question and the desired level of accuracy.

3. Penetration Velocity: Penetration velocities ranged from 0.1 mm/min to 2 m/s, reflecting the diverse range of installation methods and soil conditions considered in the literature.

2.3. Scaling of DEM Simulations

Two terms together describe the scaling in DEM, the scaling technique, and the scaling law. Scaling technique refers to the methods that are used to upscale or downscale the simulation, it tells us which part of the simulation to be scaled. Various scaling techniques have been developed for different applications namely:

- Coarse-grain
- Geometric scaling
- Exact scaling
- Particle refinement technique
- Scalping
- Hybrid scaling

Scaling laws are mathematical relationships that describe how certain properties or behaviors are scaled with system size. Vaddi (2023) [29] have mentioned all the scaling laws that has been used in DEM. The scaling laws mentioned in this literature review are:

1. Scale power index: This scaling law is based on the correlation between the forces exerted on scaled particles and the original particles [30].
2. Energy conservation law: This scaling law is based on the principle of energy conservation before and after scaling of particles [31, 32].
3. Mass conservation principle: This scaling law is based on the principle of mass conservation before and after scaling of particles [33].
4. Direct force scaling: This scaling law is based on the scaling of forces between the scaled particles and the original particles [30].
5. Equal energy density and particle density: This scaling law is based on the principle of equal energy density and particle density between the scaled particles and the original particles [34, 35, 36].
6. Dimensionless analysis for energy dissipation: This scaling law is based on the dimensionless numbers that are used to preserve the the loss of kinetic energy during inelastic collisions between particles in both the original and scaled particles [37].
7. Mechanical and dynamic similarity: This scaling law dictates that mechanical and dynamical similarity must be preserved between the original and scaled particles. To achieve this, the contact model employed should exhibit scale invariance [38, 39] .
8. Kinematic and dynamic similarity: This scaling law facilitates the preservation of similar flow conditions between the original and scaled geometries [40, 41].

9. Geometric similarity: This scaling law enables the proportional scaling (upscale or downscale) of a geometry while preserving its fundamental shape. [42, 43, 44].
10. Scaling of contact parameters: This scaling law is based on the scaling of contact parameters, such as stiffness, in direct proportion to the scale factor employed to modify the dimensions of both the particles and the geometry. [45]
11. Using particle size ratio: This is a way to categorize particle size distributions (PSDs). It is calculated as the ratio of the largest particle size to the smallest particle size in the distribution. A higher PSR indicates a wider range of particle sizes [46].

These scaling laws link the behavior of the system at different scales. These laws provide insight into the macroscopic response of the system with respect to its microscopic characteristics [29]. Given the distinct scaling laws applicable to different regimes, we will focus our subsequent investigation on the penetration regime. This selection will guide our choice of appropriate scaling techniques and corresponding scaling laws for further analysis.

Ciantia et al. used a three-dimensional discrete element model (DEM) to investigate the effect of grain crushing on cone penetration test (CPT) tip resistance in calibration chambers [36]. The model was calibrated using oedometer tests and validated by reproducing other element tests. A key aspect of the study was the upscaling technique used to simulate a realistically sized CPT. The discrete analogue was upscaled by a factor of 25, which means that the particle sizes in the simulation were 25 times larger than the actual pumice sand particles. This was done to reduce the computational cost of the simulation while maintaining the macroscopic responses of interest. The upscaling process involved adjusting particle strength, stiffness, and grain size distribution according to specific scaling laws. The researchers performed CPT simulations at two different densities and three different confinement pressures, both with and without particle crushing enabled. The results showed that cone tip resistance in the crushable material was practically insensitive to initial density, consistent with previous physical experiments. In contrast, when particle crushing was disabled, cone tip resistance increased significantly with density. The study also found that the ratio of cone tip resistance between the crushable and uncrushable simulations agreed well with previous experimental comparisons of hard and crushable soils. Overall, this study demonstrates the potential of DEM modeling to investigate the complex behavior of crushable granular materials during CPTs and highlights the importance of considering particle-scale phenomena in geotechnical engineering.

Lommen et al. investigated the application of coarse-graining, a DEM particle upscaling technique, to the simulation of large-scale bulk handling equipment [47]. The study aimed to reduce the computational cost of simulating a large volume (77 m^3) of iron ore pellets interacting with a grab unloader. The authors proposed a coarse-graining method based on the idea that the scaled system should maintain the same energy density as the original system. This involved scaling particle density, mass, moment of inertia, contact stiffness, and damping. The method was then calibrated and validated using laboratory experiments, including angle of repose tests and penetration tests. The results showed that the coarse-graining scheme accurately predicted the shearing behavior of the particles, regardless of the chosen scale. However, the penetration resistance was found to be dependent on grain size, with coarser grains leading to increased resistance. To mitigate this, the authors adjusted the sliding fric-

tion coefficient of the penetrating tip, successfully compensating for the increased resistance. The adapted coarse-graining scheme was then applied to a large-scale simulation of a grab unloader, demonstrating consistent results across different particle scales. The study concluded that particle upscaling can be effectively applied to large-scale DEM simulations, but specific grain size-dependent interactions need to be identified and adapted.

Tekeste et al. used DEM to model the interaction between soil and a bulldozer blade [48]. They aimed to establish a scaling relationship between soil reaction forces and the size of the bulldozer blade. This would allow them to predict the performance of large, industry-sized blades using simulations, which is less resource-intensive than real-world testing. The authors developed a DEM soil model that matched the behavior of Norfolk sandy loam soil in cone penetration tests. They then simulated bulldozer blades of different sizes interacting with this soil. The study used geometric scaling, which is a technique to relate the behavior of a model system to a larger, real-world system. In this case, the model system was the DEM simulation, and the real-world system was the actual soil-bulldozer interaction. The scaling law used was a power fit, which describes how the soil reaction forces change with the size of the bulldozer blade. The results showed that the DEM predictions of soil forces on the scaled bulldozer blades matched well with experimental data from soil bin tests. This suggests that the DEM model, combined with the similitude scaling law, can be a useful tool for predicting the performance of bulldozer blades.

Janda and Ooi used the DEM to model the behavior of cohesive soils during cone penetration and unconfined compression tests [49]. They employed a visco-elasto-plastic frictional adhesive contact model to simulate the interactions between soil particles. The model allowed for the simulation of the complex mechanical behavior of cohesive soils, including their stress history dependence. The study found that the DEM simulations were able to qualitatively reproduce typical cone penetration resistance profiles observed in real soils. The model also captured the effect of consolidation stress history on penetration resistance, demonstrating that soils consolidated at higher stresses exhibited greater resistance. The authors conducted a parametric study to investigate the influence of various contact model parameters on penetration resistance. They found that increasing the unloading-reloading stiffness, adhesive stiffness, and coefficient of sliding friction all led to increased penetration resistance. Additionally, the study confirmed a linear relationship between penetration resistance and undrained shear strength, consistent with empirical relationships reported in the literature. To address the computational challenges associated with simulating large-scale problems, the authors investigated the scaling of DEM contact parameters with particle size. They found that for quasi-static simulations, the stiffness parameters and the constant pull-off force could be scaled linearly with particle size (Exact scaling), while the initial pull-off force scaled quadratically. This scaling technique allowed for the simulation of larger systems while maintaining the same stress-deformation behavior as simulations with smaller particles.
McDowell et al. focused on developing a particle refinement method for DEM simulations of CPTs [50]. The authors noted that simulating an entire calibration chamber with realistically sized particles was computationally demanding. To address this, they proposed a method where smaller particles were generated near the cone penetrometer, and progressively larger particles were used further away. This approach aimed to maintain a realistic number of particle contacts at the cone tip while reducing computational time. The authors found that

using a single particle size throughout the chamber led to unrealistic results due to the migration of smaller particles into voids between larger ones. To mitigate this, they introduced a gradation method where particle size increased in sectors, which significantly improved the accuracy of the simulations. The study highlighted the importance of particle size and distribution in DEM simulations of CPTs and provided a computationally efficient method for achieving realistic results. Falagush et al. [51] used similar scaling technique as McDowell et al. [50] to investigate the effects of particle shape and particle crushing on cone penetration testing (CPT) results. The authors simulated a calibration chamber using both 90 degree and 30 degree segments to reduce computational time. The effect of particle shape was studied by either prohibiting particle rotation or using simplified two-ball clumps. Prohibiting particle rotation led to a significant increase in tip resistance compared to allowing free rotation. The use of two-ball clumps also had a substantial impact on tip resistance, with increased clump angularity resulting in higher resistance due to increased interlocking and rotational resistance. Particle crushing was simulated by replacing broken particles with two smaller particles of equal size. The results showed that particle crushing led to a considerable reduction in tip resistance, and this reduction became more pronounced as confining stress increased. The authors concluded that both particle shape and crushing significantly influence CPT results and suggested that future work should focus on using more realistic particle shapes and crushing models.

Ding et al. used DEM to study the friction analysis of large-diameter steel cylinder penetration process in sandy soils [52]. The authors developed a centrifugal model by reducing the size 100 times and increasing the corresponding acceleration of gravity. They also developed a full-scale model using the upscale theory, where the contact attributes were adjusted based on the following scaling law to maintain consistent macroscopic properties between the enlarged particles and the calibrated samples. The results showed that there was no obvious soil-plug effect during the penetration process of large diameter steel cylinders. The inside friction was found to be smaller than the outside friction. Additionally, the computational cost of the full-scale model based on the upscale theory was less than that of the centrifugal model. The study also revealed a close relationship between side friction and micro contact parameters, providing a reference for future research on cylinder or pile penetration using DEM.

Author	Number of particles	Scaling technique	Scaling law	Scaling factor	Contact model
Ciantia et al.(2016) [36]	55385	Coarse grain	Scaling of stiffness and particle strength	25	Hertz-Mindlin
Lommen et al.(2019) [47]	NS	Coarse grain	Energy density matching	5	frictional adhesive
Tekeste et al.(2020) [48]	43451	Geometric scaling	Geometric similarity	0.05	Hertz-Mindlin
Janda and Ooi (2016) [49]	15000	Exact scaling	Scaling of contact parameters	15	visco-elastoplastic
Ding et al.(2021) [52]	210995	Exact scaling	NS	100	Linear
McDowell et al.(2012) [50]	3900	Particle refinement	-	12	Linear elastic
Falagush et al.(2015) [51]	37050	Particle refinement	-	4	Linear elastic

Table 2.2: Overview of literture on scaling of DEM simulations(penetration systems)
* NS = Not specified
Note: All studies used spherical particles except Tekeste et al.(2020) which used multisphere(2 spheres)

Table 2.2 provides a comprehensive overview of the literature on scaling in Discrete Element Method (DEM) simulations, specifically focusing on penetration systems. It summarizes key aspects of various studies, including the number of particles used, the scaling technique employed, the specific scaling law applied, the scaling factor, the contact model utilized, and

the particle shape considered in each simulation. Overall, the table highlights the diversity of approaches used in scaling DEM simulations for penetration systems. Each study makes specific choices regarding the scaling technique, scaling law, scaling factor, contact model, and particle shape, depending on the research goals and computational constraints.

The literature on DEM simulation of geotechnical processes has shown a growing trend to address computational challenges through upscaling and particle refinement techniques. Various studies have investigated the effects of particle size, shape, and crushing on cone penetration tests, highlighting the importance of considering these factors for accurate simulation. The development of scaling laws has allowed for the prediction of large-scale behavior based on smaller-scale simulations, offering potential cost and time savings in geotechnical engineering. However, there are still gaps in the understanding of specific grain size-dependent interactions, the influence of different contact models, and the development of more realistic particle shapes and crushing models. Additionally, future research could explore the integration of other modeling approaches, such as the finite element method, with DEM to improve the simulation of large-scale geotechnical problems.

2.4. Conclusion

Addressing research question 1 *"What is the current state of the art research on the application of Discrete Element method in monopile installation procedure and scaling techniques?"*

The literature review reveals that the Discrete Element Method (DEM) is a valuable tool for simulating monopile installation in offshore applications. It allows for detailed analysis of soil-structure interaction, particle-scale behavior, and the effects of various parameters on penetration resistance. However, DEM simulations can be computationally expensive, especially for large-scale problems.

Several studies have used 2D DEM simulations with circular or elliptical particles to investigate the installation of monopiles in granular soils. These studies have provided insights into the micro-mechanics of soil plugging, shear band development, stress distribution, and the influence of installation methods on pile behavior. However, 2D simulations may not fully capture the complexity of 3D soil-structure interaction.

3D DEM simulations with spherical particles have been employed to study the installation of open-ended and closed-ended piles, as well as screw piles, in granular soils and weak rocks. These studies have investigated the effects of rolling resistance, pile shoes, advancement ratio, and cone apex angle on pile installation behavior and load transfer mechanisms. However, 3D simulations can be computationally demanding, limiting the size and complexity of the problems that can be analyzed.

To address the computational challenges of DEM simulations, various scaling techniques have been proposed. These techniques aim to reduce the computational cost of simulations while maintaining the accuracy of the results. Some of the scaling techniques mentioned in the literature include coarse-graining, geometric scaling, exact scaling, and particle refinement. These techniques have been applied to simulate large-scale bulk handling equipment, soil-bulldozer interaction, and cone penetration tests. However, the choice of scaling technique and the associated scaling laws depend on the specific problem and the desired level

of accuracy.

Overall, the literature review highlights the potential of DEM simulations for understanding and optimizing monopile installation processes. However, further research is needed to develop more efficient and accurate scaling techniques, as well as to validate DEM models against experimental and field data. Additionally, future studies should investigate the effects of different soil types, seabed conditions, and installation methods on monopile behavior.

3

Simulation setup and Model parameters

In this chapter, we embark on the foundational step of our research: the meticulous design of a reference DEM model that accurately simulates the monopile installation process. This model serves as the cornerstone upon which our scaling techniques will be built. To ensure both realism and computational efficiency, we will systematically investigate and select key parameters that govern the simulation's behavior.

Reference Model Development: Through a series of carefully designed simulations, we will iteratively refine parameters to achieve a balance between accuracy and computational efficiency. The resulting reference model will serve as a benchmark against which the performance of our scaled models can be assessed. For this study on monopile penetration through scour protection, fluid-particle coupling in DEM simulations is unnecessary. This is because the focus is on geotechnical scenarios with high particle density and laminar flow, where water influence is negligible. Furthermore, the drained regime ensures rapid dissipation of pore pressure, eliminating any effect of pore pressure on the rock skeleton [53].

The entirety of the discrete element method (DEM) simulations conducted in this thesis were facilitated by Altair EDEM 2023.0 [54], a cutting-edge software platform renowned for its capabilities in modeling and analyzing the behavior of granular materials. Leveraging EDEM 2023's advanced features, we were able to construct detailed and realistic simulations of monopile installation, capturing the intricate interactions between the pile, soil, and surrounding environment. All simulations presented in this chapter were conducted on DELL Alienware m15 R6 laptop equipped with an 11th Gen Intel Core i7-11800H processor, 32 GB of DDR4 RAM, and an NVIDIA GeForce RTX 3060 GPU (6 GB).

3.1. Simulation settings

3.1.1. Contact model

Teodora Barbuntoiu, stated in her thesis that complex contact models encompass specific attributes such as wear, cohesion, bonding, or the integration of elastoplasticity for compressible bulk material [53]. Hertz-Mindlin and Linear Spring are the most commonly used contact models in DEM as they are simple and computationally efficient, while Linear Spring-Dashpot is a simpler model that uses linear springs for both normal and tangential forces. It is computationally less expensive but may not capture the non-linear behavior of real materials accurately [55]. In this study, the Hertz-Mindlin contact model is used as it is efficient and accurate for force calculation. The Hertz-Mindlin model is a widely used and well-established contact model in DEM simulations, particularly for dry and non cohesive granular materials. It combines Hertzian theory for normal contact forces with Mindlin's tangential force model, resulting in a comprehensive representation of both normal and shear forces during particle interactions [56, 57].

3.1.2. Forces defined in Hertz Mindlin Contact model

Normal Force

The normal force F_n based on Hertz theory is:

$$F_n = \frac{4}{3} E^* \sqrt{R^*} \delta_n^{3/2} \tag{3.1}$$

where:

- δ_n is the normal overlap
- E^* is the equivalent Young's modulus:

$$E^* = \left(\frac{1 - \nu_1^2}{E_1} + \frac{1 - \nu_2^2}{E_2} \right)^{-1} \tag{3.2}$$

- R^* is the equivalent radius:

$$R^* = \left(\frac{1}{R_1} + \frac{1}{R_2} \right)^{-1} \tag{3.3}$$

Tangential Contact Force

The tangential force F_t based on Mindlin theory is:

$$F_t = -8 G^* \sqrt{R^* \delta_n} \delta_t \tag{3.4}$$

where:

- δ_t is the tangential displacement
- G^* is the equivalent shear modulus:

$$G^* = \left(\frac{2 - \nu_1}{G_1} + \frac{2 - \nu_2}{G_2} \right)^{-1} \tag{3.5}$$

Damping Forces
The normal and tangential damping forces are:

$$F_n^d = -2\sqrt{\frac{5}{6}}\beta\sqrt{S_n m^*}v_n^{rel} \tag{3.6}$$

$$F_t^d = -2\sqrt{\frac{5}{6}}\beta\sqrt{S_t m^*}v_t^{rel} \tag{3.7}$$

where:

- $S_n = 2E^*\sqrt{R^*\delta_n}$ is the normal stiffness
- $S_t = 8G^*\sqrt{R^*\delta_n}$ is the tangential stiffness
- m^* is the equivalent mass: $\frac{1}{m^*} = \frac{1}{m_1} + \frac{1}{m_2}$
- v_n^{rel}, v_t^{rel} are relative normal and tangential velocities
- β is the damping ratio

Coulomb Friction Limit
The tangential force is limited by Coulomb friction:

$$|F_t| \leq \mu|F_n| \tag{3.8}$$

where μ is the friction coefficient.

3.1.3. Material and Contact model properties

The accuracy of a discrete element method (DEM) simulation depends on the selection and calibration of the appropriate input parameters. For this thesis, data from the existing literature were used to define the soil and material properties in the simulations. Table 3.1 presents all the input parameters required for the DEM simulations used to model both particle-to-geometry (p-g) and particle-to-particle (p-p) interactions. These parameters, derived from literature sources (as indicated in the table), define the physical properties of the piles and particles, as well as the frictional and collisional behaviors governing their interactions. The mechanical properties of steel and granite were used as input parameters for density, shear modulus and poisson's ratio.

3.1.4. Numerical Set-up and Process Parameters

To simulate monopile installation in DEM, the selection of appropriate parameters is paramount for constructing a reference model that accurately captures the complex interplay between the pile, soil, and installation process. The parameters chosen for this thesis fall into two broad categories: geometric parameters, which define the physical attributes of the system, and soil parameters, which characterize the behavior of the granular material. In addition, the size of the simulation domain plays a crucial role in ensuring the validity of the results.

1. Geometric Parameters:
    - Velocity of the Pile: The rate at which the monopile is driven into the seabed directly

Symbol	Parameter Name	Reference	Value
ρ_g	Pile density [kg/m^3]	[58]	7850
G_g	Pile Shear modulus [GPa]	[59]	78
ν_g	Pile Poissons ratio [-]	[60]	0.28
$\mu_{s,p-g}$	Particle-pile sliding friction coefficient [-]	[61, 62]	0.5
$\mu_{r,p-g}$	Particle-pile rolling friction coefficient [-]	[63, 62]	0.05
e_{p-g}	Particle-pile restitution coefficient [-]	[53, 62]	0.6
ρ_p	Particle density[kg/m^3]	[64]	2664.3
G_p	Particle shear modulus [GPa]	[65]	0.04
ν_p	Particle Poissons ratio [-]	[65]	0.25
$\mu_{s,p-p}$	Particle-particle sliding friction coefficient [-]	[65, 61]	0.64
$\mu_{,p-p}$	Particle-particle rolling friction coefficient [-]	[65, 63]	0.1
e_{p-p}	Particle-particle restitution coefficient [-]	[53, 65]	0.75

Table 3.1: List of input model parameters needed for DEM simulation for particle-to-geometry (p-g) and particle-to-particle (p-p) interaction

influences the response of the soil and the dynamics of the installation. Choosing a velocity that reflects real-world installation practices is crucial for obtaining realistic simulation results.

- Domain Size: The size of the simulation domain must be carefully selected to ensure that boundary effects do not unduly influence the results. The domain should be large enough to accommodate the entire pile and a sufficient volume of soil to capture the soil-pile interaction.
- Shape of the Domain: The selection of the domain shape in Discrete Element Method (DEM) simulations significantly influences computational efficiency and accuracy. Square and cylindrical domains are the most commonly employed shapes due to their relative simplicity in modeling and compatibility with various physical phenomena
- Shape of the Pile: Monopiles are inherently cylindrical in shape, this section investigates the feasibility of simplifying the analysis of large diameter monopiles by representing them as plate shapes with equivalent circumferences

2. Numerical Representation of Granite Rocks:

   - Shape of the Rock (Number of Shapes): The shape of the rock particles plays a fundamental role in determining the soil's packing density, shear strength, and overall behavior. In this thesis, the number of rock shapes that can be varied within the soil bed is considered to assess the impact of particle shape diversity on the simulation results.
   - Accuracy of the Rock: The level of detail in representing the rock particles affects the computational cost and the accuracy of inter-particle interactions. Choosing an appropriate particle resolution is essential for balancing accuracy with computational efficiency.

3.1.5. Key Performance Indicatiors (KPI's)

The evaluation of monopile installation simulations requires robust and relevant metrics to assess the effectiveness and efficiency of the process. In this thesis, two primary Key Per-

formance Indicators (KPI's) are utilized to quantify the simulation results and gain insights into the installation behavior: penetration resistance and penetration work by the monopile. These KPI's offer distinct perspectives on the installation process, providing a comprehensive understanding of the interaction between the monopile and the soil.

1. Penetration resistance: Penetration resistance measures the force required to drive the monopile into the seabed at a given depth. This KPI is a critical indicator of the soil's resistance to penetration, which is influenced by various factors, including soil properties, monopile geometry, and installation velocity.
2. Penetration work: The total work done by the monopile is a measure of the energy expended during the installation process. It is calculated as the integral of the penetration resistance over the depth of penetration.

The selection of penetration resistance and the penetration work as KPIs is motivated by their direct relevance to the practical aspects of the installation of monopiles. Both KPIs are readily measurable in real-world installations, allowing direct comparison between simulations and field data. Moreover, they provide complementary information, with penetration resistance offering a detailed view of the soil response at each depth, and penetration work providing a summary measure of the overall energy requirements of the installation.

3.1.6. Timestep

In the world of DEM simulations, the choice of timestep has a considerable influence over the accuracy, stability, and efficiency of the analysis. The timestep, denoted as Δt, represents the discrete time increment used to advance the simulation through time. A well-chosen timestep is essential to capture the dynamic behavior of particles accurately while avoiding numerical instability. In this section, we delve into the importance of timestep selection, the criteria for determining an appropriate value, and the simulation-based approach employed in this thesis to identify the optimal timestep.

The time step for the Hertzian contact model is often determined on the basis of the Rayleigh wave propagation: the elastic wave propagation from one particle to the adjacent contacting particles. The Rayleigh time can be calculated from the following equation (3.9) [66].

$$t_{ray} = \frac{\pi R_{\min}\sqrt{\frac{\rho}{G}}}{0.1631v + 0.8766} \tag{3.9}$$

The timestep is directly proportional to particle size and inversely proportional to shear modulus. The shear modulus is property of soil, which cannot be changed. However, the use of multi-spheres in this thesis introduces a unique challenge. While multispheres offer greater geometric flexibility, they are composed of smaller spheres, raising the question of which radius to use for timestep calculation.
The smallest sphere within a multisphere dictates the shortest time for a stress wave to propagate through it. Using this radius in the timestep calculation would ensure stability for the entire multisphere, but it could lead to unnecessarily small timesteps, increasing computational cost. Conversely, using the overall radius of the multisphere might lead to instability as the stress wave propagation within smaller constituent spheres would not be adequately captured.

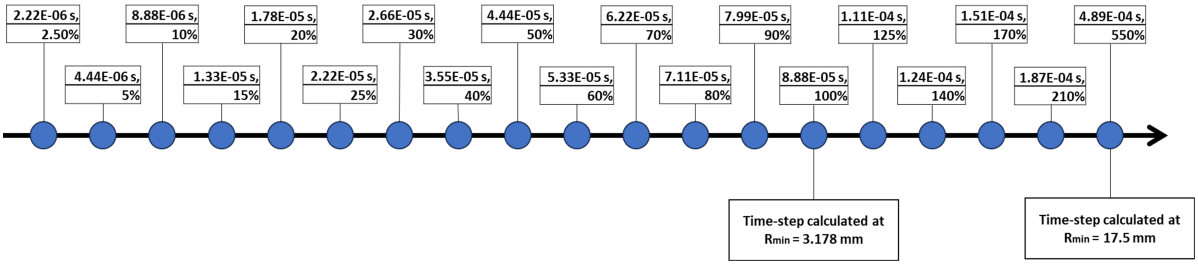

Figure 3.1: Interpolation and Extrapolation of timestep to model simulation

Interpolation and Extrapolation Approach: To address this challenge, an interpolation approach was adopted:

1. Bounding Timesteps: The timesteps were calculated for two extreme cases:

   - Lower bound (8.88e-05 s): Timestep(100% of the t_{ray}) based on the radius of the smallest sphere within the multisphere (3.178mm sphere, ensuring stability).
   - Upper bound (4.89e-04 s): Timestep(100% of the t_{ray}) based on the overall size of the multisphere (17.5 mm sphere, potentially risking instability).

   Both the timesteps were calculated properties mentioned in table 3.1 and equation (3.9)

2. Interpolation and Extrapolation: A range of time steps were interpolated and extrapolated using lower and upper bounds as reference [Figure 3.1]. This allowed for a systematic exploration of timestep values while considering the multisphere's unique structure.

A series of 19 Discrete Element Method (DEM) simulations were conducted to investigate the effect of varying timesteps on monopile installation behavior. The timesteps ranged from 2.22e-6 seconds (representing 2.5 % of the Rayleigh Time) to 4.89e-4 seconds (550% of the Rayleigh Time). This comprehensive approach aimed to identify the optimal timestep that balanced accuracy, stability, and computational efficiency.

Model setup

Real rocks were scanned using the Qlone app, creating detailed 3D models of their surfaces. These models were then imported into EDEM and converted into multi-sphere rock representations [Figure 3.2a] and traditional monopile shape, modeled as a simple cylinder [Figure 3.2b] is used for penetrating the rock bed. The DEM simulations were conducted within a square domain with dimensions sufficient to encompass the monopile and particles [Figure 3.2c]. Table 3.2 depicts the dimensions of the Monopile, Rock, and Domain used in the simulation. The monopile is displaced to 300 mm in z direction with a velocity of 100 mm/s and 50 mm/s, this approach aimed to validate the robustness of the chosen time step across varying velocity conditions.

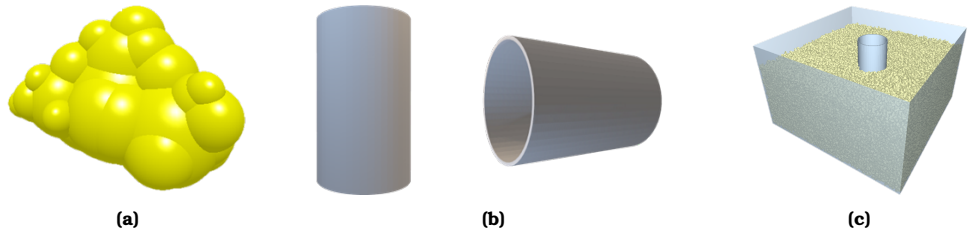

Figure 3.2: Pictorial representation of EDEM simulation components: (a) Rock sample generated using EDEM demonstrating multi-sphere approach for particle representation , (b) Monopile geometry , and (c) EDEM simulation setup showing the monopile penetration

Dimension	Value
Length of the pile	500 mm
Outer Diameter of the pile	323.9 mm
Thickness	8.8 mm
Size of the rock	35 mm
Size range of the spheres in the rock	3.178 mm -11.36 mm
Length of the domain	1650 mm
Width of the domain	1650 mm
Height of the domain	1000 mm

Table 3.2: Diemensions of Monopile, Rock and Domain

To comprehensively evaluate the impact of varying timesteps on simulation accuracy and computational efficiency, we plotted key performance indicators (KPIs) against penetration depth. The simulation results for monopile penetration, presented in figure 3.3 and 3.4, illustrate the relationship between penetration resistance and penetration work with respect to penetration depth across various timesteps expressed as percentages of the Rayleigh timestep. A consistent trend is observed across both velocities, where the simulations demonstrate stability until the timestep reaches 80%.

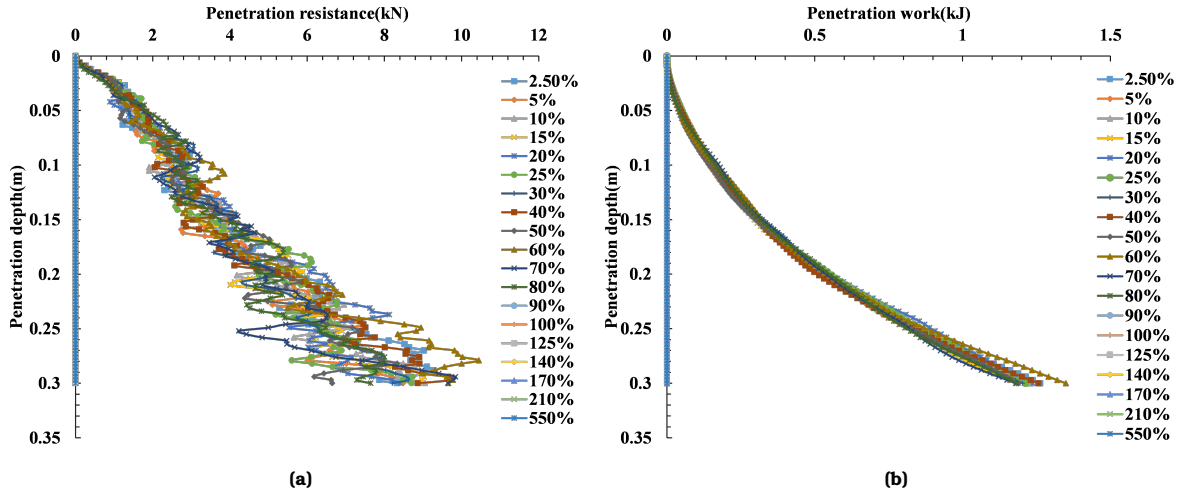

Figure 3.3: Graphical representation of timestep sensitivity analysis results for monopile penetration at 100 mm/s velocity, showing: (a) penetration resistance versus penetration depth, and (b) penetration work versus penetration depth, with timesteps ranging from 2.5% to 550% of the Rayleigh timestep.

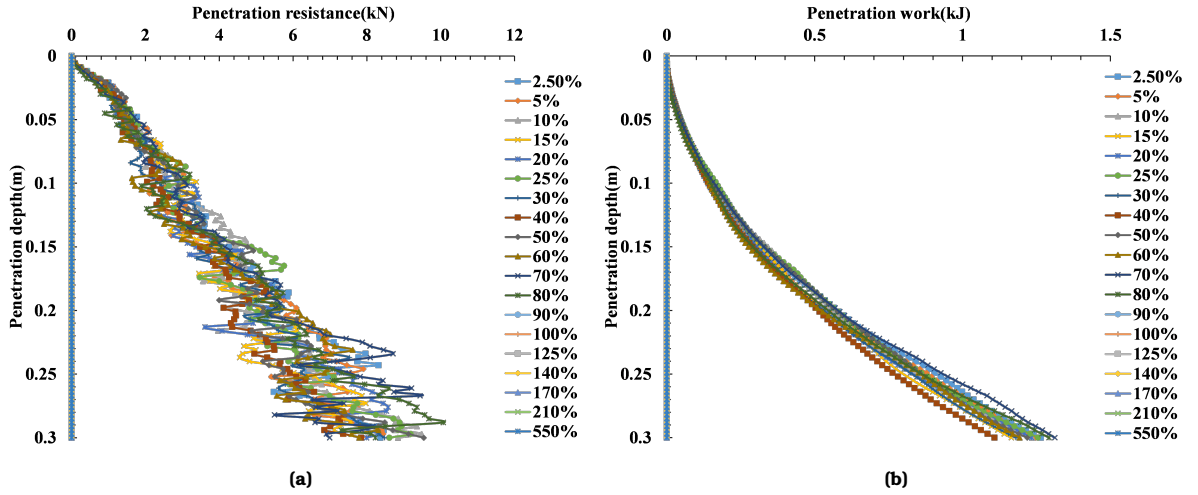

Figure 3.4: Graphical representation of timestep sensitivity analysis results for monopile penetration at 50 mm/s velocity, showing: (a) penetration resistance versus penetration depth, and (b) penetration work versus penetration depth, with timesteps ranging from 2.5% to 550% of the Rayleigh timestep.

A sharp transition occurs beyond the 80% threshold, where the simulations exhibit instability. This instability is characterized by a sudden flattening of the curves, indicating that the numerical solution no longer accurately captures the physical behavior of the system. Specifically, our findings suggest that the time-step should be calculated based on the radius of the smallest sphere within the multisphere, rather than the overall dimensions of the multisphere itself. The simulation results for penetration resistance and penetration work performed in varying Rayleigh time steps, shown in figure 3.3 and 3.4, exhibit consistent behavior up to the 80% threshold, making it difficult to determine an optimal time step based solely on this metric. Therefore, the penetration work at three different depths (0.1 m, 0.2 m, and 0.3 m) was examined to assess the divergence. A noticeable divergence in

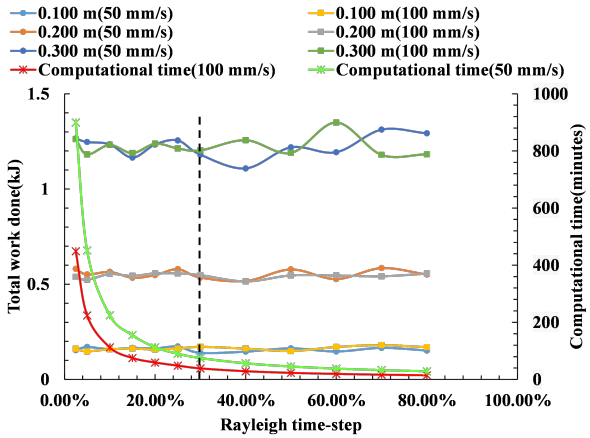

Figure 3.5: Comparison of penetration work at different depths with varying timestep and velocity

results is observed beyond the 30% Rayleigh timestep mark, with fluctuations increasing as the timestep increases. Additionally, computational time significantly impacts the feasibility of simulations. As illustrated in figure 3.5, the 30% timestep offers a substantial reduction in computational time (74 minutes for 50 mm/s and 38 minutes for 100 mm/s) compared to the 2.5% timestep (18 hours for 50 mm/s and 7.5 hours for 100 mm/s). This reduction

is crucial, especially for small-scale simulations where excessive computational time is impractical. Considering the balance between result divergence and computational efficiency, a 30% Rayleigh timestep was selected for subsequent simulations. This choice ensures a reasonable compromise between accuracy and computational cost, enabling efficient and reliable simulation results.

3.2. Geometric parameters

3.2.1. Velocity of the monopile

Monopile driving through scour layer should be penetrated at slower rate. The surface layers are typically made up of loose rock or gravel. High installation velocities can lead to excessive forces that fracture or displace these rocks, compromising the integrity of the scour protection. Rapid penetration through a scour layer can induce vibrations and shocks that could damage the installation equipment, leading to delays and increased costs. Due to the slow penetration rate, this process can be considered quasi-static, characterized by a low flow regime. Albert et al. [67] proposed a formula [Equation (3.10)] to determine the critical velocity (v_c) for the pile velocity regime (v). This formula incorporates the radius of the rock (R_{min}) and gravitational acceleration (g). Subsequent research by Feng et al. [68] and Gezgin et al. [26] used this expression to establish the maximum quasi-static penetration depth achievable by an object intruding into a granular material. Ensuring the penetration velocity remains below the critical velocity guarantees that the resistance force experienced by the object is independent of its velocity.

$$v < v_c = \frac{\sqrt{4gR_{\min}}}{10} \tag{3.10}$$

To validate the applicability of the quasi-static penetration regime, a series of numerical simulations was conducted. As an initial approximation, a grain diameter of 35mm was selected, corresponding to the largest multisphere size to be used in subsequent investigations. This yielded a calculated critical velocity of 82.5 mm/s. To assess the validity of this critical velocity, 18 discrete element method (DEM) simulations were performed. The penetration velocity was systematically varied within a range of 10 mm/s to 250 mm/s, encompassing both static and dynamic values. This comprehensive approach allowed for a thorough evaluation of the velocity-dependent behavior of the penetration process.

For velocities up to 70 mm/s, the penetration resistance curves exhibit similar trends with increasing penetration depth, a noticeable difference occurs for the velocities beyond 70 mm/s. This suggests that within this velocity range, the penetration process remains within the quasistatic regime, where the resistance force is primarily governed by the material properties and is relatively independent of the penetration velocity. The penetration work curves generally follow a similar pattern to the penetration resistance curves, with higher velocities requiring more work to achieve the same penetration depth. The consistent trends observed across different velocities below 70 mm/s. The results demonstrated a clear increase in penetration resistance at velocities exceeding 70 mm/s, aligning with the theoretical predictions based on the aforementioned formula (Equation (3.10)). This confirmed the significance of the calculated critical velocity in demarcating the transition between quasistatic and dy-

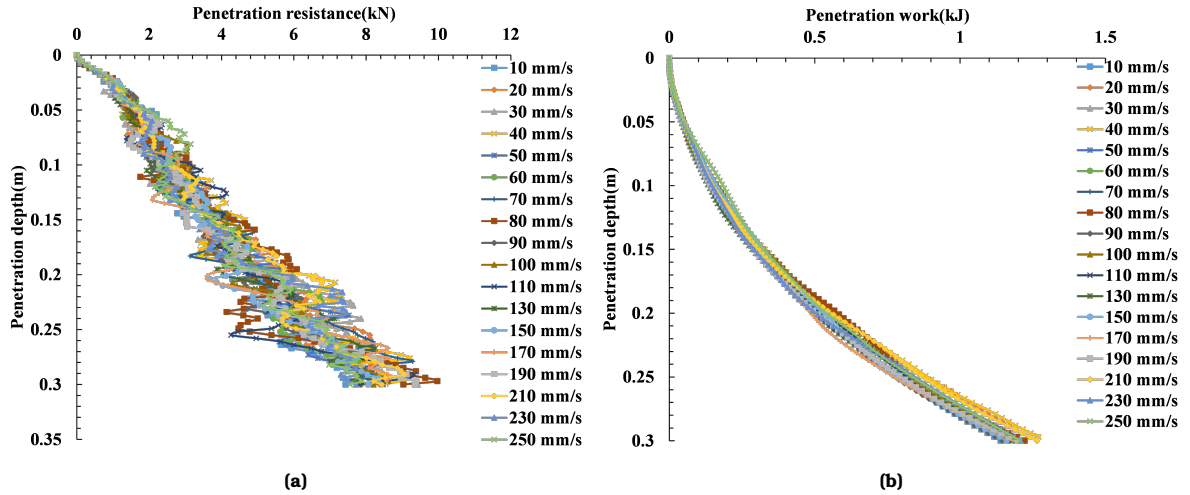

Figure 3.6: Graphical representation of velocity simulation results : (a) penetration resistance versus penetration depth, and (b) penetration work versus penetration depth, with velocity ranging from 10 mm/s to 250 mm/s of the Rayleigh timestep.

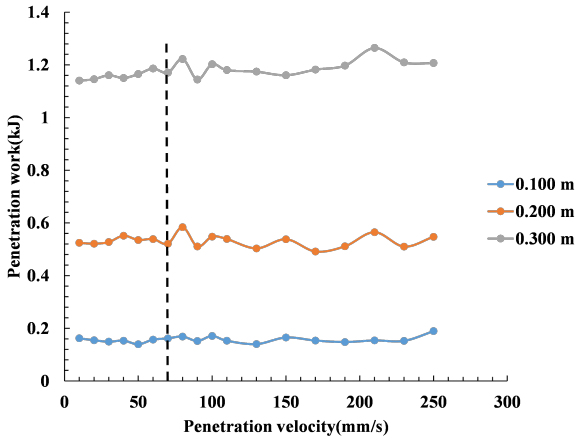

Figure 3.7: Comparison of penetration work at different depths with varying velocity

namic penetration regimes. However, to ensure the robustness of the quasistatic assumption for future investigations involving smaller rock sizes and multisphere configurations, a more conservative penetration velocity of 50 mm/s was adopted for subsequent analyses. This precautionary measure aimed to maintain the validity of the quasistatic regime even under varying particle size distributions, thereby ensuring the accuracy and reliability of the simulation results.

3.2.2. Size of the domain

The subsequent phase of the numerical study focused on optimizing the domain size to minimize computational demands while maintaining the accuracy of the penetration resistance results. To achieve this, the width of the domain(W) was systematically varied relative to the rock size(d_{rock}), with the width-to-diameter ratio (W/d_{rock}) ranging from 10 to 75.

The rationale behind this approach stems from the direct relationship between domain size and computational time. Larger domains necessitate a greater number of particles to main-

tain a consistent packing density, leading to increased computational costs due to the higher number of inter-particle interactions that need to be resolved. Therefore, it is imperative to identify the smallest domain size that does not compromise the accuracy of the penetration resistance predictions.

By performing DEM simulations varying W/d_{rock}, we aim to determine the optimal domain size that strikes a balance between computational efficiency and result accuracy. This optimization is crucial for ensuring the feasibility of future investigations involving larger and more complex particle configurations, where excessive computational times could become a limiting factor. As established in the previous section, the monopile penetration velocity is maintained at 50 mm/s.

W/d_{rock}	**Width of the domain (W) (mm)**	**Number of Particles**	**Computational Time**
10	350	4100	4 minutes
20	700	17365	10 minutes
25	870	26825	14.6 minutes
30	1050	39207	26.11 minutes
35	1225	53331	31.2 minutes
40	1400	65754	36.4 minutes
50	1750	108655	52.2 minutes
65	2275	183869	1.3 hours
75	2625	254028	5.43 hours

Table 3.3: Relationship between W/d_{rock} factor, width of the domain,number of particles and computational time

Table 3.3 presents the relationship between the W/d_{rock} factor, the corresponding number of particles in the simulation domain, and the resulting computation time. Figure 3.9 illustrates the relationship between penetration depth and both penetration resistance (Figure 3.9a) and penetration work (Figure 3.9b) for varying domain sizes, expressed as the ratio of width to particle diameter (W/d_{rock}). The elevated penetration resistance and work done for W/d_{rock} = 10 suggests that a domain size of 10 times the particle diameter may be insufficient to accurately represent the penetration process. This smaller domain likely induces boundary effects that artificially increase resistance and distort the results (Figure 3.8a). To ensure clarity and focus on the relevant trends, the curve for W/d_{rock} = 10 has been ignored, as it was deemed invalid due to significant boundary effects as discussed previously. Upon analyzing the remaining curves, a clear convergence trend is observed starting at W/d_{rock} = 30 for both penetration resistance and penetration work. This indicates that, beyond this threshold, increasing the domain size has a minimal impact on the simulation results. In other words, for W/d_{rock} values of 30 and above, the domain size is large enough to mitigate boundary effects and accurately capture penetration behavior.

However, the penetration resistance remains significantly higher for smaller domain sizes (W/d_{rock} = 20 and 25). This suggests that boundary effects still play a role in these cases, leading to an overestimation of resistance. Figure 3.9a and 3.9b shows that a domain size of at least 30 times the diameter of the particle is necessary to obtain reliable results in this simulation set-up. By selecting a domain size that is large enough to minimize boundary effects but not excessively large to avoid unnecessary computational burden, we can achieve a more accurate and efficient representation of the penetration process. Although a W/d_{rock} ratio of 30 may be sufficient to mitigate boundary effects, a slightly higher value of 40 is

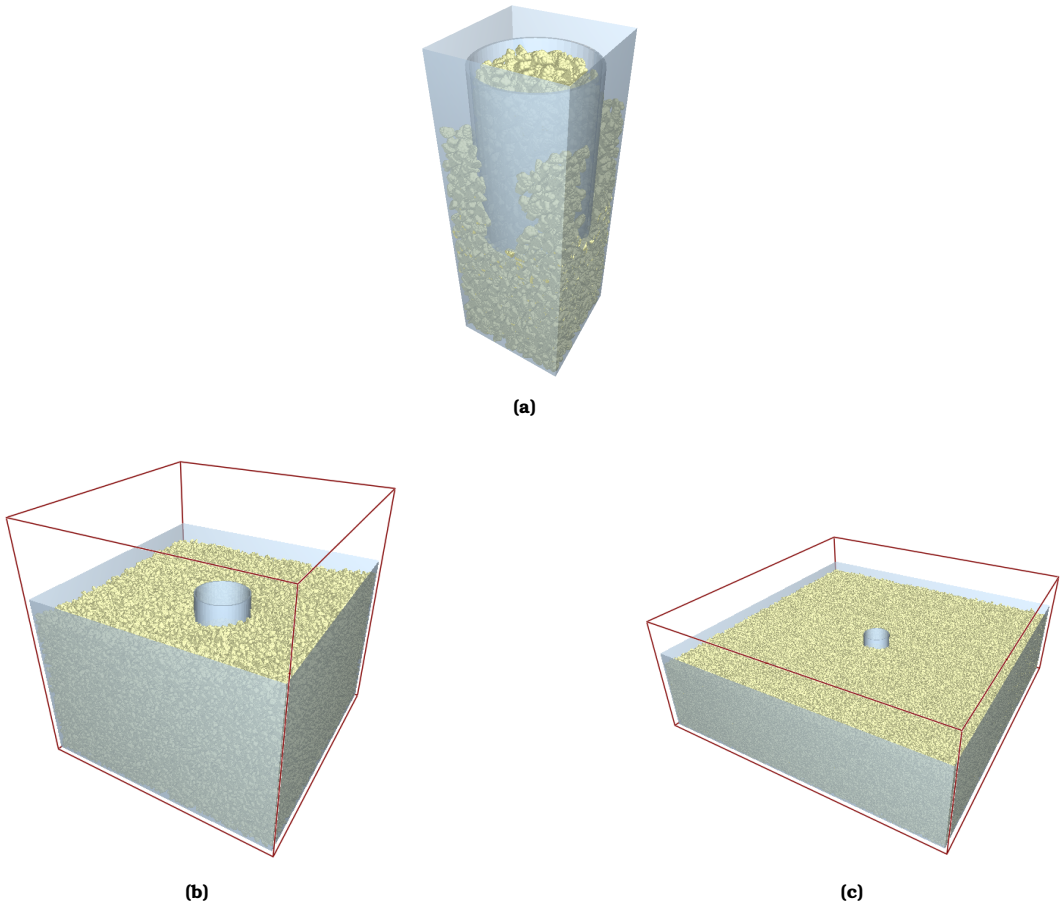

Figure 3.8: Pictorial representation of simulation domains with varying width-to-particle diameter ratios (W/d_{rock}) (a) W/d_{rock}=10 , (b) W/d_{rock}=40 and, (c) W/d_{rock}=75

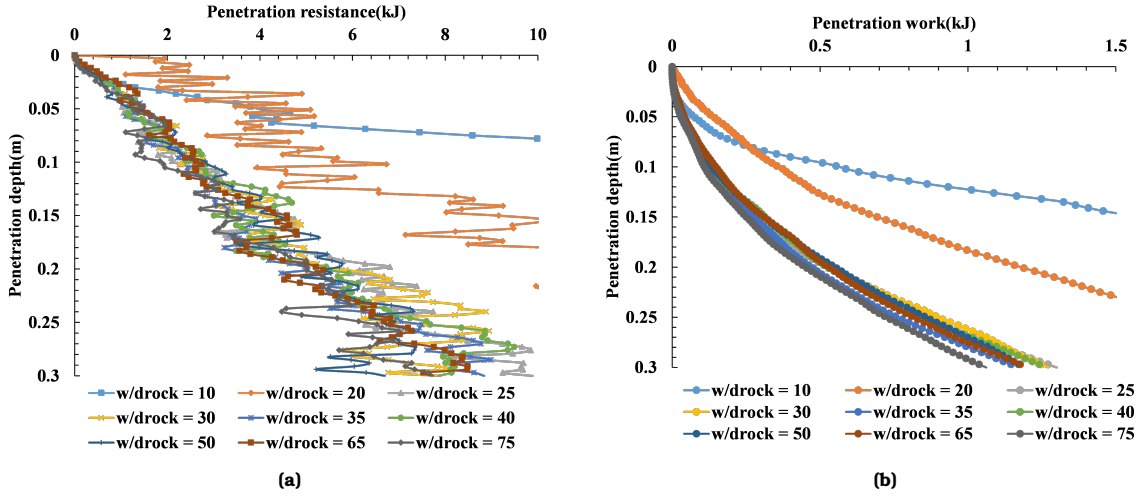

Figure 3.9: Graphical representation of domain size sensitivity analysis showing the relationship between penetration depth and (a) penetration resistance and (b) penetration work for varying domain width ratios (w/d_{rock}) ranging from 10 to 75.

chosen to provide an additional margin of safety and ensure the robustness of the simulation results and the computational time at this ratio is still less than a hour(Table 3.3). This conservative approach is particularly important for future simulations involving different rock

sizes and multi-sphere configurations, where potential boundary effects might be more pronounced. By adopting a W/d_{rock} ratio of 40, we can confidently proceed with subsequent analyses, knowing that the domain size is sufficiently large to accurately capture the penetration behavior without incurring excessive computational costs. This optimal domain size will serve as the foundation for further investigations into the effects of various parameters, such as particle size distribution and shape, on the penetration resistance of monopiles in granular media.

3.2.3. Shape of the domain

In DEM most of the simulations concerning penetration are conducted either in square or cylindrical domain. Cylindrical domains are considered because they are well suited for axisymmetric penetration problems, where the geometry and loading conditions are symmetric about a central axis and the sharp corners of a square domain can introduce artificial stress concentrations. Given the chosen domain width of 1400 mm (W/d_{rock} = 40), two possible configurations for a cylindrical domain arise (Figure 3.10), the first option is a cylindrical domain with a diameter of 1400 mm(Figure 3.10a), matching the width of the previously determined square domain; alternatively, a cylindrical domain with a diameter 1979.8 mm(Figure 3.10b) equal to the diagonal of the square domain can be considered.

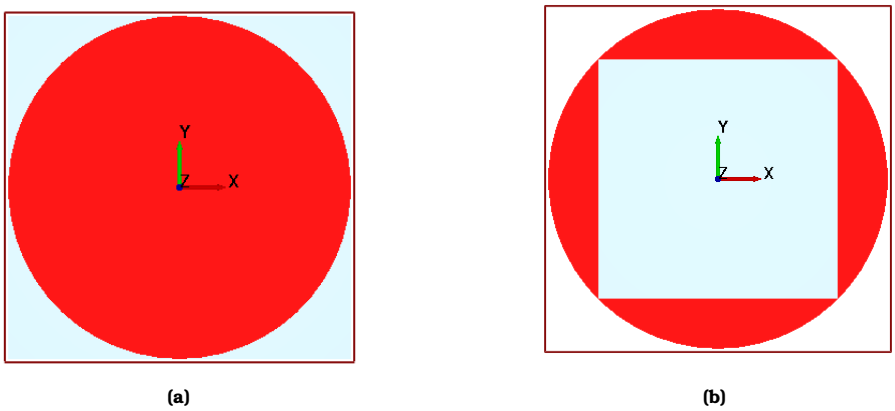

Figure 3.10: Comparison of cylindrical domain geometries relative to a square domain showing: (a) a cylindrical domain with diameter equal to the square width, and (b) a cylindrical domain with diameter equal to the square diagonal. Red regions represent the cylindrical domains while light blue regions indicate the square domain boundaries.

Figure 3.11 illustrates the effect of varying the domain shape on both penetration resistance (Figure 3.11a) and penetration work (Figure 3.11b). The results demonstrate a negligible difference in penetration behavior between the square domain (1400 mm), the cylindrical domain with equivalent diameter (1400 mm) and the cylindrical domain with equivalent diagonal (1979.8 mm). This suggests that the shape of the domain has minimal influence on the simulation results within the investigated range of penetration depths.

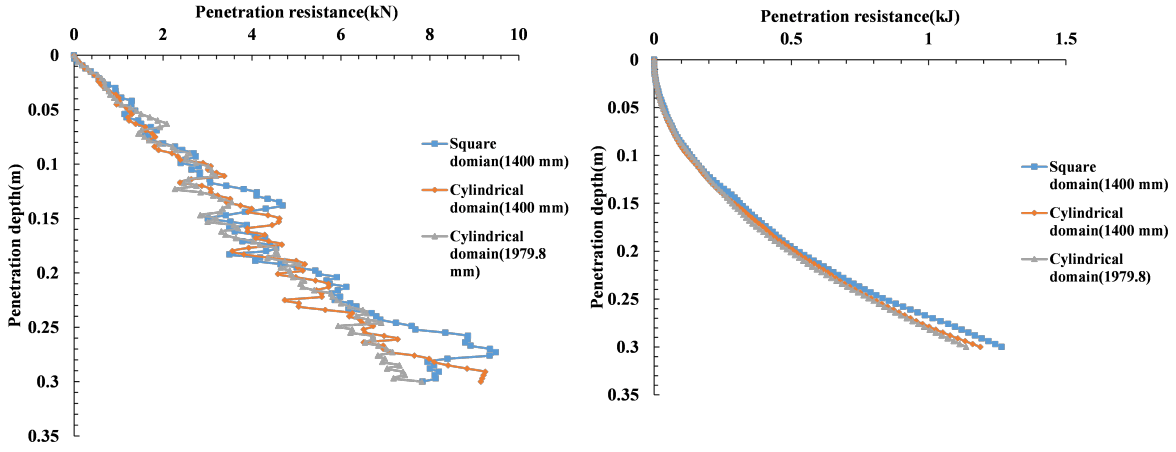

(a) Penetration resistance(N) vs. Penetration depth(m) with varying the shape of the domain

(b) Penetration work(J) vs. Penetration depth(m) with varying shape of the domain

Figure 3.11: Graphical representation of domain shape effects on penetration, comparing square domain (1400 mm) with cylindrical domains (1400 mm and 1979.8 mm diameters). The plots show (a) penetration resistance and (b) penetration work versus penetration depth in meters, demonstrating the influence of domain geometry on penetration behavior.

Given this observation, the cylindrical domain with a diameter of 1400 mm is selected for subsequent analyses. The choice of this configuration is primarily driven by the desire to optimize computational efficiency. With 54,453 particles, this configuration takes only 32 minutes hours to run, compared to 36.4 minutes for 65,754 particles and a staggering 55 minutes for 109,413 particles. By significantly minimizing the number of particles, we reduce computational time without compromising the accuracy of our simulation results.

3.2.4. Shape of the monopile

The traditional shape of a monopile is a hollow cylinder. However, for the purpose of simplifying the analysis and visualization of the penetration process, an equivalent rectangular plate can be utilized. This simplification is based on the concept of "unrolling" the cylindrical monopile(Length = 500mm, Outer diameter = 323.9 and Wall thickness = 8.8 mm) into a flat plate. A rectangular plate has the dimensions equivalent to monopile(Length = 1017.56 mm, Height = 500 mm, thickness = 8.8 mm), while reducing the complexity of the model. Figure 3.12 illustrates the dimensional comparison between plate geometry and monopile

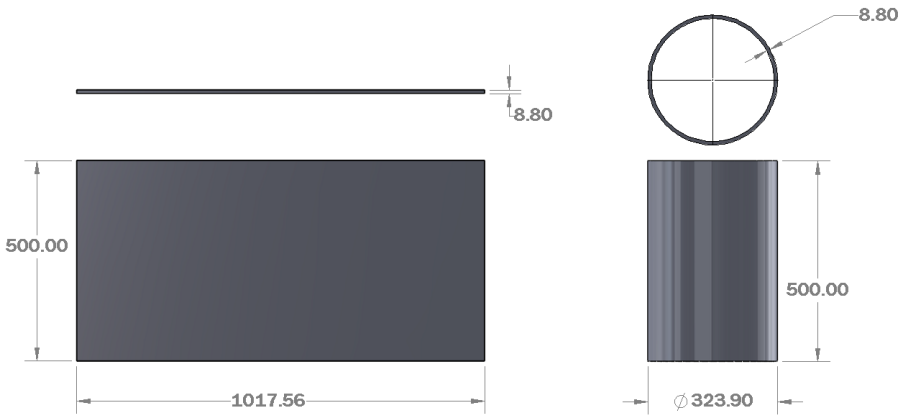

Figure 3.12: Dimensions of the plate geometry compared to monopile

The flat surface of the rectangular plate allows for easier visualization of the contact forces and deformations at the interface between the monopile and the surrounding granular medium. This can provide valuable insights into the mechanisms governing penetration resistance. Figure 3.13 illustrates the penetration resistance and penetration work as a function of penetration depth for two monopile shapes: the traditional cylindrical geometry and the simplified plate geometry. The results reveal a consistent trend in the initial stages of penetration, where both geometries experience similar resistance levels. However, as the penetration depth increases, a divergence emerges, with the plate geometry exhibiting a gradual reduction in both penetration resistance and penetration work compared to the traditional geometry. This divergence can be attributed to the "plugging effect" that occurs in the cylindrical monopile. As the monopile penetrates deeper, the soil particles displaced by its cylindrical hollow shape tend to accumulate inside the pile, forming a plug (Figure 3.14).

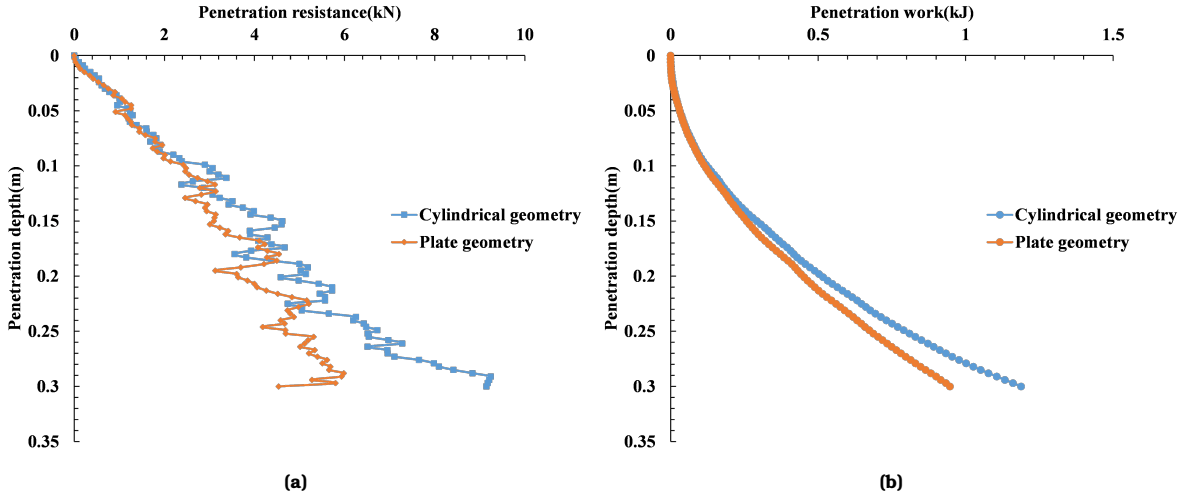

Figure 3.13: Graphical representation comparing the penetration behavior of cylindrical and plate monopile geometries, showing the relationships between penetration depth and (a) penetration resistance and (b) penetration work. The comparison demonstrates how the monopile shape influences the penetration mechanics and resistance profiles during installation.

Li et al. (2021) conducted a study on open-ended piles, finding that internal resistance,

also known as plugging resistance, is a more significant factor than external resistance in the overall penetration resistance of these piles [19]. This plug increases the effective cross-sectional area of the monopile, leading to increased frictional resistance and consequently, higher penetration resistance and penetration work. In contrast, the plate geometry does not experience this plugging effect.

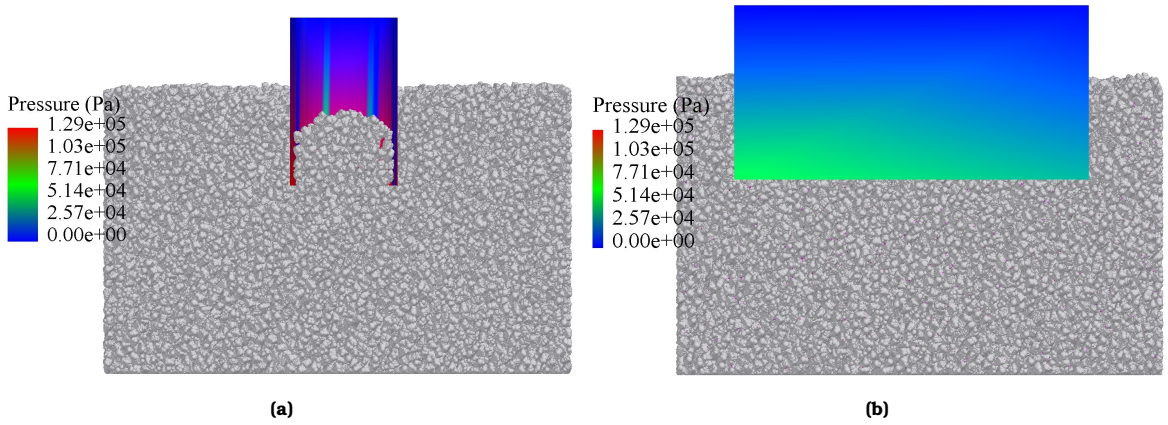

Figure 3.14: Picture depicting (a) plugging effect in monopile, (b) no plugging effect in plate geometry

The flat surface of the plate displaces soil particles laterally, minimizing the accumulation of material within the penetration zone. As a result, the resistance and work done associated with the plate geometry remain lower than those of the cylindrical monopile at greater depths. This observation underscores the importance of considering the monopile shape in penetration simulations. The plugging effect, inherent to the cylindrical geometry, can significantly influence the penetration resistance and energy requirements, particularly at greater depths. So, to accurately represent the behavior of monopile foundations in granular media, this study will continue to utilize the traditional cylindrical monopile geometry for subsequent simulations.

3.3. Rock parameters

3.3.1. Shape of the rock

The shape of individual rock particles significantly influences the behavior of granular assemblies, impacting properties such as packing density and overall mechanical response. To investigate this effect within the context of monopile penetration, this thesis explores the variation of rock shapes within the soil bed. A set of 20 distinct rock shapes was obtained through scanning and subsequently imported into the EDEM software. These shapes serve as the building blocks for constructing the granular medium in the simulations. By systematically varying the number of shapes used in each simulation, from a minimum of 2 to a maximum of 20(Figure 3.15), we aim to quantify the influence of particle shape diversity on the penetration resistance and energy requirements of the monopile.

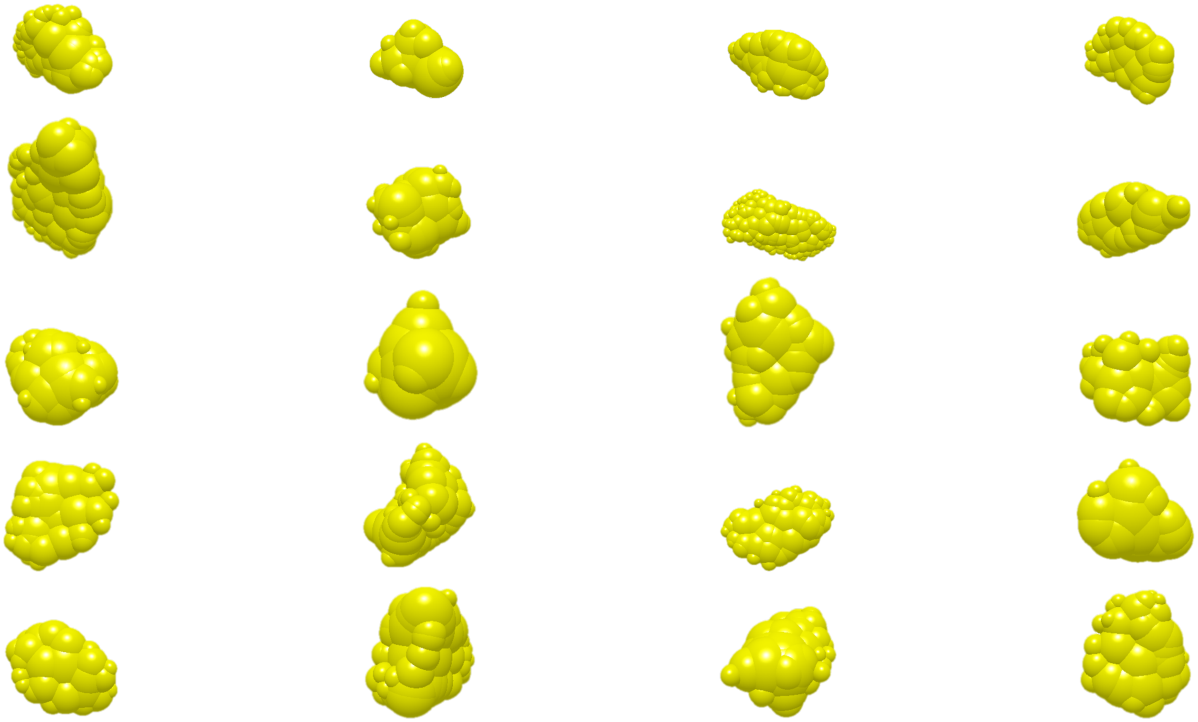

Figure 3.15: Scanned rocks generated in EDEM as multispheres

This approach allows us to assess the sensitivity of the simulation results to the level of detail used to represent the rock particles. By comparing the outcomes of simulations with varying numbers of rock shapes, we can determine whether using a limited set of shapes is sufficient to capture the essential features of the penetration process or if a more comprehensive representation is necessary for accurate predictions.

Number of shapes	Computational time
1	1.61 hours
2	1.71 hours
4	1.9 hours
6	2.71 hours
8	9.5 hours
10	10.7 hours
12	12.5 hours
14	13 hours
20	14.8 hours

Table 3.4: Computational time of DEM simulation in EDEM with varying number of rock shapes

Figure 3.16 illustrates the effect of varying the number of rock shapes on monopile penetration resistance (Figure 3.16a) and penetration work (Figure 3.16b). The results indicate a complex relationship between the number of shapes and the penetration behavior, with the curves becoming difficult to interpret as the number of shapes increases.

Further analysis was conducted by plotting the penetration resistance and penetration work at a selected depth against the number of shapes(Figure 3.17). This analysis reveals a significant increase in both the penetration resistance and the penetration work when the number

of shapes exceeds 6. This trend continues as the number of shapes further increases, suggesting that a higher diversity of particle shapes leads to greater resistance to penetration.

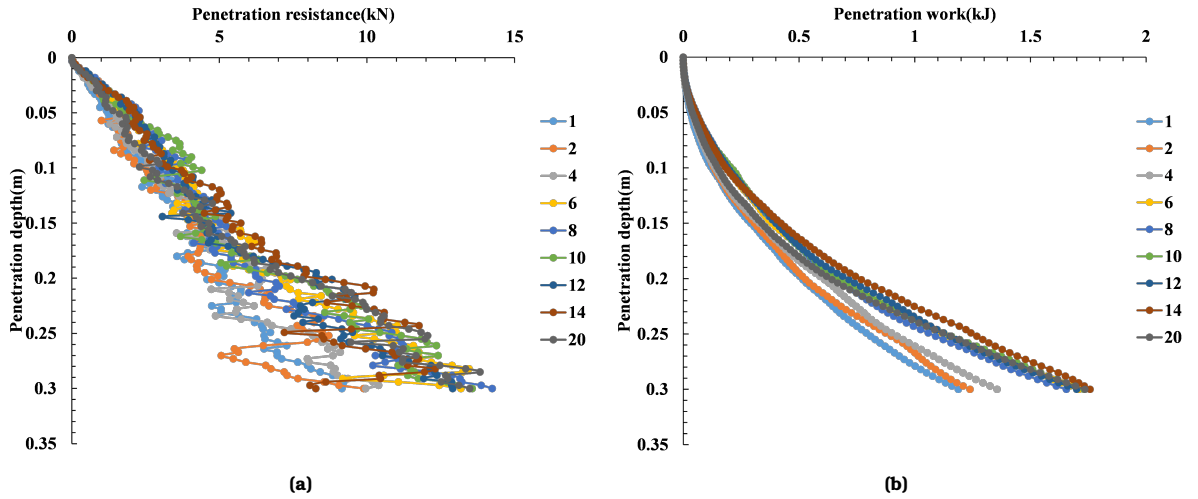

Figure 3.16: Graphical representation of penetration behavior for different rock shapes (numbered 1-20), showing the relationship between penetration depth and (a) penetration resistance and (b) penetration work. The analysis demonstrates how varying rock geometries influence the penetration mechanics and energy requirements during the penetration process

This observation can be attributed to the increased interlocking and frictional iteractions between particles with diverse shapes. As the variety of shapes increases, the particles can interlock more effectively, creating a denser and more stable packing structure. This increased packing density and interparticle friction result in higher resistance to penetration, requiring more work to achieve the same penetration depth. The significant increase in resistance observed beyond 6 shapes suggests that a maximum number of shapes is allowed to accurately capture the behavior of penetration. However, increasing the number of shapes also increases the computational time due to the increased complexity of the model.

Therefore, a balance must be struck between the level of detail used to represent the rock particles and the computational efficiency of the simulation. Based on the results presented here, it appears that using 6 or less rock shapes is sufficient to capture the essential features

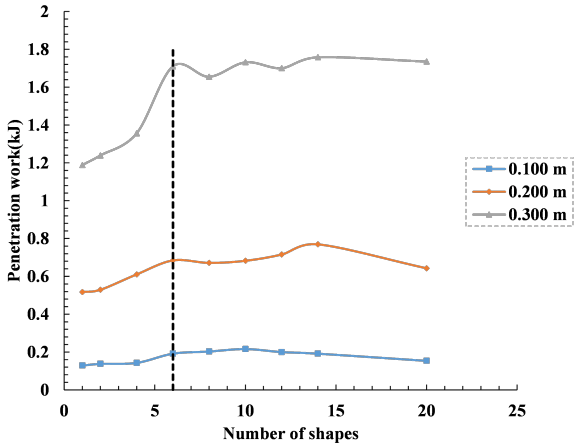

Figure 3.17: Graphical representation of Penetration work at selected depths versus Number of shapes of rocks

of the penetration process, while maintaining a reasonable computational burden. Considering the balance between accuracy and computational efficiency, a total of six distinct rock shapes will be utilized for the subsequent investigations in this study. This decision aligns with the observation that increasing the number of shapes beyond six does not significantly improve the accuracy of the results, yet incurs a higher computational cost.

3.3.2. Accuracy of the rock

The level of detail with which rock particles are represented in the numerical model can significantly influence the accuracy and computational efficiency of the simulations. In EDEM, this level of detail is controlled by the "Smoothing Value", which determines the number of multi-spheres used to approximate each rock particle. A lower accuracy value corresponds to a higher number of multi-spheres, resulting in a more detailed and accurate representation of the particle shape. In this subsection, we investigate the impact of particle accuracy on the penetration resistance and penetration work during monopile installation. To achieve this, we vary the accuracy parameter from 6 1 (highest accuracy, figure 3.18a) to (lowest accuracy, figure 3.18f) while maintaining a constant set of 4 distinct rock shapes, as determined in the previous section (Section 3.3.1). The smoothing value controls the level of detail in the rock particle representation. A higher smoothing value (e.g., 6) results in a coarser approximation of the rock shape with fewer spheres, while a lower smoothing value (e.g., 1) leads to a more detailed and accurate representation with a higher number of spheres. Decreasing the smoothing value significantly increases the number of spheres required to represent each rock type. For instance, Rock 1 requires only 41 spheres at a smoothing value of 6, but this number increases to 684 spheres at a smoothing value of 1. This increase in complexity directly translates to a longer computational time, as evidenced by the data in the table. Simulations for smoothing values of 2 and 1 were not completed due to computational limitations. The high number of spheres required for these levels of detail exceeded the available computational capacity, highlighting the trade-off between accuracy and computational cost in rock particle representation. This analysis will help us determine the optimal level of detail required to accurately capture penetration behavior while minimizing the computational burden associated with an excessively detailed model.

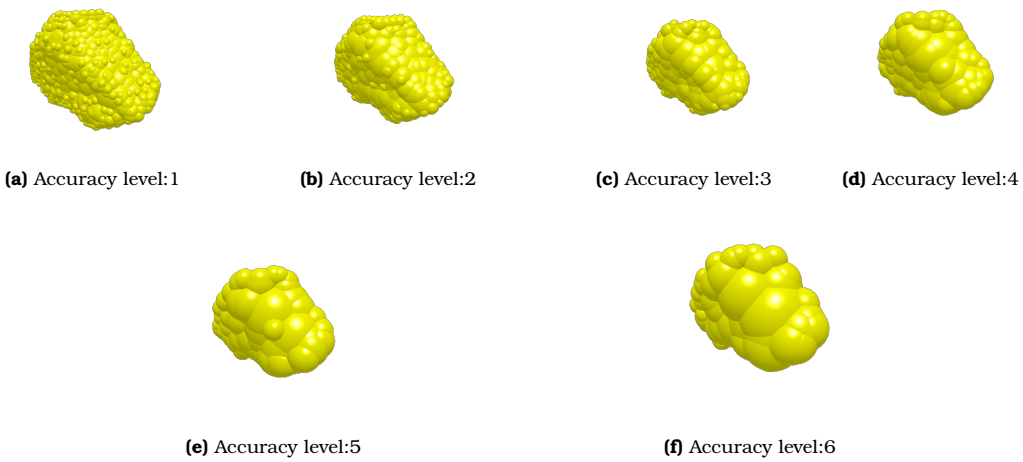

(a) Accuracy level:1 **(b)** Accuracy level:2 **(c)** Accuracy level:3 **(d)** Accuracy level:4

(e) Accuracy level:5 **(f)** Accuracy level:6

Figure 3.18: Visual representation of different levels of rock accuracy for rock 1 in EDEM

Table 3.5 displays the relationship between the smoothing value in EDEM, the corresponding number of spheres used to represent each of the six rock types, and the computational time required to generate these rock models.

Smoothing Value	Number of spheres in a rock						Number of multi spheres in simulation						Total number of spheres	Computational time
	Rock 1	Rock 2	Rock 3	Rock 4	Rock 5	Rock 6	Rock 1	Rock 2	Rock 3	Rock 4	Rock 5	Rock 6		
6	41	22	36	35	61	33	8685	8752	7210	5855	5624	8576	1,639,186	1.9 hours
5	50	29	47	46	89	45	9193	8723	7078	5811	5535	8441	2,185,049	2.5 hours
4	75	42	68	60	126	68	8498	8654	6872	9404	5779	5592	3,140,764	3.7 hours
3	119	65	128	101	221	115	8420	8493	7082	5967	5357	7886	5,153,975	13.2 hours
2	262	146	299	234	461	271	8534	8627	7193	5860	5384	7563	11,548,994	2 days(approx.)
1	684	529	721	791	984	733	8541	8500	7003	5953	5333	7407	30,773,533	10 days(approx.)

Table 3.5: Total number of spheres in a simulation with respect to smoothing value in EDEM and the required computational time to achieve it

Figure 3.19 illustrates the effect of varying the smoothing value of rock particles on both penetration resistance (Figure 3.19a) and penetration work (Figure 3.19b). The smoothing value in EDEM determines the level of detail in the rock particle representation, with lower values corresponding to higher accuracy and more detailed shapes. The results show that the penetration resistance and penetration work for a smoothing value of 6 are slightly lower compared to other values. This suggests that increasing the level of detail in the rock particle representation (by decreasing the smoothing value) leads to a marginal increase in resistance and energy requirements during penetration. However, the differences in penetration resis-

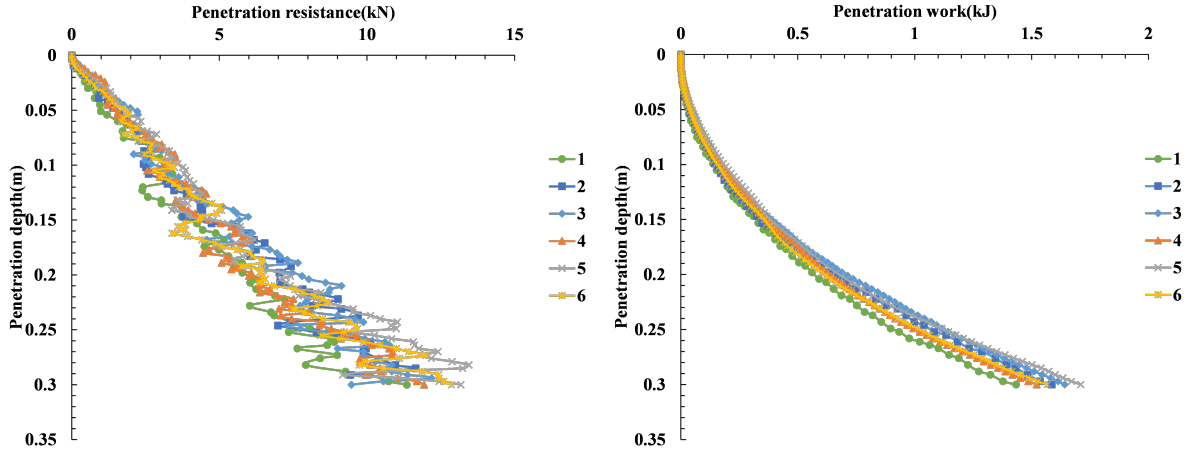

(a) Penetration resistance(N) vs. Penetration depth(m) with varying the smoothing value of the rocks

(b) Penetration work(J) vs. Penetration depth(m) with varying smoothing value of the rocks

Figure 3.19: Graphical representation of results with varying smoothing value of the rocks

tance and penetration work between smoothing values of 3, 4, and 5 are relatively small, indicating a convergence in the results as the smoothing value decreases. This suggests that beyond a certain level of detail, further increasing the accuracy of the rock particle representation does not significantly affect the penetration behavior. The slight increase in resistance and work done observed for a smoothing value of 3 could be attributed to the increased surface roughness and interlocking potential of the more detailed rock particles. However, this effect appears to be relatively minor compared to the overall convergence trend observed for smoothing values of 3 and above.

The results presented in Figure 3.19 suggest that a smoothing value of 4 or 5 provides a reasonable balance between accuracy and computational efficiency to simulate the penetration

of monopiles in granular media. Although a smoothing value of 3 may offer slightly higher accuracy, the marginal improvement in results may not justify the increased computational cost associated with the more detailed particle representation.

The results indicate that a smoothing value of 4 or 5 offers a reasonable compromise between accuracy and computational efficiency. These values provide a sufficiently detailed representation of the rock particles while maintaining manageable computational times. Therefore, subsequent simulations will utilize a smoothing value of 5 to ensure a balance between accuracy and computational feasibility.

3.4. Conclusion

This chapter established a numerical model for simulating quasistatic monopile penetration in a granular medium using the Discrete Element Method (DEM). The key parameters and modeling choices were thoroughly investigated to ensure the accuracy and efficiency of subsequent simulations.

The Hertz-Mindlin contact model was chosen to represent the interactions between the monopile and the rock particles, capturing both normal and tangential forces. The selection of rock and material properties, including density, Young's modulus, Poisson's ratio, and friction coefficients, was carefully calibrated to accurately reflect the behavior of real-world materials.

Key performance indicators (KPIs), such as penetration resistance and penetration work, were defined to assess the performance of the monopile during penetration. A suitable timestep was determined to ensure numerical stability and accuracy of the simulation results.

Extensive investigations were conducted to optimize the geometric parameters of the simulation. The optimal domain size was established by varying the width-to-diameter ratio (W/d) and analyzing the resulting penetration resistance and penetration work. A cylindrical domain with a diameter of 1400 mm (W/d = 40) was chosen for its balance of accuracy and computational efficiency.

The shape of the monopile was also investigated by comparing the traditional cylindrical geometry with a simplified rectangular plate. The cylindrical shape was ultimately selected to accurately capture the plugging effect observed in real-world monopile installations.

The rock parameters, including shape and accuracy, were explored to understand their influence on penetration behavior. A set of four different rock shapes was selected to represent the granular medium and a smoothing value of 5 was chosen to balance the accuracy of the rock particle representation with computational efficiency.

Addressing Research Question 2 in chapter 1 "What are the optimal model parameters and numerical settings for accurately and efficiently simulating monopile penetration through scour layers using DEM ?".

This chapter has laid the groundwork for the subsequent simulations by establishing a robust and reliable numerical model. The chosen contact model, material properties, KPIs, timestep,

and geometric parameters will ensure the accuracy and relevance of the simulation results to real-world monopile penetration scenarios. The optimized domain size and shape, along with the selected rock parameters, will provide a realistic representation of the granular medium, allowing for a comprehensive investigation of the factors influencing monopile penetration resistance and energy requirements.

4

Scaling of Monopile Penetration

In the previous chapter, a simulation-based methodology was used to establish a reference model for the penetration dynamics of monopile through a protective scour armor layer. The present chapter extends this foundational work by exploring scaling techniques to simulate and scaling law extrapolate the reference model to real-world, full-scale scenarios.

4.1. Scaling

Chapter 2 provided a comprehensive overview of scaling methodologies. However, the optimal combination of scaling techniques and laws for upscaling monopile penetration simulations remains a point of investigation. The design of offshore wind turbine foundations, particularly monopiles, has evolved significantly in recent years due to increasing turbine sizes and installation in deeper waters. The reference model presented in table 4.1 represents a smaller scale simulation of monopile penetration through scour armour rocks, with a domain size of 1400 mm and a monopile diameter of 323.9 mm. However, current offshore wind projects use much larger structures.

Parameter	**Value**
Domian size	1400 mm
Height of the domain	1000 mm
Outer diameter of monopile	323.9 mm
Thickness of monopile	8 mm
Length of monopile	500 mm
Size range of particles	25 mm - 35 mm
Number of particles	44,889
Velocity of the monopile	50 mm/s
Timestep	30%

Table 4.1: Parameters of a reference model

To scale this model to reflect current industry standards, we need to consider that modern monopile diameters for offshore wind turbines typically range from 8-10 meters, as evidenced

by recent projects [69]. This represents a scale factor of approximately 25 to 31.2 times the reference model's monopile diameter. When scaling the model, it's crucial to consider not just the monopile dimensions, but also the corresponding scour protection measures. In the reference model, the particle size range is 25-35 mm. However, full-scale scour protection typically uses much larger rock sizes.

Reference	**Monopile Diameter (m)**	**Water Depth (m)**	D_{50} **Rock Size (m)**
[70]	4.2	24	0.6
[71]	4.25	6-13	0.37-0.55
[71]	4.6	16-21	0.4-0.7
[70]	5.0	20-30	0.35-0.45
[72]	5.0	20-25	0.22-0.55

Table 4.2: Scour armor rock sizes for offshore monopile foundations

As shown in table 4.2, the median stone size (D_{50}) for scour protection around large monopiles ranges from 0.2 to 0.6 meters, depending on the diameter of the monopile and the depth of the water. But in our study we are desire to scale our reference monopile to XXL monopile. So we need to estimate the scour armour rock size theoretically. The design of scour protection systems for offshore wind turbine foundations requires careful consideration of various parameters to ensure practical constructability. Based on extensive laboratory studies and field observations [73], three key dimensionless parameters govern the effectiveness of scour protection.

- Scour layer extension to pile diameter ratio (w_b/D_p)
- Aspect ratio, Scour layer thickness to Scour layer extension(($A_r = h_b/w_b$)
- Scour armour rock size to pile diameter ratio (D_c/D_p)

4.1.1. Design Parameters

For the present study, the following prototype dimensions are considered:

- Pile diameter (D_p) = 8.1 m
- Scoure layer extension (w_b) = 35 m

These dimensions are scaled from laboratory model tests with a scale factor of 25, where:

- Reference pile diameter = 323.9 mm
- Refernce scour layer extension = 1400 mm

4.1.2. Determination of Design Ratios

The scour layer thickness to pile diameter ratio is calculated as:

$$\frac{w_b}{D_p} = \frac{35}{8.1} = 4.32$$

This ratio falls within the optimal range of 4-5 identified by [73], where $w_b/D_p = 4 - 5$ represents optimal protection extent

Selection of Aspect Ratio

Based on experimental studies documented in [73], an aspect ratio of:

$$A_r = \frac{h_b}{w_b} = 0.07 - 0.12$$

is selected as it:

- Falls within the recommended range ($A_r < 0.15$)
- Shows optimal performance in laboratory tests
- Aligns with successful field implementations

Calculation of Scour layer thickness

The scour layer thickness is determined using the selected aspect ratio:

$$h_b = A_r \times w_b = 0.10 \times 35 = 3.500 \text{ m}$$

4.1.3. Rock Size Determination

The rock size (D_c) is determined considering that the scour layer thickness is typically comprises 4 layers of rocks [73]:

$$h_b = 4D_c$$

$$3500 = 4D_c$$

$$D_c = 0.875 \text{ mm}$$

This yields a cover stone size to pile diameter ratio of:

$$\frac{D_c}{D_p} = \frac{0.875}{8.1} = 0.108$$

This ratio is validated against experimental findings where:

- Tested range: $0.07 \leq D_c/D_p \leq 0.24$
- Optimal performance observed at $D_c/D_p \approx 0.11$
- Field implementations showing success with similar ratios

4.1.4. Validation of Design

The selected rock size ($D_c = 0.875$ m) satisfies multiple design criteria:

1. Maintains geometric similarity with laboratory studies
2. Falls within proven ranges for all dimensionless parameters:

- $w_b/D_p = 4.32$ (optimal range: 4-5)
- $A_r = 0.12$ (recommended: < 0.15)
- $D_c/D_p = 0.13$ (tested range: 0.07-0.24)

3. Provides practically constructable rock sizes
4. Aligns with successful field experiences documented in [73]

This systematic approach ensures that the scour protection design maintains both theoretical validity through dimensionless scaling and practical applicability for field implementation, which represents a scale factor of about 25 times the reference model's particle size range.

4.1.5. Choosing scaling technique

Based on the information provided and the specific requirements for scaling both the particles and geometry for our reference, exact scaling appears to be the most appropriate technique. This choice is based on several key factors:

- Preservation of dynamic and geometric similarity: Exact scaling aims to reproduce the dynamic and energetic behavior of the unscaled problem at a larger scale. This is crucial for our simulation, as we need to accurately represent the interaction between the monopile and the scour protection rocks. By applying the scaling factor to both the geometry (monopile and domain) and particle diameter (scour protection rocks), we maintain the relative proportions and interactions of our reference model.
- Accurate representation of scale: Our reference model (Table 4.1) shows a monopile diameter of 323.9 mm, while current industry standards use monopile 8.1 meters in diameter. This represents a scale factor of approximately 25. Similarly, the size of the rock from the 25-35 mm range in the reference model must be scaled to the 0.3-0.8 m range used in full-scale projects (as shown in our earlier compilation table). Exact scaling allows us to apply this scale factor consistently across all rocks/particles of the simulation.
- Number of particles in the simulation: Unlike coarse-grain or scalping techniques, exact scaling keeps the number of particles constant. Although this technique does not reduce the number of particles, the increase in particle size increases the calculated timestep which directly reduces the computational time.
- Applicability to domain scaling: When the established scaling factor is applied to achieve the required scour protection layer extent of 35 meters (representative of full-scale installations), it leads to a proportional scaling of all domain dimensions. However,this scaling approach also results in an increase in the domain height that substantially exceeds the thickness of the scout layer by 21.5 meters.
- Retention of particle size distribution: Using exact scaling, we preserve the size distribution of the scour protection rocks. This is important because the effectiveness of scour protection depends not just on the median rock size (D_{50}).

While exact scaling will increase the absolute size of our simulation domain and particles, it does not reduce the computational complexity in terms of number of particles in the sim-

ulation. However, given the importance of accurately representing the scaled-up system for offshore wind applications, this trade-off is justified. The insights gained from such a precisely scaled model will be more directly applicable to full-scale design and analysis of scour protection systems for modern offshore wind turbine foundations.

Using exact scaling, we ensure that our scaled-up simulation maintains fidelity to the physics and dynamics of the original system, providing valuable insights that can be confidently applied to the design and optimization of scour protection for large-scale offshore wind turbine foundations.

4.2. Exact scaling

Exact scaling in DEM is crucial for simulating large-scale systems while maintaining computational efficiency and accuracy. This scaling technique that serves two key purposes in DEM modeling. First, it enables the behavior of a scaled model to be directly translated to the original physical model through established scaling conditions. Second, it allows for the creation of scaled DEM models that can accurately replicate the behavior of larger, real-world physical systems. This approach is achieved by implementing a systematic set of scaling conditions that maintain the fundamental physical relationships between the original and scaled systems.

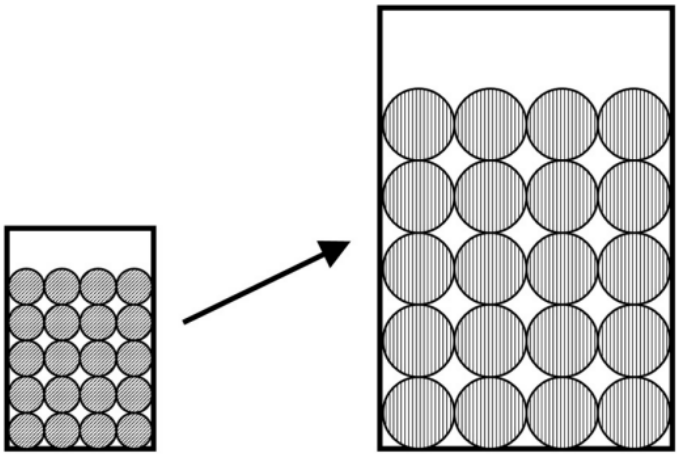

Figure 4.1: Visual representation of exact scaling [74]

Y. T. Feng and D. R. J. Owen developed a theoretical framework for upscaling discrete element models using similarity principles. They established scale factors that allow a scaled model to reproduce the behavior of a physical model exactly [75]. The approach involves choosing three basic physical quantities and their scale factors, the authors chose length, time, and mass density as the basic quantities. We choose the following(Table 4.3) physical quantities that are relavent for our research.

Quantity name	Symbol	Dimensions	Scale factor (λ)
Length	L	$[L]$	h
Time	T	$[T]$	h
Mass	M	$[\rho][L^3]$	h^3
Density	ρ	$[\rho]$	1
Displacement	u	$[L]$	h
Velocity	v	$[L][T^{-1}]$	1
Acceleration	a	$[L][T^{-2}]$	h^{-1}
Force	F	$[\rho][L^4][T^{-2}]$	h^2
Young's modulus	E	$[\rho][L^2][T^{-2}]$	1

Table 4.3: Scaling laws involved in exact scaling for various physical quantities [75].

The derived quantities - velocity, acceleration, force, and Young's modulus - exhibit systematic changes corresponding to the scaling of fundamental physical quantities. These relationships emerge from dimensional analysis and the preservation of physical similarity principles. This choice leads to the requirement that particle stress and strain must be independent of the spatial scale factor. For our model to represent the real-life scaled model, scaling the model with exact scaling with the factor of 25 gives the ideal values for both monopile and rocks. Using the basic physical quantities we mentioned in the above study, we model four different methods to scale our reference model. In Models 1 through 4, the derived quantities are determined by the scaling relationships applied to the basic quantities: length (L), time (T), and mass (M).

Velocity preservation (Scaling method 1)

In this method, we scale our reference model with the chosen scaling factor, which encompasses both geometric dimensions and the properties of the rocks, with a scaling factor of 25. Recognizing the inherent relationship between time and velocity, we initiate the scaling process by adjusting the time dimension. This manipulation maintains a constant velocity, while resulting in a reduction in acceleration by a factor of 25. Consequently, the forces experienced within the system are magnified by the square of the scaling factor, leading to a substantial increase of 625 times. Table 4.4 shows the reference and scaled values for Model 1.

Quantity name	Dimensions	Reference value	Scale factor	Scaled value
Width of the domain	[L]	1400 mm	25	35 m
Length of the monopile	[L]	500 mm	25	12.500 m
Outer diameter of monopile	[L]	323.9 mm	25	8.1 m
Thickness of monopile	[L]	8.8 mm	25	0.22 m
Displacement	[L]	300 mm	25	7.500 m
Size of the rocks	[L]	25 mm - 35 mm	25	0.575 m - 0.875 m
Time	[T]	6 s	25	150 s
Mass of the rocks	[M]	1835 kg	25^3	2.86×10^7 kg
Mass of the monopile	[M]	34.12 kg	25^3	5.33×10^5 kg
Density	$[\rho]$	2664.3 kg/m^3	1	2664.3 kg/m^3
Velocity	$[L][T]^{-1}$	50 mm/s	1	50 mm/s
Acceleration	$[L][T]^{-2}$	9.8 m/s^2	25	0.392 m/s^2
Youngs Modulus	$[\rho][L]^2[T]^{-2}$	4×10^7	25	4×10^7
Force	$[\rho][L]^4[T]^{-2}$	F	25^2	625F

Table 4.4: Selected physical quantities, symbols, dimensions and scale factors for scaling method 1

The simulation has been designed incorporating the aforementioned parameters, particular attention must be given to the generation and settlement of scaled rocks. Given that gravitational acceleration is reduced by a factor of 25, it is imperative to ensure proper particle settlement prior to initiating the penetration phase. Failure to achieve adequate settlement may result in particles exhibiting unrealistic behavior, such as ejection from the simulation domain, thereby compromising the consistency and validity of the results. To mitigate this risk, a controlled settlement period is incorporated into the simulation protocol, allowing the scaled rock particles to reach a stable configuration under the modified gravitational conditions. To reach the stable configuration, the particle generation was run for longer period and make sure the total kinetic energy of the particles is approximately zero. This ensures the robustness and reliability of the subsequent penetration simulations.

Time Preservation (Scaling method 2)

This model closely mirrors Model 1, with the exception of deliberate modifications to time, velocity, acceleration, and force parameters. Notably, time remains unscaled, resulting in a direct scaling of velocity by a factor of 25. Consequently, acceleration is also scaled by the same factor, while force undergoes a more substantial scaling, amplified to the fourth power of 25. The reason for choosing this alternate scaling method that scales velocity and acceleration is because the previous scaled model, even though it is scaled with factor 25 to the real-life scale the model, it imitates the reference model at larger scale through altered gravity conditions, by this alternative approach we aim to model a simulation that replicate the behavior of real-world physical system. Table 4.5 depicts the scaled values calculated for Model 2.

Quantity name	Dimensions	Reference value	Scale factor	Scaled value
Width of the domain	[L]	1400 mm	25	35 m
Length of the monopile	[L]	500 mm	25	12.5 m
Outer diameter of monopile	[L]	323.9 mm	25	8.1 m
Thickness of monopile	[L]	8.8 mm	25	220 mm
Displacement	[L]	300 mm	25	7.5 m
Size of the rocks	[L]	25 mm - 35 mm	25	0.575 m - 0.875 m
Time	[T]	6 s	1	6 s
Mass of the rocks	[M]	1835 kg	25^3	2.86×10^7 kg
Mass of the monopile	[M]	34.12 kg	25^3	5.33×10^5 kg
Density	[ρ]	2664.3 kg/m^3	1	2664.3 kg/m^3
Velocity	[L][T]$^{-1}$	50 mm/s	25	11.25 m/s
Acceleration	[L][T]$^{-2}$	9.81 m/s^2	25	245.25 m/s^2
Youngs Modulus	[ρ][L]^2[T]$^{-2}$	4×10^7	25	2.5×10^9
Force	[ρ][L]^4[T]$^{-2}$	F	25^4	390,625F

Table 4.5: Selected physical quantities, symbols, dimensions and scale factors for scaling method 2

Gravity Preservation (Scaling method 3)

In contrast to Models 1 and 2, which required adjustments to time and velocity parameters and consequently introduced an artificial gravity condition unattainable in real-world scenarios, this model operates under standard gravitational conditions. This adherence to normal gravity enables the model to demonstrate its intrinsic behavior at a larger scale, providing a more authentic representation of the full-scale phenomenon. The preservation of natural gravitational forces in this model facilitates a more accurate simulation of the system's dynamics and interactions, enhancing the validity and applicability of this numerical results

to real-world conditions. Table 4.6 shows the scaled values calculated for Model 3

Quantity name	Dimensions	Reference value	Scale factor	Scaled value
Width of the domain	[L]	1400 mm	25	35 m
Length of the monopile	[L]	500 mm	25	12.5 m
Outer diameter of monopile	[L]	323.9 mm	25	8.1 m
Thickness of monopile	[L]	8.8 mm	25	220 mm
Displacement	[L]	300 mm	25	7.5 m
Size of the rocks	[L]	25 mm - 35 mm	25	0.575 m - 0.875 m
Time	[T]	6 s	25	150 s
Mass of the rocks	[M]	1835 kg	25^3	2.86×10^7 kg
Mass of the monopile	[M]	34.12 kg	25^3	5.33×10^5 kg
Density	[ρ]	2664.3 kg/m^3	1	2664.3 kg/m^3
Velocity	[L][T]$^{-1}$	50 mm/s	1	50 mm/s
Acceleration	[L][T]$^{-2}$	9.81 mm/s^2	1	9.81 m/s^2
Youngs Modulus	[ρ][L]^2[T]$^{-2}$	4×10^7	1	4×10^7
Force	[ρ][L]^4[T]$^{-2}$	F	25^2	625F

Table 4.6: Selected physical quantities, symbols, dimensions and scale factors scaling method 3

Froude Principle (Scaling method 4)

Despite Model 3's incorporation of real-world gravitational acceleration ($g = 9.81$ m/s^2), the mere inclusion of gravity does not guarantee dimensional similarity across scales. This gap in scaling compliance is addressed through the implementation of Froude scaling principles, which provide a systematic framework for maintaining dynamic similarity between reference and scaled simulations. The application of Froude scaling ensures that the relative magnitudes of inertial and gravitational forces remain consistent across different geometric scales, thus preserving the essential dynamics of the system. Froude scaling is a dimensional analysis technique used in DEM simulations to maintain dynamic similarity between scaled systems [40]. The Froude number (Fr) represents the ratio of inertial forces to gravitational forces:

$$Fr = \frac{v}{\sqrt{gL}} \tag{4.1}$$

where:

- v is velocity
- g is gravitational acceleration
- L is characteristic length

The reference model, with dimensions of 500 mm and an operational velocity of 50 mm/s under standard gravity ($g = 9.81$ m/s^2), was scaled up by a factor (λ) of 25 using Froude scaling principles. According to Froude scaling laws, while lengths scale directly with λ, velocities scale with the square root of λ. Consequently, the scaled-up velocity (v_2) can be calculated as:

$$v_2 = v_1\sqrt{\lambda} = 50 \text{ mm/s} \times \sqrt{25} = 250 \text{ mm/s} \tag{4.2}$$

The temporal scaling factor follows the same square root relationship, where:

$$t_2 = t_1\sqrt{\lambda} = t_1 \times \sqrt{25} = 5t_1 \tag{4.3}$$

Thus, the time scale in the scaled-up system is 5 times longer than in the reference model, maintaining dynamic similarity between the two systems while preserving the Froude number across scales. However, a significant consequence of implementing Froude scaling, when time is scaled by a factor of $\sqrt{h}$, it impacts Young's modulus of the material. Through dimensional analysis of the basic physical quantities, it was determined that the Young's modulus scales linearly with the scaling factor h. The Young's modulus must scale proportionally with factor of 25 to preserve the system's dynamic behavior. This scaling relationship has significant implications for material behavior in the scaled simulation, particularly in how it affects contact interactions and force transmission between particles.

The implementation of Froude scaling demonstrates that the time parameter must be scaled by a factor of 5, allowing the preservation of real-world gravitational conditions while maintaining compliance with dimensional scaling laws. This scaling approach ensures dynamic similarity between the reference and scaled models. Table 4.7 presents the basic quantities derived for the scaled model, illustrating the application of the Froude scaling principles to the fundamental parameters. The preservation of gravitational acceleration (g) across scales, coupled with the systematic scaling of other parameters, ensures that the dynamic behavior of the system remains consistent between the reference and scaled models. This preservation of gravitational conditions necessitates an increase in the Young's modulus of the rock material proportional to the scaling factor (in this case, 25). Consequently, the forces acting within the scaled model are magnified by the cube of the scaling factor. This cubic relationship arises from the interplay between the scaled dimensions and the preserved gravitational acceleration, leading to a significant amplification of forces within the scaled system. This scaling method provides a robust foundation for extending simulation results to full-scale applications.

Quantity name	**Dimensions**	**Reference value**	**Scale factor**	**Scaled value**
Width of the domain	[L]	1400 mm	25	35 m
Length of the monopile	[L]	500 mm	25	12.5 m
Outer diameter of monopile	[L]	323.9 mm	25	8.1 m
Thickness of monopile	[L]	8.8 mm	25	220 mm
Displacement	[L]	300 mm	25	7.5 m
Size of the rocks	[L]	25 mm - 35 mm	25	0.575 m - 0.875 m
Time	[T]	6 s	$\sqrt{25}$	30 s
Mass of the rocks	[M]	1835 kg	25^3	2.86×10^7 kg
Mass of the monopile	[M]	34.12 kg	25^3	5.33×10^5 kg
Density	[ρ]	2664.3 kg/m^3	1	2664.3 kg/m^3
Velocity	[L][T]$^{-1}$	50 mm/s	$\sqrt{25}$	250 mm/s
Acceleration	[L][T]$^{-2}$	9.81 m/s^2	1	9.81 m/s^2
Youngs Modulus	[ρ][L]^2[T]$^{-2}$	4×10^7	25	1×10^9
Force	[ρ][L]^4[T]$^{-2}$	F	25^3	15,625F

Table 4.7: Selected physical quantities, symbols, dimensions and scale factors scaling method 4

Our current numerical model domain incorporated a rock bed height of 25 meters for simu-

lation purposes, this significantly exceeds typical scour protection thicknesses implemented in the field. The thickness of scour protection typically follows a multi-layered approach, consisting of a filter layer and an armor layer. We calculated the thickness of the scour armour layer to be 3.5m, which is 4 times the median stone diameter. This is further supported by [76], that typical scour protection thicknesses in operational wind farms range from 1m to 2m. The Horns Rev 1 offshore wind farm, a well-documented case study, implements a scour protection system with a total thickness of 1.8m, comprising a 0.6m filter layer and 1.2m armor layer [77].

The implementation of a realistic scour protection system in our numerical model requires a total thickness of 3.5m for the armor layer, following industry standards discussed in the previous section. The volume of the remaining domain must be filled with sand particles to accurately represent the conditions of the seabed. However, it takes approximately 100 trillion sand particles to fill the current domain size with particles of natural sand dimensions.

Given the computational limitations of current hardware resources, simulating such a vast number of individual particles is impractical. The computational cost would be prohibitive in terms of both memory requirements and processing time. To address this limitation while maintaining the physical relevance of our simulation, a coarse-graining technique will be implemented to upscale the particle size.

4.3. Coarse grain

The coarse grain method in DEM is a technique used to speed up simulations of large systems of particles. In traditional DEM, each individual particle is modeled and tracked separately, which can be computationally expensive for very large systems. The coarse-grain method addresses this by grouping multiple original particles into single, larger, "coarse grained" particles [78]. These coarse particles have their properties (such as size, mass, etc.) adjusted to represent the collective behavior of the original particles they replace. This significantly reduces the number of particles in the simulation, leading to faster computation times.

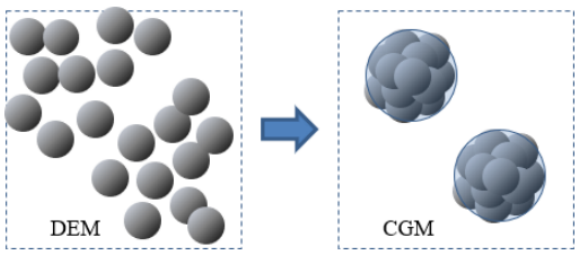

Figure 4.2: Concept of DEM-CGM: original particles (left), equivalent coarse grains (right) [79]

The relationship between the original particle diameter (d_p) and the coarse-grained particle diameter (d_g) is typically expressed as

$$d_g = NPG^{\frac{1}{3}} \cdot d_p \tag{4.4}$$

* NPG = number of particles per grain

The scale factor, which determines the size ratio between the original particles and the scaled particles, is a crucial parameter in this process. However, there is no universally applicable "maximum" scale factor. The optimal choice depends on a balance between accuracy requirements and computational constraints and is heavily influenced by factors such as material properties, flow behavior, and the specific goals of the simulation. For example, while simpler granular flows might allow for larger-scale factors (e.g., 10 or higher), complex materials with cohesive or plastic behavior often necessitate smaller factors (e.g., 2-5) to accurately capture their behavior [78, 80].

It is crucial to validate the coarse-grained model against experimental data or original scale simulations to ensure that the chosen scale factor adequately represents the physics of the system. This validation process helps determine the acceptable level of accuracy compromise for the particle in computational efficiency. Researchers have explored various scale factors in different applications, with studies on cohesive materials often employing smaller factors to preserve bulk behavior, while simulations of silo flow with simpler materials have successfully utilized larger factors [81]. To investigate the upper bounds of particle scaling, two distinct simulation series were designed and executed. Table 4.8 shows the details of the simulations modeled to explore the coarse-grain technique. The first series employed direct upscaling of particles while maintaining the original interaction parameters constant. The second series implemented a coarse grain technique, where particle upscaling was accompanied by a systematic modification of the particle interaction properties to preserve the bulk mechanical response. Through comparative analysis of these simulation sets, the maximum permissible scale factor that maintains the fidelity of the granular system's behavior could be determined.

Table 4.8: Contact parameters at different coarse grain factors

Parameter	**Base Case**	**SF 2**	**SF 3**	**SF 4**	**SF 5**	**SF 10**	**SF 15**	**SF 20**	**SF 30**
Particle Size (mm)	0.6	1.2	1.8	2.4	3.0	6	9	12	18
Shear Modulus (Pa)	4×10^7	2×10^7	1.33×10^7	1×10^7	8×10^6	4×10^6	2.6×10^6	2×10^6	1.3×10^6
Static Friction Coef.	0.7	0.35	0.233	0.175	0.14	0.07	0.046	0.035	0.023
Rolling Friction Coef.	0.05	0.025	0.0167	0.0125	0.01	0.005	0.0033	0.0025	0.0016

*Notes: SF = scale factor

In the scaled parameters simulations, shear modulus, static friction coefficient, and rolling friction coefficient were scaled down by the respective scale factors. Common parameters across all simulations: Penetration velocity: 1 mm/s, Particle properties: Poisson's ratio: 0.27, Density: 2100 kg/mş, Coefficient of restitution: 0.3

Despite using the coarse grain scaling approach to a factor of 20, which significantly reduced the computational demands for the scour protection layer, simulation of the complete domain with realistic sand particles remains computationally prohibitive. Calculations indicate that approximately 180 billion particles would still be required to represent the sand bed portion of the domain with a particle size of 12 mm, far exceeding current computational capabilities. To address this limitation while maintaining physical relevance, a modified approach was developed in which the upscaled simulation model was rescaled to match the dimensions of the reference model. In this configuration, the thickness of the scour protection layer was translated to 140 mm, and the rest of the domain is filled with coarse-grained rock particles. This hybrid approach aims to balance computational feasibility with physical accuracy, particularly in the critical scour protection zone where particle-monopile interactions are most significant.

4.4. Hybrid scaling

The hybrid scaling approach in the DEM represents an advanced computational strategy that synthesizes multiple scaling techniques to optimize computational efficiency while preserving the fidelity of large-scale particle system simulations [82].

Mohajeri et al. used coarse grain and geometric scaling together in hybrid scaling. In the particle scaling phase, the approach implements systematic particle size enlargement coupled with a corresponding reduction in particle population, adhering to established scaling laws to maintain bulk behavioral characteristics [82]. This is followed by geometric scaling of the system boundaries and equipment dimensions, enabling the simulation of industrial-scale processes. A distinguishing feature of hybrid scaling is its ability to accommodate complex material behaviors, particularly in cohesive and elastoplastic bulk solids. The methodology allows independent scaling factors for particle properties and geometric dimensions, offering enhanced flexibility compared to traditional scaling approaches. This adaptability facilitates the preservation of critical material behaviors while achieving substantial gains in computational efficiency. The validation protocol typically encompasses comparative analyses between scaled simulations and laboratory-scale experiments or fully resolved numerical simulations. This methodology can be integrated with both bulk and in situ calibration methodologies, potentially enabling parameter calibration independent of process configuration.

The hybrid scaling approach developed in this research represents a novel combination of exact scaling and coarse grain methodologies to effectively simulate monopile penetration through scour armour layer. This approach strategically applies different scaling techniques to distinct regions of the simulation domain based on their physical significance and computational demands. In the critical scour armor layer, where accurate representation of particle-monopile interaction is essential, exact scaling principles are implemented. This preserves the fundamental physics of penetration mechanics while the system can calculate and capture the behavior of full scale system . The exact scaling component maintains geometric similarity and force relationships through careful consideration of dimensionless parameters and scaling laws derived from basic physical quantities. Simultaneously, the underlying sand bed, which primarily serves as a supporting medium, is modeled using coarse grain methodology. This approach systematically increases particle size while adjusting interaction parameters to maintain bulk mechanical behavior. The coarse-graining of the sand layer significantly reduces the number of particles required for simulation while preserving the essential characteristics of the granular medium's response to loading. The integration of these two scaling methodologies creates a computationally efficient framework that maintains physical accuracy. Figure 4.3 shows conceptual design of hybrid scaling in EDEM.

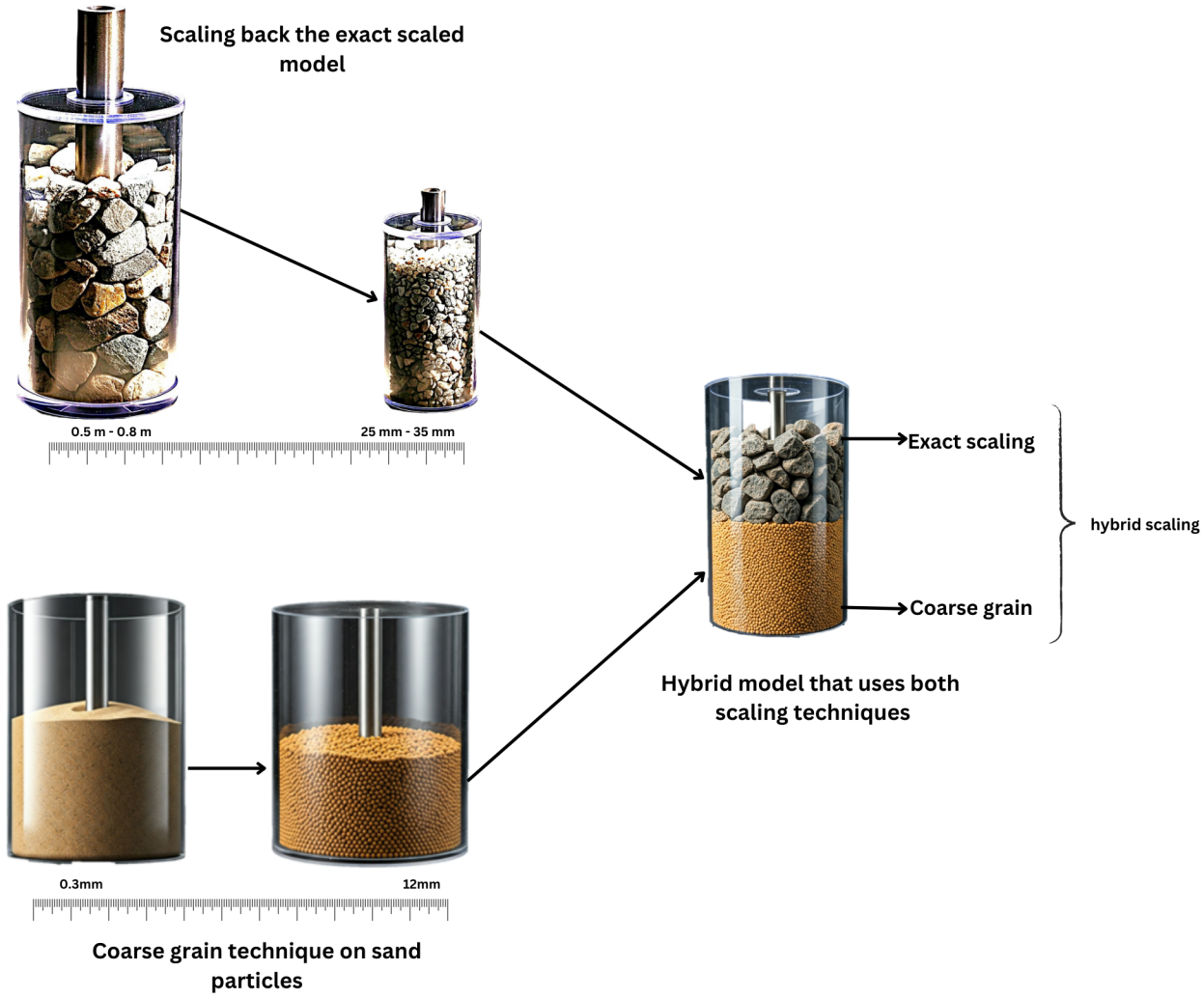

Figure 4.3: Conceptual design of hybrid scaling.
The figures are generated using AI, Google Imagen 3

This hybrid approach enables the simulation of industrial-scale monopile installations through scour armour layers while managing computational resources effectively. The methodology preserves the detailed particle-scale interactions in the scour armor layer where they significantly influence penetration resistance, while efficiently representing the mechanical response of the deeper sand layers where bulk behavior is the primary concern. This innovative combination of scaling techniques demonstrates how strategic application of different scaling methodologies can overcome the computational limitations typically associated with large-scale DEM simulations while maintaining physical fidelity in critical regions of the model.

To validate the hybrid scaling approach, three different simulation configurations were implemented, each employing different coarse-grain scaling factors for the sand particles while maintaining identical scour protection layer properties. The first and second configurations used sand particles scaled by a factors of 10 and 15, resulting in a particle diameter of 6 mm and 9 mm, the final configuration employed a more moderate scaling factor of 20, yield-

ing particles of 12 mm diameter. Table 4.9 depicts the simulation settings of three different configurations of hybrid scaling.

Parameter	**Scour Protection Layer**	**Underlying Sand Layer**		
	Exact Scaling (Scaling method 4)	**Coarse Grain**		
Scale Factor	1	20	15	10
Particle Size Range	25 mm - 35 mm	12 mm	9 mm	6 mm
Layer height	145 mm		800 mm	
Velocity	50 mm/s			
Gravitational Acceleration	9.8 m/s^2			
Shear modulus	4×10^7 Pa	2×10^6	2.6×10^6	4×10^6
Static friction Coef.	0.64	0.035	0.046	0.07
Rolling friction Coef.	0.1	0.0025	0.0033	0.005
Number of Particles	∼8500	∼617000	∼1.4 million	∼5 million

Table 4.9: Configuration of hybrid scaling simulations

This systematic variation in particle size scaling was designed to evaluate the sensitivity of the simulation results to the degree of coarse-graining applied to the sand particles. This validation approach enables a more comprehensive understanding of the capabilities and limitations of the hybrid scaling methodology, providing crucial guidance for future applications in similar geotechnical scenarios.

4.5. Conclusion

This chapter has established a comprehensive framework for scaling DEM simulations of monopile penetration through scour protection layers. Through careful theoretical analysis and systematic development, three distinct scaling approaches have been formulated to address the computational challenges of full-scale simulations while maintaining physical accuracy.

The exact scaling methodology was developed with four variant models, each addressing different aspects of scaling:

- Scaling method 1 maintains constant velocity while reducing gravitational acceleration
- Scaling method 2 preserves time while scaling velocity and gravity
- Scaling method 3 attempts to maintain real-world gravitational conditions but lacks theoretical foundation in terms of dimensional scaling laws, limiting its applicability for systematic scaling
- Scaling method 4 implements Froude scaling principles, providing a theoretically sound framework that both preserves real-world gravitational conditions and follows dimensional scaling laws derived from basic physical quantities

Among these, scaling method 4 emerged as the most promising approach for real-world applications. While scaling method 3 attempted to preserve gravitational conditions, Model 4's implementation of Froude scaling principles provides a more robust solution by simultaneously maintaining gravitational conditions and ensuring proper dimensional scaling relationships.

This theoretical foundation enables Model 4 to accurately simulate full-scale monopile installations while preserving both gravitational effects and dynamic similarity. The scaling factor of 25 allows the reference model to be scaled up to dimensions representative of modern offshore wind turbine foundations, with the monopile diameter increasing from 323.9 mm to 8097.5 mm, while maintaining proper physical relationships between all system parameters.

The coarse-grain approach was formulated to address the specific challenges of simulating the granular medium, particularly the sand layer beneath the scour protection. This methodology enables systematic upscaling of particle sizes while preserving bulk behavioral characteristics through appropriate scaling of interaction parameters. Through careful consideration of particle size distribution and contact mechanics, this approach significantly reduces computational demands while maintaining the essential granular physics of the system.

A hybrid scaling strategy was also developed, synthesizing elements of both exact scaling and coarse graining approaches. This novel approach aims to optimize computational efficiency while maintaining accuracy. By applying exact scaling to the scour protection layer while utilizing coarse graining for the underlying sand bed, this method provides a practical solution for simulating complete installation scenarios.

Addressing research question 3, "What kind of scaling technique and scaling laws can be used specifically to upscale the simulation of monopile penetration in DEM?", this chapter demonstrates that a combination of scaling approaches is most effective:

- Exact scaling (scaling method 4) with Froude similarity principles enables accurate representation of monopile-rock interaction at full scale, preserving both gravitational and dynamic effects
- Coarse graining allows for efficient simulation of large sand volumes by upscaling particle size while maintaining bulk behavior
- Hybrid scaling combines these approaches to create computationally feasible simulations that accurately represent both the scour protection layer and underlying sand bed

The theoretical framework established in this chapter provides a foundation for the systematic evaluation of these scaling approaches, which will be validated through numerical simulations and analyzed in Chapter 5. Particular attention has been paid to ensuring that each scaling methodology preserves the essential physics of monopile-rock interaction while offering practical advantages for industrial-scale simulations. This comprehensive approach to scaling methodologies addresses the fundamental research question regarding optimal scaling techniques for representing real-field scenarios, while establishing clear criteria for evaluating their effectiveness in subsequent numerical investigations.

5

Results and Discussions

The preceding chapters established both the theoretical study for scaling DEM simulations and the robust numerical methodology for simulating monopile penetration through scour armour layer. This chapter presents and analyzes the results obtained from implementing three distinct scaling approaches: exact scaling, coarse grain scaling, and hybrid scaling. Our analysis focuses on two key performance indicators (KPIs) identified in Chapter 3: penetration resistance and penetration work. These KPIs provide quantitative measures for evaluating the effectiveness of each scaling technique in preserving the essential physics of monopile-rock interaction while reducing computational demands. For each scaling approach, we examine:

- The accuracy of the scaled simulations compared to the reference model
- The computational efficiency gains achieved
- The practical limitations and implementation challenges encountered

The results are organized into three main sections, corresponding to each scaling technique. In each section, we first present the quantitative results, followed by a detailed discussion of the physical mechanisms and computational aspects. Special attention is paid to the trade-offs between computational efficiency and physical accuracy, as these considerations are crucial for the practical application of these techniques in industrial-scale simulations. This systematic analysis aims to identify the most suitable scaling approach for simulating monopile penetration through scour protection layers, ultimately addressing our primary research question regarding the optimal scaling technique for representing real-field scenarios.

5.1. Exact Scaling

The exact scaling approach, as detailed in Chapter 4, aims to preserve the fundamental physics of monopile-rock interaction while scaling up the system dimensions to match real-world installations. This section presents the results from four distinct exact scaling methods, each employing different scaling strategies to address specific aspects of the monopile penetration process. Table 5.1 highlight the key differences among the four methods we used in

Exact scaling.

Parameter	Scaling method 1	Scaling method 2	Scaling method 3	Scaling method 4
Gravity (m/s^2)	0.39	245.25	9.81	9.81
Velocity (mm/s)	50	1250	50	250
Time (s)	150	6	150	30
Force	25^2F	25^4F	25^2F	25^3F
Young's Modulus (Pa)	4×10^7	2.5×10^9	4×10^7	1×10^9
Stability	Stable	Unstable	Stable	Stable
Run time	2.4 hrs	-	2.4 hrs	1.67 hrs

Table 5.1: Comparison of Exact Scaling Methods for Monopile Penetration Simulation

By comparing these four methods, we aim to identify which exact scaling strategy best balances the competing demands of physical accuracy and computational feasibility for large-scale monopile installations.

5.1.1. Scaling method 1

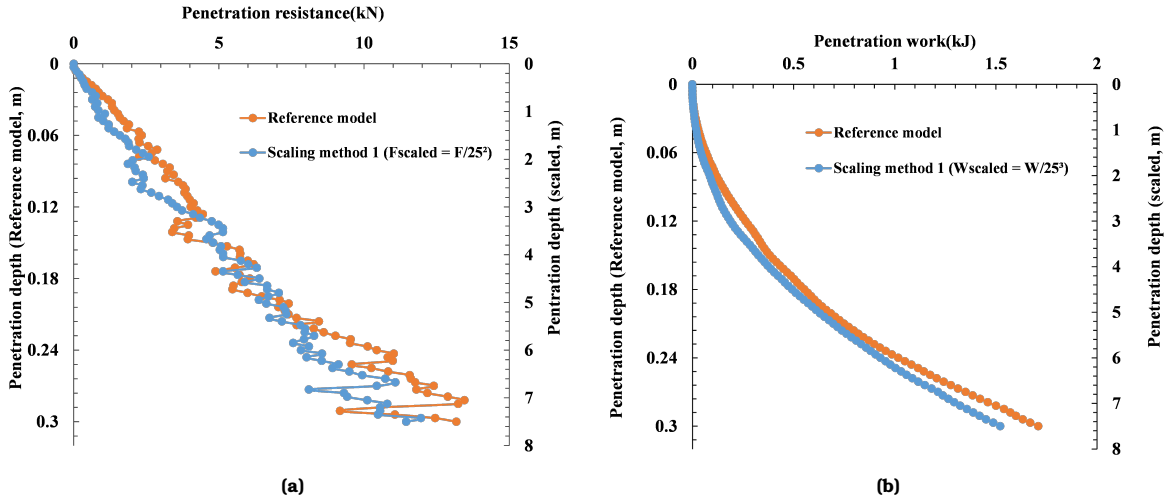

Figure 5.1: Results of scaling method 1 exact scaling simulation (scale factor = 25) compared to reference model: (a) Penetration resistance versus depth, and (b) Penetration work versus depth.

Scaling method 1 implements an exact scaling approach where gravitational acceleration is reduced by the scaling factor while maintaining constant velocity. Figure 5.1a compares the penetration resistance between the scaled model and the reference model across the penetration depth. A particularly significant finding is that the resistance values of the scaled model align with the theoretically predicted scaling factor of 25^2 (calculated as the square of the geometric scaling factor of 25), derived from the dimensional analysis of basic physical quantities as detailed in Chapter 4. This quantitative agreement validates the scaling laws developed for this method and demonstrates the predictive power of exact scaling in preserving force relationships across different scales. The scaled model shows good agreement with the reference model, particularly in capturing the overall trend of increasing resistance with depth.

The total work done during penetration, shown in figure 5.1b, demonstrates excellent agreement between the scaled and reference models. This strong correlation supports the the-

oretical basis of our scaling approach and confirms that the energy requirements of the penetration process are accurately preserved despite the reduced gravitational conditions. The success of Scaling method 1 can be attributed to its fundamental approach of maintaining constant velocity while reducing gravitational acceleration. This strategy preserves the quasi-static nature of the penetration process while allowing for the simulation of small scale systems at larger scale. The reduction in gravitational acceleration effectively compensates for the increased particle sizes and system dimensions, enabling the scaled model to reproduce the mechanical behavior observed in the reference model. However, it is important to note that this scaling approach introduces certain physical limitations. The reduced gravity environment creates conditions that deviate from real-world installations. This deviation becomes particularly relevant when considering strongly gravity-dependent phenomena, such as particle settling and void formation during penetration.

Despite these limitations, Scaling method 1 verified the scaling laws associated with the scaling technique. The quantitative agreement with theoretical scaling predictions makes it a reliable tool for preliminary design studies of monopile installations.

5.1.2. Scaling method 2

This method explores an alternative exact scaling approach where time remains unscaled, leading to direct scaling of velocity and acceleration parameters. This approach, while theoretically sound, revealed significant practical limitations in implementation due to software constraints and physical instabilities. During the simulation design phase, it was observed that the EDEM software encountered limitations in accommodating the intended acceleration input value due to its abnormally large magnitude. Consequently, the value was reduced by half to 122625 mm/s^2. Despite this adjustment, the simulation exhibited instability, with particles being ejected from the system as they attempted to settle. This behavior underscores the challenges associated with simulating systems under such extreme acceleration conditions.

Even with this reduced acceleration value, the simulation exhibited severe instability. The primary manifestation of this instability was the ejection of particles from the simulation domain during the particle settling phase, prior to the commencement of monopile penetration. This behavior can be attributed to several factors:

- Excessive Inertial Forces: The scaled acceleration values, even at half the theoretical requirement, generated inertial forces that overwhelmed the inter-particle contact forces, leading to unrealistic particle behavior.
- Numerical Integration Issues: The combination of high velocities and accelerations created challenges for the numerical integration schemes employed by the DEM solver, potentially introducing cumulative errors in particle position and velocity calculations.
- Contact Model Limitations: The standard Hertz-Mindlin contact model, while suitable for the reference simulation, may not adequately capture particle interactions under such extreme dynamic conditions.

The particle ejection phenomenon made it impossible to establish a stable initial configuration, which is crucial for meaningful penetration analysis. This fundamental instability

prevented the collection of reliable data for penetration resistance and work done.

These findings highlight a critical limitation in the practical application of exact scaling when time remains unscaled. The resulting acceleration requirements can exceed both software capabilities and the physical validity range of standard DEM contact models. These results suggest that while scaling method 2's scaling approach is mathematically valid, its practical implementation is not possible for both numerical and real-life environment. For large-scale monopile simulations, alternative scaling strategies that avoid extreme intertial/body forces may be more appropriate.

5.1.3. Scaling method 3

Scaling method 3 attempted to maintain real-world gravitational conditions while scaling the system dimensions. The results, presented in Figure 5.2, demonstrate significant limitations of this approach compared to the reference model, it fails to capture the theoretical value calculated using dimensional analysis.

Figure 5.2a illustrates the penetration resistance versus penetration depth for both the scaled and reference models. A stark disparity is evident between the two responses. Although the reference model exhibits a gradual increase in penetration resistance with depth, the scaled model shows dramatically higher resistance values than a factor of 25^2. This deviation from expected behavior suggests fundamental inconsistencies in the scaling methodology. Although higher penetration resistance and work are expected in the scaled model when compared to the Scaling method 1 as it acts under real-world gravitational conditions instead of altered. The inconsistencies in the scaling laws makes it impossible to verify the results.

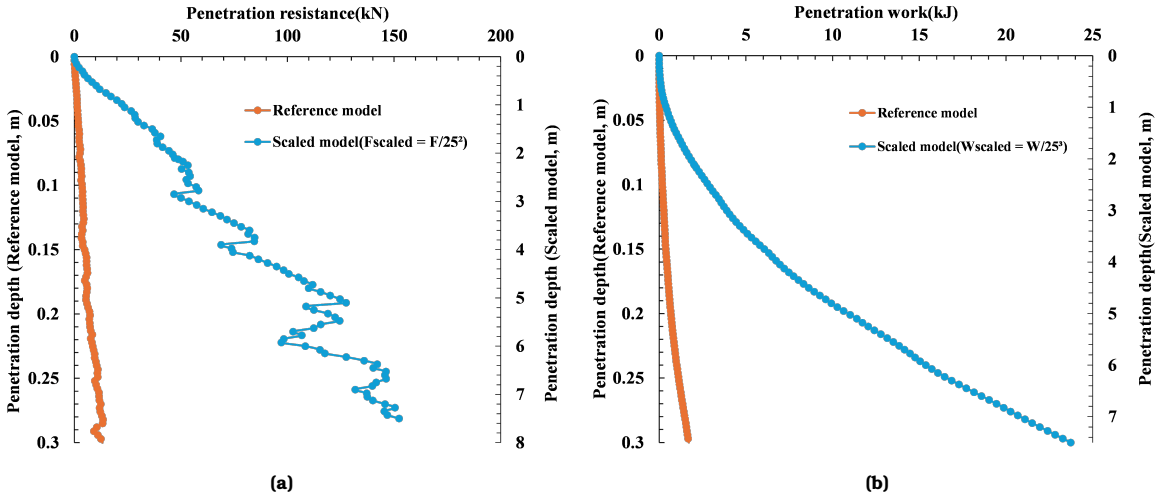

Figure 5.2: Results of Scaling method 3 DEM simulations (scale factor = 25) compared to reference model: (a) Penetration resistance versus depth, and (b) Penetration work versus depth.

The penetration work versus depth relationship, shown in Figure 5.2b, further highlights the limitations of Scaling method 3. The scaled model, with work values scaled by 25^3, demonstrates a markedly different energy accumulation pattern compared to the reference model. This divergence suggests that the preservation of gravitational acceleration alone, without proper consideration of dimensional scaling laws, leads to results that cannot be verified

theoretically.

The key deficiency in Scaling method 3 becomes apparent through its parameter selection. Although the model maintains gravitational acceleration at 9.81 m/s^2 and geometric scaling (domain dimensions from 1400 mm to 35 m, monopile diameter from 323.9 mm to 8.1 mm), it fails to establish proper relationships between the velocity, time, and force parameters. The over prediction of penetration resistance of the scaled model, characterized by sharp fluctuations and unrealistic force magnitudes, indicates that the particle-particle and particle-monopile interactions are not being properly scaled. These inconsistencies can be attributed to the failure of scaling method 3 to adhere to fundamental dimensional scaling laws, which are essential to maintain physical similarity across different scales.

The results of scaling method 3 underscore the importance of employing a theoretically sound scaling approach that considers all relevant physical quantities and their interrelationships. The model's inability to accurately predict penetration resistance and work demonstrates that preserving gravitational conditions alone is insufficient for reliable scaling of DEM simulations. This limitation makes Model 3 unsuitable for practical applications in monopile installation modeling

5.1.4. Scaling method 4

Scaling method 4 implemented Froude scaling principles to maintain dynamic similarity between the scaled and reference models. The results, shown in Figure 5.3, demonstrate the effectiveness of the scaling approach.

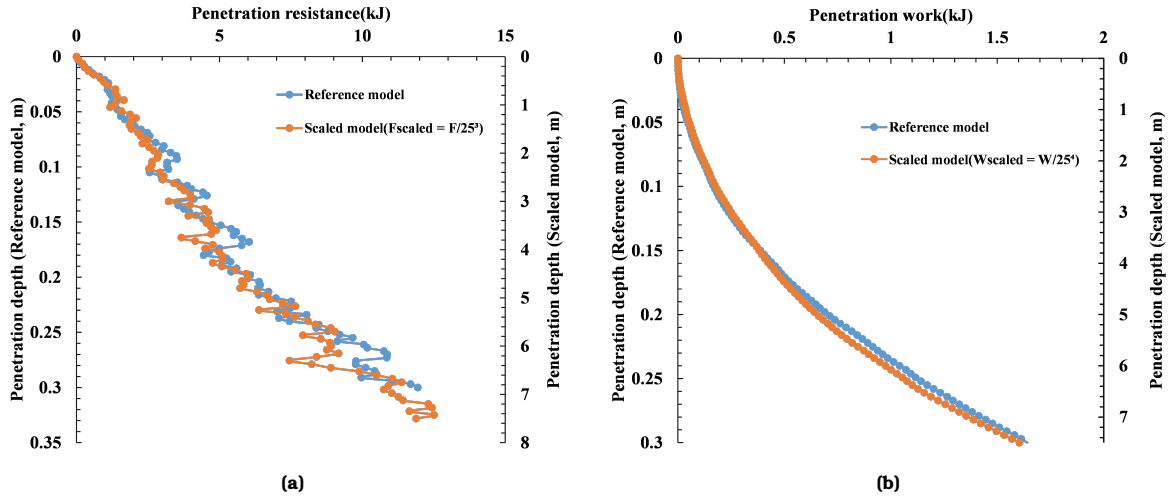

Figure 5.3: Results of scaling method 4 DEM simulation (scale factor = 25) compared to reference model: (a) Penetration resistance versus depth, and (b) Penetration work versus depth.

Figure 5.3a presents the penetration resistance versus penetration depth for both the scaled model (scaled by a factor of 25) and the reference model. The results show good agreement with the overall trend, and both models exhibit similar patterns of resistance increase with depth. The scaled model, following the scaling laws derived from the preservation of the Froude number ($Fr = \frac{v}{\sqrt{gL}}$), maintains physical similarity while adjusting the dimensions of the system. The penetration work versus depth relationship, illustrated in Figure 5.3b, shows

a particularly strong correlation between the scaled and reference models. This agreement validates the theoretical basis of the Froude scaling approach, confirming that the energy requirements of the penetration process are accurately preserved across scales. The implementation of Froude scaling led to specific parameter adjustments as detailed in Table 4.7:

- Geometric parameters were scaled by a factor of 25 (domain dimensions: 35000 mm, monopile length: 12500 mm)
- Time was scaled by $\sqrt{25}$, resulting in a 30s penetration duration
- Velocity was scaled by $\sqrt{25}$, yielding 250 mm/s
- Acceleration remained constant at 9810 mm/s^2, to maintain real-world gravitational conditions
- Young's modulus was scaled by a factor of 25, increasing from 4×10^7 to 1×10^9
- The penetration resistance was scaled by 25^3

The results demonstrate that this approach successfully maintains both static and dynamic similarity while operating under realistic gravitational conditions. The successful implementation of the preservation of the Froude number in Scaling method 4 provides a robust framework for scaling up laboratory-scale DEM simulations to industrial-scale applications while maintaining physical realism. This approach offers particular advantages for modeling monopile installation in scour protection layers, where both gravitational and inertial effects play crucial roles in system behavior.

5.2. Coarse Grain

The coarse grain approach was investigated using scaling factors ranging from 1 to 30, with results presented in Figures 5.4 and 5.5. This methodology aims to reduce computational demands by scaling up the particle size ($d_g = NPG^{1/3} \cdot d_p$) while preserving bulk behavior through appropriate scaling of particle properties and interaction parameters.

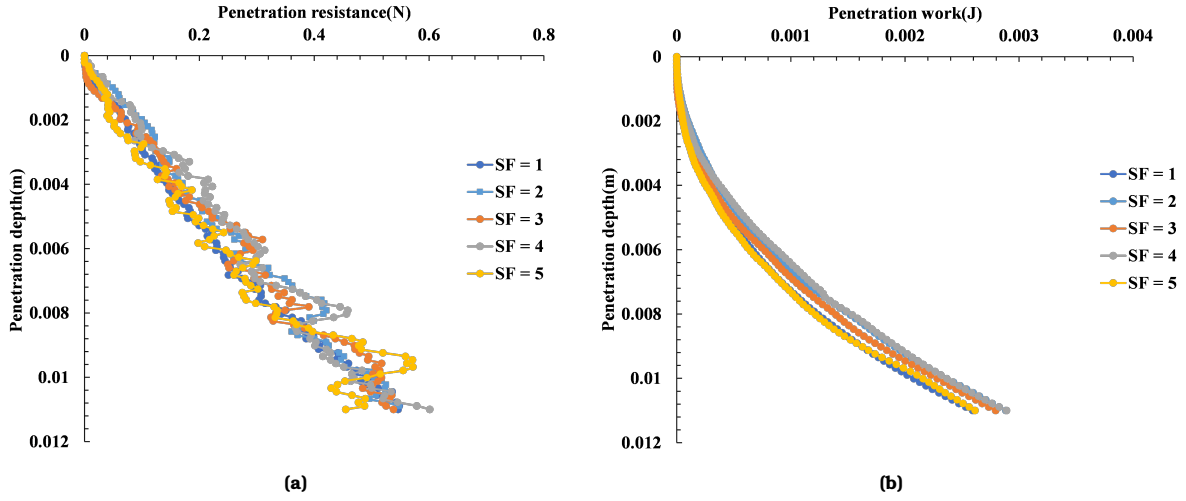

Figure 5.4: Results of coarse grain simulations (scale factor = 1-5: (a) Penetration resistance versus depth (without coarse grain), and (b) Penetration resistance depth (with coarse grain).

Figure 5.4 presents the results of simulations for both penetration resistance (figure 5.4a)

and the total work done (figure 5.4b) with the coarse-grain technique. For scaling factors 2 through 5, the coarse-grained simulations shows good agreement with the base model (scale factor = 1) which is depicted in the figure 5.4.

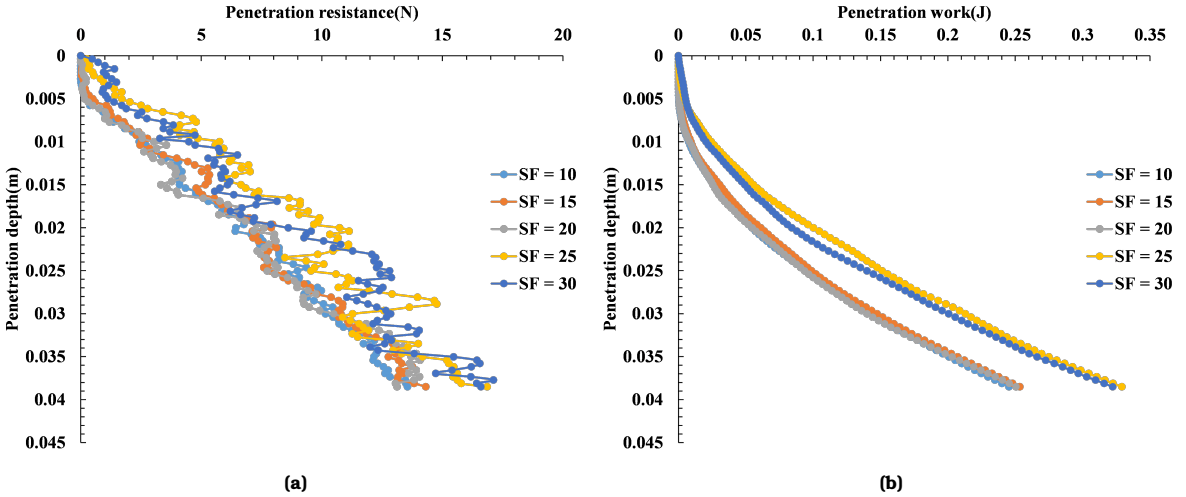

Figure 5.5: Results of coarse grain simulations (scale factor(SF) = 10-30: (a) Penetration work versus depth (without coarse grain), and (b) Penetration work versus depth (with coarse grain).

However, for further scale factors after 5, the "wall effect" phenomenon comes into play in DEM simulations, where the ratio between particle size and domain dimensions becomes critical. With the particle diameter increasing from 0.6 mm in the reference model to 18 mm at scale factor 30, while maintaining the same domain width of 120 mm, the number of particles spanning the domain width reduces significantly. This reduction in the particle-to-domain size ratio leads to artificial boundary effects that influence force transmission patterns within the granular assembly. The particle size-to-domain width size ratio should be atleast 30 as discussed in Section 3.2.2.

To study further scale factors, we scale up the geometry with factor 5 to ensure the particle size-to-domain width ratio is greater than 30. The results from scale factor 10 to 30 were presented in Figure 5.5. Figure 5.5b presents the penetration resistance and figure 5.5b shows the corresponding penetration work done results. The penetration resistance demonstrates consistent behavior for scale factors up to 2, with curves following similar patterns and magnitudes. However, a clear divergence emerges when the scaling factor reaches 25. The penetration work results illustrated in Figure 5.5b corroborate this finding. While the curves remain closely grouped for scale factors up to 20, a noticeable deviation occurs at SF = 25, This transition point at SF = 25 appears to represent a critical threshold where the coarse-grain approach begins to lose its physical accuracy.

However, we cannot compare all the scale factors as there is variation in geometry from factors above 5 which leads to higher penetration resistance. This makes it impossible to compare with the base model (SF = 1), to make this possible we choose stress as KPI (Stress is defined as the force per unit area acting on a material). By comparing the stress values across different scale factors, we can assess whether the coarse grain technique preserves the bulk behavior of the original system. Normalizing results using stress on the geometry as a KPI

provides a clear visualization of how different scaling factors compare across the entire range tested. As shown in the figure 5.6, when the penetration resistance is converted to stress (N/mmš), we observe a compelling pattern that helps validate the coarse-grain's approach limitations.

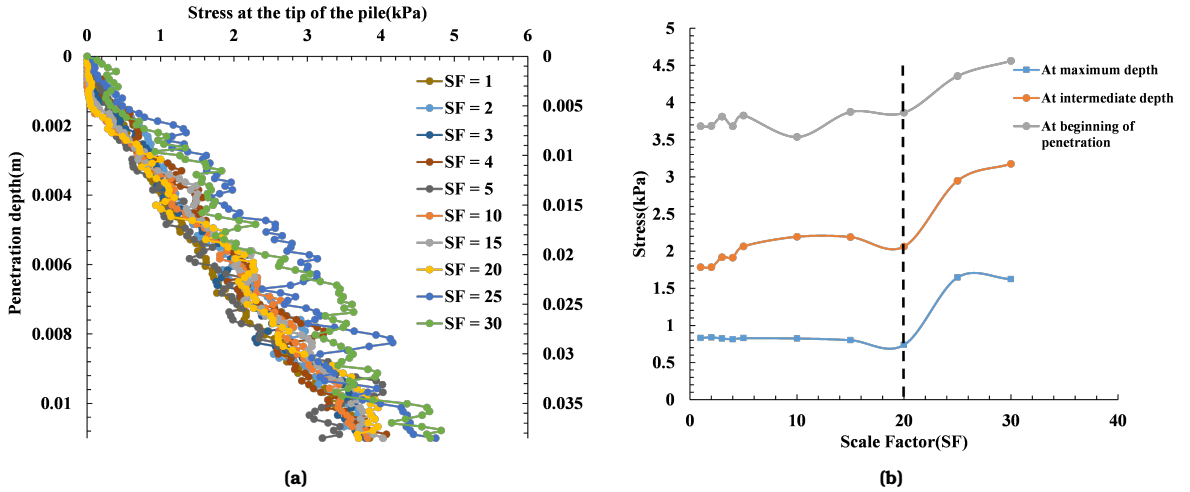

Figure 5.6: Depiction of coarse grain results with stress as KPI: (a) Stress on the geometry vs Penetration depth, and (b) Stress on the geometry at various depths

Figure 5.6a shows the stress curves for scaling factors from 1 to 30 demonstrate remarkably consistent behavior, clustering together throughout the penetration depth. This collapse of the curves onto essentially the same path indicates that the fundamental physics of the penetration process is preserved across this range of scaling factors. The similarity in stress profiles suggests that the force transmission mechanisms and particle-monopile interactions remain physically representative despite the increasing particle sizes. To give more clearer picture of the results we plot stress at three different depth with varying scale factors(figure 5.6b. The key insight is that coarse-graining remains valid up to a critical scale factor between 20 for this system. Beyond that, the abstracted particles no longer behave like the true granular material. The chart makes it easy to see this transition point.

This normalized representation confirms that SF=20 represents the practical upper limit for coarse-graining in this application. The stress-based analysis provides a more definitive validation of this threshold, as it accounts for the geometric effects of scaling and allows for direct comparison across all scaling factors. This finding is particularly valuable for establishing guidelines for future DEM simulations of monopile penetration, as it demonstrates the range within which coarse graining can be reliably applied.

The implementation of scale factor 20 achieved a significant reduction in computational demands (147.5 hrs for scale factor 1 to 0.24 hrs for scale factor 20) while maintaining simulation accuracy. This dramatic improvement in computational efficiency, while still preserving the essential physics of the system up to scale factor 20, represents a practical solution for simulating large-scale monopile installations. The ability to reduce the particle count while maintaining accuracy aligns with the primary goal of coarse-graining: to enable the simulation of industrial-scale systems.

5.3. Hybrid Scaling

The implementation of hybrid scaling, which combines elements of both exact scaling and coarse graining approaches (figure 5.7), demonstrates the penetration mechanics of the monopile through the scour protection layer. Figure 5.8 presents two KPI's - penetration resistance and penetration work - revealing important insights into the effectiveness of this combined scaling approach.

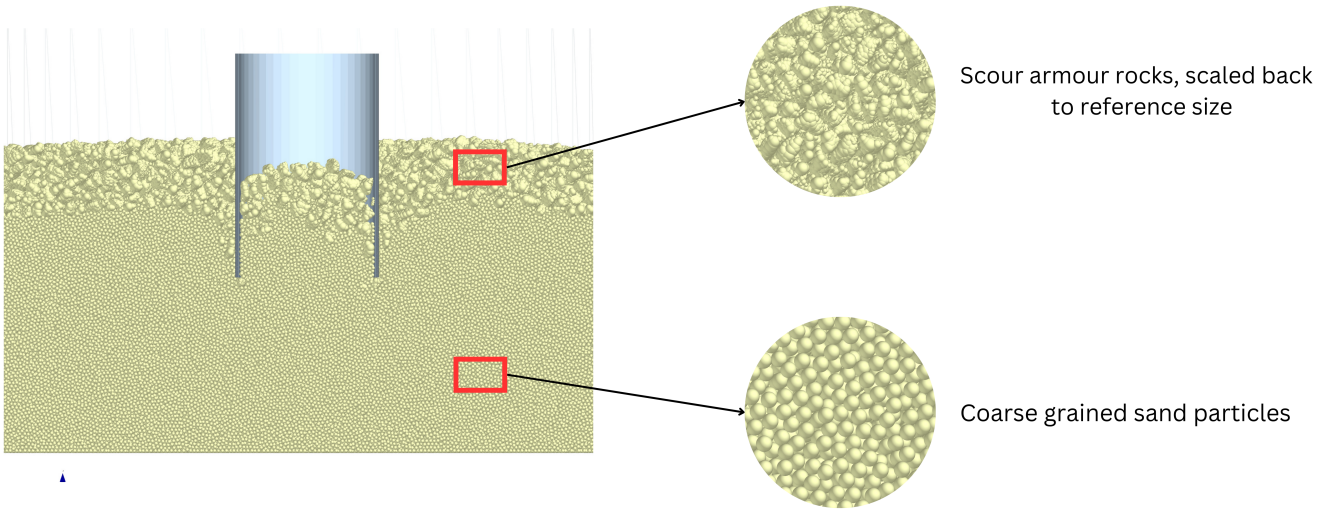

Figure 5.7: Simulation setup of Hybrid scaling

The hybrid scaling simulations reveal distinctive patterns in both penetration resistance and work during monopile installation through the scour protection system. The results can be analyzed in two distinct phases, demarcated by the transition from scour rock interaction to sand bed penetration at approximately 0.15 m depth.
In the initial phase (0-0.15 m), both the penetration resistance and work curves (figure 5.8) demonstrate remarkable agreement between the reference model and hybrid scaled models across all coarse grain factors (CG = 10, 15, and 20). This consistency validates the effectiveness of the hybrid scaling approach in the scour protection zone, where exact scaling principles were applied to the rock layer. The close alignment of results suggests that the fundamental physics of monopile-rock interaction is preserved, regardless of the underlying sand bed's scaling factor.
However, a pronounced deviation emerges beyond 0.15 m depth, characterized by significantly lower penetration resistance (figure 5.8a) in the hybrid models compared to the reference case. This divergence stems from the fundamental difference in domain composition: the hybrid models incorporate a coarse-grained sand bed beneath the scour rocks, while the reference model contains no underlying material but the domain is completely filled with scour rocks. The penetration resistance profiles of the hybrid models show systematically reduced magnitudes, with values approximately 75% lower than the reference model at maximum penetration depth.

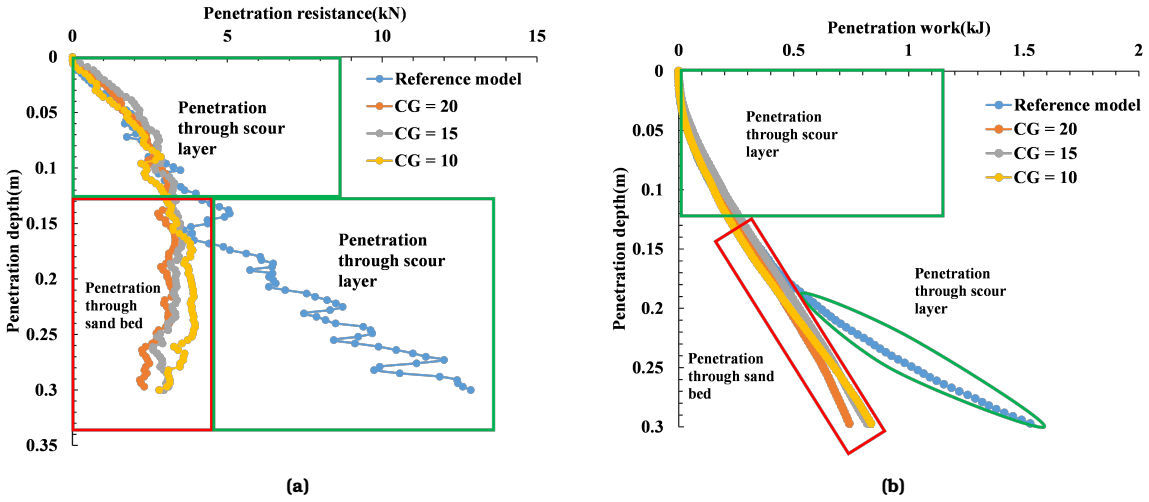

Figure 5.8: Results of hybrid scaling simulations : (a) Penetration resistance versus depth, and (b) Penetration work versus depth.
*NOTES: CG = Coarse grain scale factor

The penetration work results (figure 5.8b) mirror the behavioral pattern of penetration resistance, exhibiting excellent agreement in the scour rock layer followed by marked divergence in the sand bed region as expected because the penetration resistance through sand bed is less than through scour rock layer. The penetration work required for penetration in the hybrid models is substantially less than the reference model. This difference becomes more pronounced with increasing depth, as evidenced by the growing separation between the work curves. Notably, despite these deviations, the hybrid models consistently capture the general trends of both increasing penetration resistance and penetration work with depth at all selected coarse grain factors (CG = 10, 15, and 20).

The computational efficiency of the hybrid scaling approach with CG 15 required approximately 30 hours of computational time, while CG 20 demonstrated improved efficiency, completing the simulation in 15 hours. CG 10, which theoretically have demanded greater computational resources, so I necessitated it with enhanced computational infrastructure, resulting in a processing time of 24 hours. Notably, despite these significant variations in computational demands, all scale factors exhibited remarkably consistent results in terms of penetration resistance and work profiles. This consistency in outcomes, coupled with the substantial reduction in computational time, strongly supports the selection of scale factor 20 as the optimal parameter for coarse graining in hybrid scaling applications. The combination of computational efficiency and maintained accuracy makes this scale factor particularly advantageous for practical implementation. This finding significantly advances the trade-off between computational feasibility and simulation accuracy in DEM modeling of monopile penetration. Achieving reliable results with reduced computational overhead enhances the practical applicability of hybrid scaling methods in engineering applications, particularly in scenarios where computational resources may be constrained.

This balance of computational efficiency and accuracy positions scale factor 20 as the recommended parameter for future hybrid scaling simulations in similar applications, offering a robust solution for modeling complex monopile installation processes. The hybrid scaling approach successfully addresses several key challenges.

- Computational Efficiency: By implementing different scaling strategies for different regions of the domain, the approach achieves a significant reduction in computational demands while maintaining physical accuracy where it matters most.
- Physical Accuracy: The results indicate that the essential physics of the penetration process are preserved, particularly in the critical scour protection layer, where particle-monopile interactions are most significant.

These results validate the theoretical framework developed in Chapter 4, demonstrating that hybrid scaling can effectively bridge the gap between computational feasibility and physical accuracy in simulating monopile installation through scour protection layers. The success of this approach opens new possibilities for simulating larger-scale systems while maintaining the essential physical characteristics of the penetration process.

5.4. Conclusion

This chapter has systematically evaluated the reliability and accuracy of three distinct scaling approaches for DEM simulations of monopile penetration through scour protection layers. Through detailed analysis of penetration resistance and penetration work, each scaling method demonstrated unique strengths and limitations.

The exact scaling approach, particularly scaling method 4 that implements the Froude scaling principles, proved to be highly reliable in maintaining physical similarity while scaling the dimensions of the system. The preservation of both gravitational conditions and dynamic similarity through the Froude number matching resulted in consistent force relationships and energy requirements across scales. This approach successfully scaled the reference model (323.9 mm diameter) to full-scale dimensions (8097.5 mm diameter) while maintaining the essential physics of the penetration process.

The coarse grain approach demonstrated an effective reduction in computational demands up to a scale factor of 20, beyond which accuracy began to deteriorate. Key findings include:

- Reliable results for scale factors 1-20 with proper parameter scaling
- Significant reduction in computational time (147.5 hrs for scale factor 1 to 0.24 hrs for scale factor 20)
- Clear upper limit at scale factor 20, regardless of domain size adjustments

The hybrid scaling strategy successfully developed a two-layer simulation (sand layer at bottom and scour layer in top) by combining the advantages of both approaches, offering:

- High accuracy in the critical scour protection layer through exact scaling
- Computational efficiency through selective application of coarse-graining
- Practical feasibility for industrial-scale simulations

Limitations

- The study focuses primarily on the penetration phase of monopile installation, excluding other critical phases such as self-penetration and hammering.

- The research does not include experimental validation of the scaled models, which would further strengthen the reliability and applicability of the findings.
- The current model has limitations in simulating the behavior of the sand bed beneath the scour layer in larger domains, which presents a challenge for future investigations.

Assumptions

- The study assumes quasi-static penetration conditions, which may not fully capture the dynamic effects during monopile penetration.
- The simulations do not account for the effects of water-particle coupling, which could influence the penetration resistance in certain scenarios. For the application of quasi-static penetration of pile through the scour protection layer, no geotechnical concerns are predicted concerning the instabilities of the scour protection due to the particle-fluid interaction.
- The research focuses primarily on as scour rock armour layer, neglecting the filter layer as scour layer is primarily composed with armor layer.

Addressing research question 4, *How reliable and accurate are the scaled DEM simulations ?* This study demonstrates that scaled DEM simulations can achieve high reliability and accuracy when:

- Appropriate scaling techniques are selected on the basis of specific simulation requirements.
- Proper scaling laws are applied with careful consideration of physical principles.
- Scaling limits are respected (particularly for coarse-graining).

The validation through penetration resistance and work measurements confirms that these scaling approaches can reliably represent full-scale monopile installation processes, provided their respective limitations are properly considered. The successful implementation of these scaling techniques opens new possibilities for efficient simulation of industrial-scale offshore wind turbine installations while maintaining physical accuracy. This comprehensive evaluation establishes a robust framework for selecting and implementing appropriate scaling techniques in DEM simulations of monopile penetration, providing practical guidelines for future research and industrial applications.

6

Conclusions and Recommendations

This research has investigated and developed scaling techniques for modeling monopile installation through scour protection layers using the Discrete Element Method (DEM). Through systematic analysis of different scaling approaches, theoretical framework development, and numerical validation, this study has addressed the fundamental challenges of simulating industrial-scale offshore wind turbine installations while sequentially maintaining computational feasibility, addressing each research question formulated in Chapter 1.

6.1. Conclusions

6.1.1. Main Research Question

Which scaling techniques can be applied to model offshore wind turbine monopile installation and represent real field scenarios?

This research has demonstrated that a combination of scaling approaches is most effective for modeling offshore wind turbine monopile installation and representing real field scenarios. The exact scaling approach with Froude similarity principles enables accurate representation of monopile-rock interaction at full scale, preserving both gravitational and dynamic effects. The coarse-graining technique allows for efficient simulation of large sand volumes by upscaling particle size while maintaining bulk behavior. The hybrid scaling strategy combines these approaches to create computationally feasible simulations that accurately represent both the scour protection layer and the underlying sand bed. The findings of this study provide valuable insights and practical guidelines for researchers and industry professionals involved in the design and optimization of offshore wind turbine foundations. The developed scaling techniques contribute to the advancement of DEM simulations as a powerful tool for understanding and predicting the behavior of monopile installations in increasingly challenging offshore environments.

6.1.2. Sub Research Questions

(RQ1): *What is the current state of the art research on the application of the discrete element method in monopile installation procedure and scaling techniques?*

The literature review revealed that while DEM is well-established for modeling pile penetration, significant challenges remain in scaling these simulations to industrial applications. The current research landscape demonstrates both the capabilities and limitations of DEM in this domain, particularly concerning the computational demands of full-scale modeling.

Various scaling techniques have been developed to address these computational limitations, including exact scaling, coarse-graining, and hybrid approaches. Each approach offers distinct advantages and limitations, particularly in maintaining physical accuracy while reducing computational demands. The findings from the literature review establish a strong foundation for developing and evaluating scaling approaches for monopile installation simulations, setting the stage for the detailed investigation presented in subsequent chapters.

(RQ2): *What are the optimal model parameters and numerical settings for accurately and efficiently simulating monopile penetration through scour layers using DEM?*

Chapter 3 established a robust numerical model through systematic parameter investigation and optimization. The Hertz-Mindlin contact model, combined with carefully calibrated material properties, was found to provide an accurate representation of particle-particle and particle-monopile interactions. A suitable timestep was determined to ensure the numerical stability and accuracy of the simulation results. Extensive investigations were conducted to optimize the geometric parameters of the simulation, including the domain size and shape, monopile geometry, and rock parameters. The optimal domain size was established by varying the width-to-diameter ratio (W/d) and analyzing the resulting penetration resistance and penetration work. The cylindrical shape was ultimately selected for the monopile to accurately capture the plugging effect observed in real-world installations. The rock parameters, including shape and accuracy, were explored to understand their influence on penetration behavior. The chosen contact model, material properties, key performance indicators, timestep, and geometric parameters collectively ensure the accuracy and relevance of the simulation results to real-world monopile penetration scenarios. The optimized domain size and shape, along with the selected rock parameters, provide a realistic representation of the granular medium, allowing for a comprehensive investigation of the factors influencing monopile penetration resistance and energy requirements.

(RQ3): *What kind of scaling technique and scaling laws can be used specifically to upscale the simulation of monopile penetration in DEM?*

Chapter 4 established a comprehensive framework for scaling DEM simulations of monopile penetration through scour protection layers. The investigation has led to the development and theoretical validation of three distinct scaling approaches. The exact scaling approach, particularly Model 4, which implements the Froude scaling principles, proved to be highly reliable in maintaining physical similarity while scal-

ing the system's dimensions. The preservation of both gravitational conditions and dynamic similarity through the Froude number matching resulted in consistent force relationships and energy requirements across scales. The coarse grain approach effectively reduced computational demands up to a scale factor of 20, beyond which accuracy began to deteriorate. Key findings showed reliable results for scale factors 1-20 with proper parameter scaling, a reduction from 6 billion to 617000 particles while maintaining accuracy, and a clear upper limit at scale factor 20, regardless of domain size adjustments. The hybrid scaling strategy successfully combined the advantages of both approaches, offering high accuracy in the critical scour protection layer through exact scaling, computational efficiency through selective application of coarse-graining, and practical feasibility for industrial-scale simulations.

(RQ4): *How reliable and accurate are the scaled DEM simulations?*
This study demonstrates that scaled DEM simulations can achieve high reliability and accuracy when appropriate scaling techniques are selected based on specific simulation requirements, proper scaling laws are applied with careful consideration of physical principles, and scaling limits are respected (particularly for coarse-graining). The validation through penetration resistance and work measurements confirms that these scaling approaches can reliably represent full-scale monopile installation processes, provided their respective limitations are properly considered. The successful implementation of these scaling techniques opens new possibilities for efficient simulation of industrial-scale offshore wind turbine installations while maintaining physical accuracy. This comprehensive evaluation establishes a robust framework for selecting and implementing appropriate scaling techniques in DEM simulations of monopile penetration, providing practical guidelines for future research and industrial applications.

6.2. Recommendations

(RQ5): *What are the remaining gaps that can be studied further to address future challenges in offshore wind turbine installation, such as larger turbines or different seabed conditions ?*
For future research, several promising avenues can be explored to further enhance the understanding and applicability of scaling techniques in DEM simulations of monopile penetration through scour protection layers. Investigating alternative scaling technique combinations, such as combining scalping, particle refinement techniques, and geometric scaling, could offer unique advantages in terms of computational efficiency and physical accuracy. Employing different contact models and comparing their performance across scales could provide valuable insights into the robustness and generalizability of the scaling techniques.

Validating scaled simulations against experimental data is crucial for establishing the credibility of the scaling methodologies and their applicability to real-world scenarios. Conducting a series of controlled experiments using the reference model and subsequently scaling it up to larger dimensions would allow researchers to assess the ac-

curacy and reliability of the scaling techniques in capturing the essential physics of monopile penetration through scour protection layers.

Another important aspect to consider is the current models limitation in simulating the behavior of the sand bed beneath the scour layer in bigger domains, such as the current domain. Developing strategies to accurately represent the sand beds behavior while maintaining computational feasibility is a significant challenge that requires further investigation.

By exploring these research directions, future studies can contribute to the design and optimization of offshore wind turbine foundations in increasingly challenging environments, such as those encountered with larger turbines or different seabed conditions. The insights gained from this study provide a solid foundation for further advancements in the field, ultimately supporting the sustainable development of offshore wind energy.

References

[1] Athanasios Tsetas, Apostolos Tsouvalas, and Andrei V Metrikine. “Installation of large-diameter monopiles: introducing wave dispersion and non-local soil reaction”. In: *Journal of Marine Science and Engineering* 9.3 (2021), p. 313. URL: https://doi.org/10.3390/jmse9030313.

[2] Sergio Sánchez, José-Santos López-Gutiérrez, Vicente Negro, and M Dolores Esteban. “Foundations in offshore wind farms: Evolution, characteristics and range of use. Analysis of main dimensional parameters in monopile foundations”. In: *Journal of Marine Science and Engineering* 7.12 (2019), p. 441. URL: https://www.mdpi.com/2077-1312/7/12/441.

[3] Nia Kajastie. *A short review of foundation design for Offshore Wind Turbines*. Apr. 2024. URL: https://www.geplus.co.uk/opinion/a-short-review-of-foundation-design-for-offshore-wind-turbines-22-04-2024/.

[4] Erica Bush and Lance Manuel. “Foundation models for offshore wind turbines”. In: *47th AIAA aerospace sciences meeting including the new horizons forum and aerospace exposition*. 2009, p. 1037. URL: https://www.caee.utexas.edu/prof/Manuel/Papers/BushManuel_AIAA-2009-1037.pdf.

[5] Vicente Negro, José-Santos López-Gutiérrez, M Dolores Esteban, Pablo Alberdi, Mario Imaz, and José-María Serraclara. “Monopiles in offshore wind: Preliminary estimate of main dimensions”. In: *Ocean Engineering* 133 (2017), pp. 253–261. URL: https://doi.org/10.1016/j.oceaneng.2017.02.011.

[6] Devender Gujjula, Satya Kiran Raju Alluri, G Dhinesh, R Panneer Selvam, and MV Ramana Murthy. “Installation Analysis of Monopile for Offshore Wind Data Collection Platform in High Tidal Environment”. In: *Proceedings of the Fourth International Conference in Ocean Engineering (ICOE2018) Volume 2*. Springer. 2019, pp. 431–440. URL: https://link.springer.com/chapter/10.1007/978-981-13-3134-3_32.

[7] Britta Bienen, Shengsheng Fan, Maximilian Schröder, and Mark F Randolph. “Effect of the installation process on monopile lateral response”. In: *Proceedings of the Institution of Civil Engineers-Geotechnical Engineering* 174.5 (2021), pp. 530–548. URL: https://doi.org/10.1680/jgeen.20.00219.

[8] Nuo Duan, Yi Pik Cheng, Mingfei Lu, and Zhenkui Wang. "DEM investigation of sand response during displacement pile installation". In: *Ocean Engineering* 230 (2021), p. 109040. URL: https://doi.org/10.1016/j.oceaneng.2021.109040.

[9] Annevisser. *OMM, geofabrics to develop Scour Protection Solution*. Mar. 2014. URL: https://www.offshorewind.biz/2014/03/11/omm-geofabrics-to-develop-scour-protection/.

[10] *OPIS*. Dec. 2023. URL: https://grow-offshorewind.nl/project/opis.

[11] Guedes Soares Carlos. *Developments in Renewable Energies Offshore: Proceedings of the 4th International Conference on Renewable Energies Offshore (RENEW 2020, 12-15 October 2020, Lisbon, Portugal)*. CRC Press, 2020. URL: https://doi.org/10.1201/9781003134572.

[12] Fabricio Fernández, Eurípedes do Amaral Vargas, and Raquel Quadros Velloso. "A 3D discretization procedure for the material point method (MPM)". In: *Computational Particle Mechanics* 7 (2020), pp. 725–733. URL: https://doi.org/10.1007/s40571-019-00303-7.

[13] *XL Monopiles*. Nov. 2015. URL: https://www.esru.strath.ac.uk/EandE/Web_sites/14-15/XL_Monopiles/technical.html.

[14] Maarten Veld, Arjan Roest, and Jort van Wijk. "Airborne noise emission measurement during near-shore monopile installation in The Netherlands". In: Sept. 2023.

[15] Martijn Wittingen, K. Visser, M. Godjevac, J. Ye, Ehab El Amam, A Breijs, and Remmelt van der Wal. *Offshore Wind Turbine Monopile Foundation Installation with a Dynamic Positioned Vessel: A feasibility study by modeling*. Oct. 2018. URL: https://repository.tudelft.nl/islandora/object/uuid%3A9a6f1edb-e780-4184-8b6c-2b346714c680.

[16] *Jan De Nul orders monopile installation system for its Floating Installation Vessel Les Alizés*. Nov. 2021. URL: https://www.jandenul.com/news/jan-de-nul-orders-monopile-installation-system-its-floating-installation-vessel-les-alizes.

[17] Ricardo Gurevitz Esposito, Raquel Quadros Velloso, Eurípedes do Amaral Vargas Jr, and Bernadete Ragoni Danziger. "Multi-scale sensitivity analysis of pile installation using DEM". In: *Computational Particle Mechanics* 5 (2018), pp. 375–386.

[18] Junwei Liu, Nuo Duan, Liang Cui, and Na Zhu. "DEM investigation of installation responses of jacked open-ended piles". In: 14.6 (June 2019). DOI: 10.1007/S11440-019-00817-7.

[19] Lichen Li, Wenbing Wu, Hao Liu, and Barry Lehane. "DEM analysis of the plugging effect of open-ended pile during the installation process". In: *Ocean Engineering* 220 (2021), p. 108375.

[20] Wenhan Zhong, Hanlong Liu, Qi Wang, Wengang Zhang, Yongqin Li, Xuanming Ding, and Longlong Chen. "Investigation of the penetration characteristics of snake skin-inspired pile using DEM". In: 16.6 (Jan. 2021). DOI: 10.1007/S11440-020-01132-2.

[21] Jian Zhou, Qiwei Jian, Jiao Zhang, and Jian-jun Guo. "Coupled 3D discrete-continuum numerical modeling of pile penetration in sand". In: 13.1 (Jan. 2012). DOI: 10.1631/JZUS.A1100172.

[22] Michail Komodromos, Gaël Combe, and Gioacchino Viggiani. "Grain-scale DEM study of open-ended pipe pile penetration in granular soils". In: *EPJ Web of Conferences*. Vol. 249. EDP Sciences. 2021, p. 11007.

[23] Xiangyu Zhang and Behzad Fatahi. "Assessing axial load transfer mechanism of open-ended tubular piles penetrating in weak rocks using three-dimensional discrete element method". In: 137 (Sept. 2021). DOI: 10.1016/J.COMPGEO.2021.104267.

[24] Yaseen Umar Sharif, Michael John Brown, Benjamin Cerfontaine, Craig Davidson, Matteo Oryem Ciantia, Jonathan Adam Knappett, Jonathan David Ball, Andrew Brennan, Charles Augarde, Will Coombs, et al. "Effects of screw pile installation on installation requirements and in-service performance using the discrete element method". In: *Canadian geotechnical journal* 58.9 (2021), pp. 1334–1350.

[25] O. M. Hunt, Kyle B. OHara, and Y.M. Chen. "Numerical and Physical Modeling of the Effect of the Cone Apex Angle on the Penetration Resistance in Coarse-Grained Soils". In: 23.2 (Feb. 2023). DOI: 10.1061/(asce)gm.1943-5622.0002626.

[26] Ahmet Talha Gezgin, Behzad Soltanbeigi, and Ozer Cinicioglu. "Discrete-element modelling of pile penetration to reveal influence of soil characteristics". In: *Proceedings of the Institution of Civil Engineers-Geotechnical Engineering* 175.4 (2022), pp. 365–382. URL: https://doi.org/10.1680/jgeen.20.00134.

[27] Na Zhu, Liang Cui, Junwei Liu, Junwei Liu, Mingming Wang, Hui Zhao, and Jia Ning. "Discrete element simulation on the behavior of open-ended pipe pile under cyclic lateral loading". In: 144 (May 2021). DOI: 10.1016/J.SOILDYN.2021.106646.

[28] Yu Peng, Zhen-Yu Yin, and Xuanming Ding. "Analysis of particle corner-breakage effect on pile penetration in coral sand: model tests and DEM simulations". In: 60.5 (Nov. 2022). DOI: 10.1139/cgj-2022-0038.

[29] Anil Vaddi. "Scaling techniques and Scaling laws in the Discrete Element Method: A Systematic Literature Review, report no: 2023.MME.8836". In: (July 2023).

[30] Ei L Chan and Kimiaki Washino. "Coarse grain model for DEM simulation of dense and dynamic particle flow with liquid bridge forces". In: *Chemical Engineering Research and*

Design 132 (2018), pp. 1060–1069. URL: https://doi.org/10.1016/j.cherd.2017.12.033.

[31] Yoshihiro Kosaku, Yuki Tsunazawa, and Chiharu Tokoro. "Investigating the upper limit for applying the coarse grain model in a discrete element method examining mixing processes in a rolling drum". In: *Advanced Powder Technology* 32.11 (2021), pp. 3980–3989. URL: https://doi.org/10.1016/j.apt.2021.08.039.

[32] Yoshihiro Kosaku, Yuki Tsunazawa, and Chiharu Tokoro. "A coarse grain model with parameter scaling of adhesion forces from liquid bridge forces and JKR theory in the discrete element method". In: *Chemical Engineering Science* 268 (2023), p. 118428. URL: https://doi.org/10.1016/j.ces.2022.118428.

[33] Ruihuan Cai, Zhichao Hou, and Yongzhi Zhao. "Numerical study on particle mixing in a double-screw conical mixer". In: *Powder technology* 352 (2019), pp. 193–208. URL: https://doi.org/10.1016/j.powtec.2019.04.065.

[34] M Javad Mohajeri, CV Rhee, and Dingena L Schott. "Coarse graining of adhesive elasto-plastic DEM contact models in quasi-static processes". In: *13th International Conference on Bulk Materials Storage, Handling & Transportation*. 2019. URL: https://www.researchgate.net/publication/337732082_Coarse_graining_of_adhesive_elasto-plastic_DEM_contact_models_in_quasi-_static_processes.

[35] Stef Lommen, Mohammadjavad Mohajeri, Gabriel Lodewijks, and Dingena Schott. "DEM particle upscaling for large-scale bulk handling equipment and material interaction". In: *Powder Technology* 352 (2019), pp. 273–282. URL: https://doi.org/10.1016/j.powtec.2019.04.034.

[36] Matteo Oryem Ciantia, Matteo Oryem Ciantia, Marcos Arroyo, Joanna Butlanska, and Antonio Gens. "DEM modelling of cone penetration tests in a double-porosity crushable granular material". In: 73 (Mar. 2016). DOI: 10.1016/J.COMPGEO.2015.12.001.

[37] Suranita Kanjilal and Simon Schneiderbauer. "A revised coarse-graining approach for simulation of highly poly-disperse granular flows". In: *Powder Technology* 385 (2021), pp. 517–527. URL: https://doi.org/10.1016/j.powtec.2021.02.015.

[38] Subhash C Thakur, Jin Y Ooi, and Hossein Ahmadian. "Scaling of discrete element model parameters for cohesionless and cohesive solid". In: *Powder Technology* 293 (2016), pp. 130–137. URL: https://doi.org/10.1016/j.powtec.2015.05.051.

[39] Hideya Nakamura, Hiroyuki Fujii, and Satoru Watano. "Scale-up of high shear mixer-granulator based on discrete element analysis". In: *Powder Technology* 236 (2013), pp. 149–156. URL: https://doi.org/10.1016/j.powtec.2012.03.009.

[40] Angga Pratama Herman, Jieqing Gan, and Aibing Yu. "GPU-based DEM simulation for scale-up of bladed mixers". In: *Powder technology* 382 (2021), pp. 300–317. URL: https://doi.org/10.1016/j.powtec.2020.12.045.

[41] Eva Siegmann, Dalibor Jajcevic, Charles Radeke, Dieter Strube, Karsten Friedrich, and Johannes G. Khinast. "Efficient Discrete Element Method Simulation Strategy for Analyzing Large-Scale Agitated Powder Mixers". en. In: *Chemie Ingenieur Technik* 89.8 (2017), pp. 995–1005. DOI: 10.1002/cite.201700004. URL: https://onlinelibrary.wiley.com/doi/abs/10.1002/cite.201700004.

[42] Priscila M Esteves, Douglas B Mazzinghy, Roberto Galéry, and Luís CR Machado. "Industrial vertical stirred mills screw liner wear profile compared to discrete element method simulations". In: *Minerals* 11.4 (2021), p. 397. URL: https://doi.org/10.3390/min11040397.

[43] Richard J Garrity, C Paul Kolthoff, Carl A Reaves, and Robert L Schafer. "A test comparison of model and full-size bulldozer blades". In: *SAE Transactions* (1968), pp. 2495–2511. URL: http://www.jstor.org/stable/44580810.

[44] Yu Nagata, Yuki Tsunazawa, Kouji Tsukada, Yuichi Yaguchi, Yosuke Ebisu, Kohei Mitsuhashi, and Chiharu Tokoro. "Effect of the roll stud diameter on the capacity of a high-pressure grinding roll using the discrete element method". In: *Minerals Engineering* 154 (2020), p. 106412. URL: https://doi.org/10.1016/j.mineng.2020.106412.

[45] Alvaro Janda and Jin Y Ooi. "DEM modeling of cone penetration and unconfined compression in cohesive solids". In: *Powder Technology* 293 (2016), pp. 60–68. URL: https://doi.org/10.1016/j.powtec.2015.05.034.

[46] Alireza Ahmadi, Stefan Larsson, and Carl Wersäll. "Scaling granular material with polygonal particles in discrete element modeling". In: *Particuology* 75 (2023), pp. 151–164. URL: https://doi.org/10.1016/j.partic.2022.07.005.

[47] Stef Lommen, Mohammadjavad Mohajeri, Gabriel Lodewijks, and Dingena L. Schott. "DEM particle upscaling for large-scale bulk handling equipment and material interaction". In: 352 (June 2019). DOI: 10.1016/J.POWTEC.2019.04.034.

[48] Mehari Z. Tekeste, Thomas R. Way, Zamir Syed, and R.L. Schafer. "Modeling soil-bulldozer blade interaction using the discrete element method (DEM)". In: 88 (Apr. 2020). DOI: 10.1016/J.JTERRA.2019.12.003.

[49] Alvaro Janda and Jin Y. Ooi. "DEM modeling of cone penetration and unconfined compression in cohesive solids". In: 293 (May 2016). DOI: 10.1016/J.POWTEC.2015.05.034.

[50] Glenn R. McDowell, O. Falagush, and Hai-Sui Yu. "A particle refinement method for simulating DEM of cone penetration testing in granular materials". In: 2.3 (Sept. 2012). DOI: 10.1680/GEOLETT.12.00036.

[51] O. Falagush, Glenn R. McDowell, and Hai-Sui Yu. "Discrete Element Modeling of Cone Penetration Tests Incorporating Particle Shape and Crushing". In: 15.6 (Dec. 2015). DOI: 10.1061/(ASCE)GM.1943-5622.0000463.

[52] Xiaobin Ding, Yu Shi, Rui Chen, and Mi Zhou. "Friction anlysis of large diameter steel cylinder penetration process using 3D-DEM". In: *Granular Matter* 23 (2021), pp. 1–15. URL: https://doi.org/10.1007/s10035-021-01086-6.

[53] Teodora Brbunoiu. *Assessing the drivability of a monopile through the rock armour layer: An analysis using Discrete Element Method and small-scale testing*. Nov. 2023. URL: https://repository.tudelft.nl/record/uuid:b85939ce-2d14-4107-8b09-dd2dcafc2e8b.

[54] URL: https://altair.com/edem.

[55] Helio A Navarro and Meire P de Souza Braun. "Determination of the normal spring stiffness coefficient in the linear spring–dashpot contact model of discrete element method". In: *Powder technology* 246 (2013), pp. 707–722. URL: https://doi.org/10.1016/j.powtec.2013.05.049.

[56] Heinrich Hertz. In: *Journal für die reine und angewandte Mathematik* 1882.92 (1882), pp. 156–171. DOI: doi:10.1515/crll.1882.92.156. URL: https://doi.org/10.1515/crll.1882.92.156.

[57] R. D. Mindlin. "Compliance of Elastic Bodies in Contact". In: *Journal of Applied Mechanics* 16.3 (Apr. 2021), pp. 259–268. ISSN: 0021-8936. eprint: https://asmedigitalcollection.asme.org/appliedmechanics/article-pdf/16/3/259/6746333/259_1.pdf. URL: https://doi.org/10.1115/1.4009973.

[58] Run Liu, Long Zhou, Ji-jian Lian, and Hong-yan Ding. "Behavior of Monopile Foundations for Offshore Wind Farms in Sand". In: *Journal of Waterway, Port, Coastal, and Ocean Engineering* 142.1 (2016), p. 04015010. URL: https://ascelibrary.org/doi/abs/10.1061/%28ASCE%29WW.1943-5460.0000312.

[59] Editor Engineeringtoolbox. *Modulus of rigidity*. Sept. 2023. URL: https://www.engineeringtoolbox.com/modulus-rigidity-d_946.html.

[60] Editor Engineeringtoolbox. *Poissons ratio*. Apr. 2024. URL: https://www.engineeringtoolbox.com/poissons-ratio-d_1224.html.

[61] J Byerlee. "Rock friction and earthquake prediction". In: *(No Title)* (1978), p. 615. URL: https://link.springer.com/book/10.1007/978-3-0348-7182-2.

[62] Mustafa Ucgul, John M Fielke, and Chris Saunders. "Defining the effect of sweep tillage tool cutting edge geometry on tillage forces using 3D discrete element modelling". In: *Information Processing in Agriculture* 2.2 (2015), pp. 130–141. URL: https://doi.org/10.1016/j.inpa.2015.07.001.

[63] Jorge Paulino Pereira. "Rolling friction and shear behaviour of rock discontinuities filled with sand". In: *International Journal of Rock Mechanics and Mining Sciences* 34.3-4 (1997), 244–e1. URL: https://doi.org/10.1016/S1365-1609(97)00037-3.

[64] Andrew Alden. *The density of common rocks and minerals*. Jan. 2020. URL: https://www.thoughtco.com/densities-of-common-rocks-and-minerals-1439119.

[65] M Combarros Garcia, HJ Feise, S Strege, and A Kwade. "Segregation in heaps and silos: Comparison between experiment, simulation and continuum model". In: *Powder Technology* 293 (2016), pp. 26–36. URL: https://doi.org/10.1016/j.powtec.2015.09.036.

[66] Kimiaki Washino, Ei L Chan, Koki Miyazaki, Takuya Tsuji, and Toshitsugu Tanaka. "Time step criteria in DEM simulation of wet particles in viscosity dominant systems". In: *Powder Technology* 302 (2016), pp. 100–107. URL: https://doi.org/10.1016/j.powtec.2016.08.018.

[67] R Albert, MA Pfeifer, A-L Barabási, and P Schiffer. "Slow drag in a granular medium". In: *Physical review letters* 82.1 (1999), p. 205. URL: https://doi.org/10.1103/PhysRevLett.82.205.

[68] Yajie Feng, Raphael Blumenfeld, and Caishan Liu. "Support of modified Archimedes' law theory in granular media". In: *Soft matter* 15.14 (2019), pp. 3008–3017. URL: 10.1039/C8SM02480D.

[69] Satish Jawalageri, Subhamoy Bhattacharya, Soroosh Jalilvand, and Abdollah Malekjafarian. "A comparative study on load assessment methods for offshore wind turbines using a simplified method and OpenFAST simulations". In: *Energies* 17.9 (2024), p. 2189. URL: https://doi.org/10.3390/en17092189.

[70] Leen De Vos, Julien De Rouck, Peter Troch, and Peter Frigaard. "Empirical design of scour protections around monopile foundations: Part 1: Static approach". In: *Coastal Engineering* 58.6 (2011), pp. 540–553. DOI: 10.1016/j.coastaleng.2011.02.001.

[71] Richard JS Whitehouse, John M Harris, James Sutherland, and Jon Rees. "The nature of scour development and scour protection at offshore windfarm foundations". In: *Marine Pollution Bulletin* 62.1 (2011), pp. 73–88. DOI: 10.1016/j.marpolbul.2010.09.007.

[72] Minghao Wu, Leen De Vos, Carlos Emilio Arboleda Chavez, Vasiliki Stratigaki, Tiago Fazeres-Ferradosa, Paulo Rosa-Santos, Francisco Taveira-Pinto, and Peter Troch.

"Large scale experimental study of the scour protection damage around a monopile foundation under combined wave and current conditions". In: *Journal of Marine Science and Engineering* 8.6 (2020), p. 417. URL: https://doi.org/10.3390/jmse8060417.

[73] Thor Ugelvig Petersen. "Scour around offshore wind turbine foundations". In: (2014). URL: https://findit.dtu.dk/en/catalog/5450f3238b8b17265f000002.

[74] Thomas Roessler and André Katterfeld. "Scaling of the angle of repose test and its influence on the calibration of DEM parameters using upscaled particles". In: *Powder technology* 330 (2018), pp. 58–66. URL: https://doi.org/10.1016/j.powtec.2018.01.044.

[75] YT Feng and DRJ Owen. "Discrete element modelling of large scale particle systemsI: exact scaling laws". In: *Computational Particle Mechanics* 1 (2014), pp. 159–168. URL: 10.1007/s40571-014-0010-y.

[76] R.J.S. Whitehouse, J.M. Harris, J. Sutherland, and J. Rees. "The nature of scour development and scour protection at offshore windfarm foundations". In: *Marine Pollution Bulletin* 62 (2011), pp. 73–88. URL: https://doi.org/10.1016/j.marpolbul.2010.09.007.

[77] A.W. Nielsen, X. Liu, B.M. Sumer, and J. Fredsøe. *Flow and bed shear stresses in scour protections around a pile in a current*. Tech. rep. Coastal Engineering, 2014, pp. 20–35. URL: https://doi.org/10.1016/j.coastaleng.2012.09.001.

[78] Xin Jiang. "Research on Coarse-Grained Discrete Element Model and Optimization for Fine Particles". In: *Coatings* 12.10 (2022), p. 1483. URL: https://doi.org/10.3390/coatings12101483.

[79] Erasmo S. Napolitano, Alberto Di Renzo, and Francesco P. Di Maio. "Coarse Graining in Discrete Element Modelling (DEM-CFD) of High Solids Loading Cyclones". In: *Chemical Engineering Transactions* 86 (2021), pp. 1–6. ISSN: 2283-9216. URL: https://www.aidic.it/icheap15/programma/401napolitano.pdf.

[80] Hideya Nakamura, Hiroharu Takimoto, Naoki Kishida, Shuji Ohsaki, and Satoru Watano. "Coarse-grained discrete element method for granular shear flow". In: *Chemical Engineering Journal Advances* 4 (2020), p. 100050. URL: https://doi.org/10.1016/j.ceja.2020.100050.

[81] G. Lu, J.R. Third, and C.R. Müller. "Discrete element models for non-spherical particle systems: From theoretical developments to applications". In: *Chemical Engineering Science* 127 (2015), pp. 425–465. DOI: 10.1016/j.ces.2014.11.050.

[82] M Javad Mohajeri, Rudy LJ Helmons, Cees van Rhee, and Dingena L Schott. "A hybrid particle-geometric scaling approach for elasto-plastic adhesive DEM contact models".

In: *Powder technology* 369 (2020), pp. 72–87. URL: https://doi.org/10.1016/j.powtec.2020.05.012.

A

Research paper

Optimization of DEM Simulation Time of Monopile Penetration through Scour Rock Layer using Scaling

Anil Kumar Vaddi[1], Hao Shi[1*] and Dingena Schott[2]

***Abstract*— This study investigates the feasibility of scaling Discrete Element Method (DEM) simulations to model the penetration of monopiles through protective scour armour layers in offshore wind turbine installations. A reference model is constructed to simulate monopile penetration through a scour protection layer composed of granular material. Three distinct scaling approaches are investigated: exact scaling, coarse-graining technique, and hybrid scaling. The results of this study show that scaled DEM simulations can achieve high reliability and accuracy when appropriate scaling techniques are selected based on specific simulation requirements, proper scaling laws are applied with careful consideration of physical principles, and scaling limits are respected. The successful implementation of these scaling techniques opens new possibilities for efficient simulation of industrial-scale offshore wind turbine installations while maintaining physical accuracy.**

I. INTRODUCTION

The installation of monopiles for offshore wind turbines has become increasingly challenging as the industry moves toward larger structures in deeper waters. Monopiles, typically 4-6 meters in diameter have traditionally been the foundation of choice for offshore wind installations in shallow waters. However, the emergence of XXL monopiles exceeding 7 meters in diameter and 150 meters in length has introduced new complexities to the installation process [1]. The successful installation of these structures requires careful consideration of soil conditions, installation methods, and the interaction between the monopile and the surrounding medium [2]. Experimental studies provide valuable information on the complex interactions between the monopile, the scour protection layer, and the underlying soil. However, conducting full-scale experimental studies in deep waters is practically impossible due to several challenges, including the immense size and weight of monopiles, the vast depths involved, harsh environmental conditions, and the costs associated. Although reduced-scale models offer a more practical alternative, they have limitations, including scaling effects and significant construction and operating costs. Given these challenges, numerical simulations provide a valuable alternative for investigating monopile penetration through scour layers. Several numerical methods can simulate the penetration of monopiles through scour rocks, including the Finite Element Method (FEM), the Discrete Element Method (DEM), the Material Point Method (MPM), and the Computational Fluid Dynamics (CFD). However, DEM is the most appropriate numerical method as this method captures the contact characteristics of particles and simulates large-deformation events. The major setback that DEM has is the simulation time which leads to higher computational cost. The simulation time increases as the number of particles increases; even simulating laboratory systems might be difficult as trillions of particles are required and would be cumbersome even if a supercomputer is deployed. This study uses scaling techniques in DEM to simulate monopile penetration in a reasonable time by reducing the number of particles. The primary goal is to identify scaling techniques that can be applied to model monopile penetration and represent real-field scenarios.

The penetration mechanics of piles in granular media has been extensively studied through various approaches. Early work by Esposito et al. used two-dimensional DEM simulations to investigate the effects of installation methods and particle rotation on stress distribution and porosity changes around displacement piles [3]. Further, Liu et al. explored the micro-mechanics of soil plugging in open-ended piles, revealing that plug resistance concentrates within a zone 2-3 times the pile diameter above the base [4]. The complexity of pile-soil interaction was further illuminated by Li et al. who demonstrated that plugging is more prevalent in jacked piles compared to dynamically installed ones [5]. Three-dimensional analyses have provided additional insights into the penetration process. Zhou et al. developed a coupled discrete-continuum model that preserved the discrete nature of soil near the pile while efficiently modeling the far-field response [6]. Komodromos et al. advanced this understanding by examining the influence of rolling resistance on soil response during pile installation [7], while Zhang and Fatahi investigated load transfer mechanisms in weak rocks using three-dimensional DEM [8].

To further reduce the computational demands of the DEM simulations have led researchers to explore various scaling techniques. Ciantia et al. successfully implemented particle upscaling by a factor of 25 while maintaining the key mechanical responses of crushable granular materials [9]. Lommen et al. demonstrated the effectiveness of coarse-graining in large-scale bulk handling simulations, though they noted limitations in capturing penetration resistance

*This work is supported by Delft University of Technology

[1]Anil Kumar Vaddi is with the Faculty of Mechanical Engineering, Department of Maritime and Transport Technology, Delft University of Technology, 2628 CD Delft, The Netherlands

[1*]Hao Shi is with the Faculty of Mechanical Engineering, Department of Maritime and Transport Technology, Delft University of Technology, 2628 CD Delft, The Netherlands

[2]Dingena Schott is with the Faculty of Mechanical Engineering, Department of Maritime and Transport Technology, Delft University of Technology, 2628 CD Delft, The Netherlands

accurately [10]. A significant advancement came through Tekeste et al. who established scaling relationships between soil reaction forces and equipment size using geometric scaling principles [11]. The challenge of scaling up both particles and geometry was studied by Janda and Ooi [12]. They explored scaling of contact parameters with particle size and scaling up the geometry with the same scale factor in quasi-static processes, while McDowell et al. studied a particle refinement method, which focuses on scaling particles at a specific region specifically for penetration problems [13], [14]. These efforts are combined in a work by Mohajeri et al., who proposed a hybrid particle-geometric scaling approach that efficiently handles the larger scale DEM simulations bulk solids with a minimized computational time [33]. The development of hybrid scaling approaches represents a promising direction for balancing computational efficiency with physical accuracy in modeling complex geotechnical processes. This progression of research demonstrates the evolution from a basic understanding of pile penetration mechanics to sophisticated scaling techniques that enable practical simulation of large-scale installations. However, there are no studies simulating monopile through multispheres specifically through scour rocks. Understanding the behavior of monopile foundations during installation in deep waters, particularly when penetrating through scour protection layers, is crucial for the design and optimization of offshore wind farms. This study focuses on using scaling techniques in DEM to simulate monopile penetration through the scour rock armor layer.

II. SIMULATION SETUP AND MODEL PARAMETERS

The development of an accurate reference model is crucial for studying monopile installation through scour protection layers using the Discrete Element Method (DEM). This section presents a systematic investigation of key parameters that govern the simulation's behavior, focusing on achieving a balance between computational efficiency and physical accuracy. All simulations were conducted using Altair EDEM 2023.0 on a DELL Alienware m15 R6 laptop with an 11th Gen Intel Core i7-11800H processor integrating 8 willow clove processor cores(16 threads), 32 GB RAM, and an NVIDIA GeForce RTX 3060 GPU with 6 GB memory.

A. Discerete Element Method

1) Contact model and Material properties: The Hertz-Mindlin contact model was selected for its ability to accurately represent both normal and tangential forces in particle interactions. This model combines Hertzian theory for normal contact forces with Mindlin's tangential force model, making it particularly suitable for dry, non-cohesive granular materials [15], [16]. The model incorporates the following force components.
The Normal force is given by:

$$F_n = \frac{4}{3} E^* \sqrt{R^*} \delta_n^{3/2} \tag{1}$$

where E^* is the equivalent Young's modulus:

$$E^* = \left(\frac{1-\nu_1^2}{E_1} + \frac{1-\nu_2^2}{E_2} \right)^{-1} \tag{2}$$

The tangential force is given by:

$$F_t = -8G^* \sqrt{R^* \delta_n} \delta_t \tag{3}$$

Damping forces are expressed as:

$$F_n^d = -2\sqrt{\frac{5}{6}} \beta \sqrt{S_n m^*} v_{rel}^n \tag{4}$$

Material properties were carefully calibrated based on existing literature, with parameters including particle density, shear modulus, and Poisson's ratio selected to represent granite rocks accurately The material parameters used in the simulation are defined as:

TABLE I: contact parameters used in DEM simulation

Parameter	Symbol	Value	Reference
Pile density	ρ_g	7850 kg/m^3	[17]
Pile shear modulus	G_g	78 GPa	[18]
Pile Poisson's ratio	ν_g	0.28	[19]
Particle density	ρ_p	2664.3 kg/m^3	[20]
Particle shear modulus	G_p	0.04 GPa	[21]
Particle Poisson's ratio	ν_p	0.25	[21]
Particle-pile sliding friction	$\mu_{s,p-g}$	0.5	[22], [23]
Particle-pile rolling friction	$\mu_{r,p-g}$	0.05	[23], [24]
Particle-particle sliding friction	$\mu_{s,p-p}$	0.64	[21], [22]
Particle-particle rolling friction	$\mu_{r,p-p}$	0.1	[21], [23]

2) Model Configuration: The initial model configuration was established to create a reference case for timestep sensitivity analysis. The monopile was modeled as a cylindrical structure with specific dimensions chosen to represent a scaled version of typical offshore installations. The geometry consisted of a pile length of 500 mm, an outer diameter of 323.9 mm, and a wall thickness of 8.8 mm (fig. 1). These dimensions were selected to maintain realistic proportions while keeping the simulation computationally tractable. For

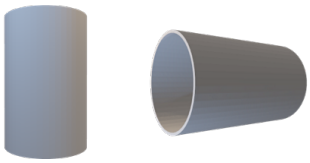

Fig. 1: Monopile geometry designed in solidworks and imported to EDEM

the granular medium, real rocks were scanned using the Qlone application to create detailed 3D models of their surfaces. These scans were then imported into EDEM and converted into multi-sphere representations (fig. 2). Each rock particle ranged in size from 25 mm to 35 mm, with constituent spheres varying from 3.178 mm to 11.36 mm in diameter. This multi-sphere approach allowed for accurate representation of complex particle geometries while maintaining computational efficiency. The simulation domain was designed to be sufficiently large to minimize boundary effects while remaining computationally feasible. A cubic

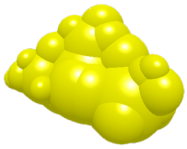

Fig. 2: Rock sample generated using EDEM demonstrating multi-sphere approach for particle representation

domain was implemented with dimensions of 1650 mm in length and width, and a height of 1000 mm (fig. 3). These domain dimensions were carefully chosen to ensure that the distance from the monopile to the domain boundaries was at least four times the monopile diameter, following established guidelines for minimizing boundary effects in DEM simulations. The monopile was configured to penetrate to a depth of 300 mm, providing sufficient data to analyze the penetration resistance and work done during the installation process. This configuration served as the foundation for

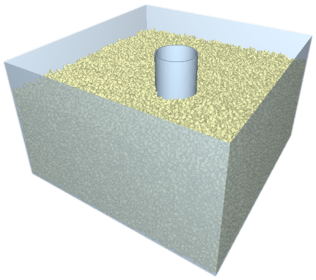

Fig. 3: EDEM simulation setup showing the monopile penetration

subsequent parametric studies and provided a robust baseline for evaluating different scaling approaches. The dimensions were carefully documented to ensure reproducibility and to facilitate comparison with other research in the field.

3) Key Performance Indicators(KPIs): Two primary metrics were established to evaluate simulation performance:

Penetration Resistance: Measures the force required to drive the monopile into the seabed at various depths Penetration Work: Quantifies the total energy expended during the installation process

These KPIs were selected for their direct relevance to practical installation procedures and their ability to provide complementary information about the penetration process.

4) Timestep: The Rayleigh timestep (t_{ray}) was calculated using [25]:

$$t_{ray} = \frac{\pi R_{min}\sqrt{\rho/G}}{0.1631\nu + 0.8766} \tag{5}$$

The penetration velocity was set at 100 mm/s and 50 mm/s for different simulation cases, allowing for investigation of velocity-dependent effects on the timestep sensitivity. Through systematic investigation of timesteps ranging from 2.5% to 550% of t_{ray}, we determined that 30% of t_{ray} provides optimal balance between accuracy and computational efficiency.

B. Geometric Parameters

The optimization of geometric parameters plays a crucial role in ensuring both accuracy and computational efficiency in DEM simulations of monopile penetration. This section presents a systematic investigation of key geometric parameters, including penetration velocity, domain characteristics, and monopile configuration.

1) Penetration Velocity: The selection of appropriate penetration velocity is fundamental for maintaining quasi-static conditions during monopile installation through scour protection layers. Following Albert et al., the critical velocity (v_c) for pile penetration was determined using [26]:

$$v_c = \sqrt{\frac{4gR_{min}}{10}} \tag{6}$$

where g is gravitational acceleration and R_{min} is the radius of the rock particle.

For the maximum rock diameter of 35 mm, this yielded a critical velocity of 82.5 mm/s. To validate this threshold, simulations were conducted with velocities ranging from 10 mm/s to 250 mm/s. Results demonstrated consistent penetration resistance patterns up to 70 mm/s, beyond which dynamic effects became significant. A conservative penetration velocity of 50 mm/s was selected for subsequent analyses to ensure maintenance of quasi-static conditions.

2) Domain size Optimization: Domain size configuration focused on investigating various width-to-particle diameter ratios (W/drock) to establish optimal simulation boundaries. The analysis examined ratios ranging from 10 to 75, with particular attention to boundary effects and computational efficiency (table II.

TABLE II: Domain size optimization results

W/d_{rock}	Width (mm)	Particles	Computation Time
10	350	4,100	4 min
20	700	17,365	10 min
25	870	26,825	14.6 min
30	1050	39,207	26.22 min
35	1225	53,331	31.2 min
40	1400	65,754	36.4 min
50	1750	108,655	52.2 min
65	2275	183,869	1.4 h
75	2,625	254,028	5.43 h

3) Domain shape Configuration: Two domain shapes were investigated: cylindrical and square. For a square domain width of 1400 mm, two cylindrical configurations were tested (fig. 4):

- Cylinder diameter equal to square width (1400 mm)
- Cylinder diameter equal to square diagonal (1979.8 mm)

Results showed negligible differences in penetration resistance between these configurations. The cylindrical domain with a 1400 mm diameter was selected for its optimal combination of accuracy and computational efficiency, requiring only 54,453 particles compared to 65,754 for the square domain.

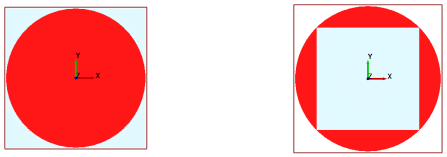

Fig. 4: Comparison of domain shapes showing (a) cylindrical domain with width-matched diameter, (b) cylindrical domain with diagonal-matched diameter. Red regions represent cylindrical domains while light blue indicates square domain boundaries.

4) Monopile Configuration: The study compared traditional cylindrical monopile geometry with a simplified plate representation. The cylindrical monopile had dimensions:

- Length: 500 mm
- Outer diameter: 323.9 mm
- Wall thickness: 8.8 mm

The equivalent plate dimensions were:

- Length: 1017.56 mm
- Height: 500 mm
- Thickness: 8.8 mm

C. Rock Parameters

The accurate representation of rock particles in DEM simulations is crucial for modeling monopile penetration through scour protection layers. This section presents a systematic investigation of rock shape diversity and rock accuracy.

1) Shape Representation: Twenty distinct rock shapes were obtained through 3D scanning using the Qlone application and subsequently imported into EDEM as multi-sphere approximations. These scanned shapes provided realistic representations of actual scour protection rocks, capturing their irregular geometries and angular features. The number of shapes used in simulations was systematically varied from 2 to 20 to investigate the influence of shape diversity on penetration behavior. Table III shows the required computational time required with the increase in shapes

TABLE III: Computational requirements for varying rock shape diversity

Number of Shapes	Computational Time
1	1.61 h
2	1.71 h
4	1.9 h
6	2.71 h
8	9.5 h
10	10.7 h
12	12.5 h
14	13 h
20	14.8 h

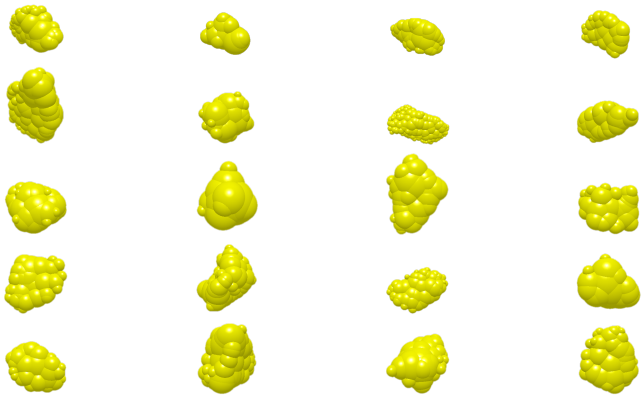

Fig. 5: Scanned rocks generated in EDEM as multispheres

2) Rock Accuracy: The "smoothing value" parameter in EDEM controls the resolution of individual rock particles, determining the number of constituent spheres used to approximate each rock shape. The investigation covered smoothing values from 1 (highest resolution) to 6 (lowest resolution). Table IV shows how the number of spheres increases in the simulation as I change the smoothing value.

Smoothing Value	Number of Spheres per Rock Type					
	Rock 1	Rock 2	Rock 3	Rock 4	Rock 5	Rock 6
6	41	22	36	35	61	33
5	50	29	47	46	89	45
4	75	42	68	60	126	68
3	119	65	128	101	221	115
2	262	146	299	234	461	271
1	684	529	721	791	984	733

TABLE IV: Sphere count for different smoothing values

3) Results and Analysis: Let me restructure the results in a more cohesive narrative form:

The penetration velocity analysis revealed important insights about maintaining quasi-static conditions during monopile installation. When testing the maximum rock diameter of 35 mm, calculations established a critical velocity threshold of 82.5 mm/s. Through systematic investigation with velocities ranging from 10 mm/s to 250 mm/s, the simulations demonstrated consistent penetration resistance patterns up to 70 mm/s. Beyond this threshold, dynamic effects began to dominate the system behavior. Based on these findings, a conservative penetration velocity of 50 mm/s was selected for subsequent analyses to ensure reliable quasi-static conditions throughout the penetration process.

The domain configuration investigation yielded clear relationships between boundary effects and computational efficiency. Domains with width-to-particle diameter ratios (W/drock) less than 30 showed significant boundary interference that compromised result accuracy. While ratios above 40 maintained consistent results, they offered minimal improvement in accuracy despite substantially increased computational demands. The cylindrical domain configuration with a 1400 mm diameter emerged as the optimal choice, requiring only 54,453 particles compared to the 65,754

needed for an equivalent square domain. The computational time analysis revealed a nonlinear relationship with domain size, ranging from just 4 minutes for the smallest ratio (W/drock = 10) to 5.43 hours for the largest (W/drock = 75).

The monopile configuration study demonstrated crucial differences between cylindrical and plate geometries, particularly regarding the plugging effect (fig. 6). The cylindrical geometry exhibited significant particle accumulation inside the pile during penetration, a phenomenon absent in the plate geometry. This plugging effect led to measurably increased penetration resistance and work requirements at greater depths, validating the importance of maintaining cylindrical geometry for an accurate representation of real-world installation behavior.

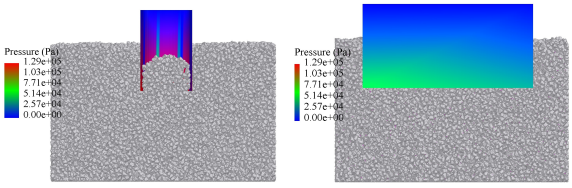

Fig. 6: Picture depicting (a) plugging effect in monopile, (b) no plugging effect in plate geometry

The rock parameter optimization revealed several critical relationships between geometric accuracy and computational efficiency. Through systematic testing, six distinct rock shapes emerged as the optimal number, providing sufficient variety to capture realistic behavior while maintaining manageable computation times. The investigation of smoothing values showed that levels 4 and 5 achieved the best balance between geometric accuracy and computational efficiency. Higher resolution settings, particularly smoothing value 1, while offering the most accurate representation, required prohibitively long computation times of approximately 10 days. The particle count analysis showed significant variation across smoothing values, ranging from 41 to 984 spheres per rock depending on the resolution level. Importantly, while shape diversity beyond six distinct forms showed minimal improvement in performance metrics, the computational time continued to increase substantially, establishing a clear practical limit for shape variety in the simulations.

III. SCALING

The reference model developed for monopile penetration simulation, while computationally tractable, represents a scaled-down version of industrial installations. Modern offshore wind turbines utilize monopiles with diameters ranging from 8-10 meters, necessitating a scale factor of approximately 25 to bridge the gap between our reference model (diameter 323.9 mm) and full-scale installations (target diameter 8.1 m).

A. Scour Protection Design Parameters

When scaling the model, it's crucial to consider not just the monopile dimensions, but also the corresponding scour protection measures. In the reference model, the particle size range is 25-35 mm. However, full-scale scour protection typically uses much larger rock sizes ranging 0.2 m - 0.6 for a monopile diameter 4 m - 5m ([27] - [29]). The design of scaled scour protection followed established dimensionless parameters:

$$\frac{w_b}{D_p} = \frac{35}{8.1} = 4.32 \tag{7}$$

where w_b represents scour layer extension and D_p is pile diameter.

The aspect ratio was selected as:

$$A_r = \frac{h_b}{w_b} = 0.10 \tag{8}$$

yielding a scour layer thickness of:

$$h_b = A_r \times w_b = 0.10 \times 35 = 3.5 \text{ m} \tag{9}$$

The cover stone size (D_c) was determined based on the four-layer criterion:

$$D_c = \frac{h_b}{4} = 0.875 \text{ m} \tag{10}$$

These parameters ensure geometric similarity with established design guidelines while maintaining practical constructability, which represents a scale factor of about 25 times the reference model's particle size range. Based on the information provided and the specific requirements for scaling both the particles and geometry for our reference, exact scaling(with factor 25) appears to be the most appropriate technique.

B. Exact Scaling Technique

The implementation of exact scaling for monopile penetration simulations aims to bridge the gap between laboratory-scale models and industrial applications. This section presents the theoretical framework and numerical implementation of exact scaling, with particular focus on scaling the reference model to the industrial scale while managing computational demands. Exact scaling maintains fundamental physical relationships between the original and scaled systems through systematic application of scaling laws. The approach preserves both geometric and dynamic similarity by scaling basic physical quantities - length, time, mass

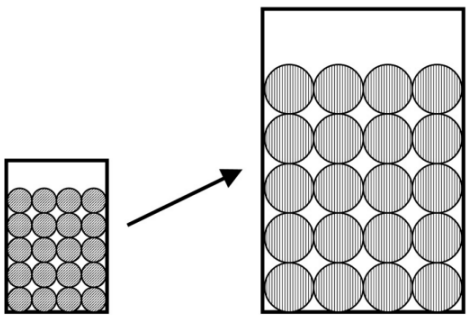

Fig. 7: Visual representation of exact scaling [30]

and and density - from which other parameters are derived [31]. For this study, a scale factor of 25 was selected to match current industry requirements, scaling the reference monopile diameter from 323.9 mm to 8097.5 mm. Four distinct scaling methods were developed and evaluated, each employing different approaches to preserve critical physical parameters.

- Scaling Method 1 maintained constant velocity while reducing gravitational acceleration.
- Scaling Method 2 preserved time while scaling velocity and gravity.
- Scaling Method 3 attempted to maintain real-world gravitational conditions, but does not establish any scaling laws.
- Scaling Method 4 implemented Froude scaling principles to ensure that it implements the real-world gravitational conditions while maintaining scaling laws.

The Froude scaling relationship is given by:

$$Fr = \frac{v}{\sqrt{gL}} \tag{11}$$

where v is velocity, g is gravitational acceleration, and L is characteristic length [32]. The below table shows the scaling of various physical quantities

TABLE V: Exact scaling laws

Physical Quantity	Dimensions	Scaling method 1	Scaling method 2	Scaling method 3	Scaling method 4
Length	[L]	25L	25L	25L	25L
Time	[T]	25T	1	25T	$\sqrt{25}$
Mass	[M]	25M	25M	25M	25M
Density	ρ	1	1	1	1
Velocity	$[L][T]^{-1}$	1	25	1	$\sqrt{25}$
Acceleration	$[L][T]^{-2}$	1/25	25	1	1
Young's Modulus	$[\rho][L]^2[T]^{-2}$	1	25^2	1	25
Force	$[\rho][L]^4[T]^{-2}$	25^2	25^4	25^2	25^3

The implementation of a realistic scour protection system in our numerical model requires a total thickness of 3.5m for the armor layer, following industry standards discussed in the previous section. The volume of the remaining domain must be filled with sand particles to accurately represent the conditions of the seabed. However, it takes approximately 100 trillion sand particles to fill the current domain size with particles of natural sand dimensions.

Given the computational limitations of current hardware resources, simulating such a vast number of individual particles is impractical. The computational cost would be prohibitive in terms of both memory requirements and processing time. To address this limitation while maintaining the physical relevance of our simulation, a coarse-graining technique will be implemented to upscale the particle size.

C. Coarse Grain Technique

The coarse grain technique is used to speed up simulations of large systems of particles. In traditional DEM, each individual particle is modeled and tracked separately, which can be computationally expensive for very large systems. The coarse-grain method addresses this by grouping multiple original particles into single, larger, "coarse grained" particles [34]. The coarse grain approach addresses the computational challenges of simulating the sand bed beneath the scour protection layer. The particle diameter scaling follows:

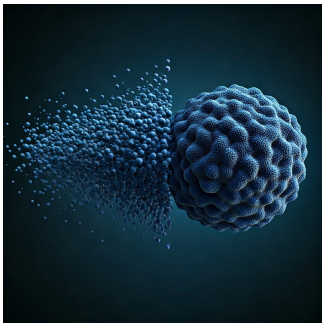

Fig. 8: Concept of DEM-CGM: original particles (left), equivalent coarse grain (right).
(This is an AI generated picture, Google Imagen 3)

$$d_g = NPG^{1/3} \cdot d_p \tag{12}$$

- d_g= Scaled particle diameter
- d_g= Original particle diameter
- NPG = Number of Particles per Grain

Contact parameters were systematically scaled as shown in Table VI and Table VII. Scale factors from 1 to 30 were investigated to determine optimal upscaling limits.

TABLE VI: Contact parameters for lower scale factors (SF 2-5)

Parameter	Base Case	SF 2	SF 3	SF 4	SF 5
Particle Size (mm)	0.6	1.2	1.8	2.4	3.0
Shear Modulus (Pa)	4×10^7	2×10^7	1.33×10^7	1×10^7	8×10^6
Static Friction Coef.	0.7	0.35	0.233	0.175	0.14
Rolling Friction Coef.	0.05	0.025	0.0167	0.0125	0.01

TABLE VII: Contact parameters for higher scale factors (SF 10-30)

Parameter	SF 10	SF 15	SF 20	SF 30
Particle Size (mm)	6	9	12	18
Shear Modulus (Pa)	4×10^6	2.6×10^6	2×10^6	1.3×10^6
Static Friction Coef.	0.07	0.046	0.035	0.023
Rolling Friction Coef.	0.005	0.0033	0.0025	0.0016

Note: SF = scale factor. Common parameters across all simulations: Penetration velocity: 1 mm/s, Particle properties: Poisson's ratio: 0.27, Density: 2100 kg/ms, Coefficient of restitution: 0.3

Calculations indicate that approximately 120 billion particles would still be required to represent the sand bed portion of the domain even with a particle size of 18 mm, far exceeding current computational capabilities. To address this limitation while maintaining physical relevance, a modified approach was developed in which the upscaled simulation model was rescaled to match the dimensions of the reference

model. In this configuration, the thickness of the scour protection layer was translated to 140 mm, and rest of the domain is filled with the coarse-grained rock particles. This hybrid approach aims to balance computational feasibility with physical accuracy, particularly in the critical scour protection zone where particle-monopile interactions are most significant.

D. Hybrid Scaling Implementation

The hybrid scaling approach in the DEM represents an advanced computational strategy that synthesizes multiple scaling techniques to optimize computational efficiency while preserving the fidelity of large-scale particle system simulations [33]. A novel hybrid approach was developed combining exact scaling for the scour protection layer with coarse graining for the underlying sand bed. This methodology employs:

- Froude scaling (Method 4) for rocks in scour protection layer
- Coarse graining with scale factors (20) for sand bed
- Layer-specific parameter optimization

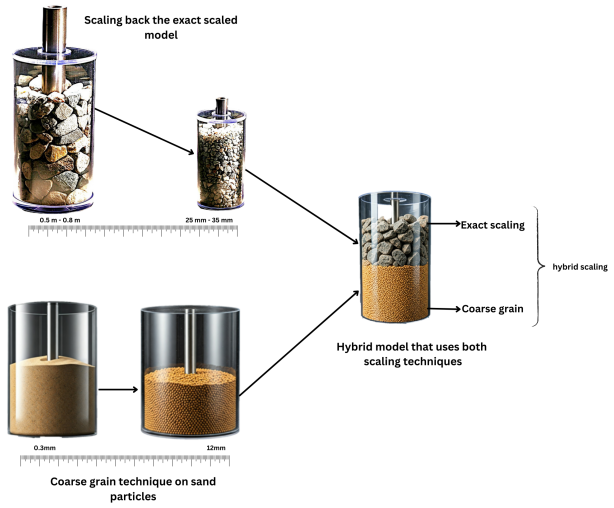

Fig. 9: Conceptual design of hybrid scaling.
(This is an AI generated picture, Google Imagen 3)

The hybrid approach addresses the computational challenges of full-scale simulation while maintaining physical accuracy in critical regions. This methodology enables practical simulation of industrial-scale installations while preserving essential particle-scale interactions in the scour protection layer. To validate the hybrid scaling approach, three different simulation configurations were implemented, each employing different coarse-grain scaling factors for the sand particles while maintaining identical scour protection layer properties. The first and second configurations used sand particles scaled by a factors of 10 and 15, resulting in a particle diameter of 6 mm and 9 mm, the final configuration employed a more moderate scaling factor of 20, yielding particles of 12 mm diameter. Table VIII depicts the simulation settings of three different configurations of hybrid scaling.

TABLE VIII: Configuration of hybrid scaling simulations

Parameter	**Scour Protection Layer**	**Underlying Sand Layer**		
	Exact Scaling	**Coarse Grain**		
Scale Factor	25	20	15	10
Particle Size Range	25 mm - 35 mm	12 mm	9 mm	6 mm
Layer height	145 mm		800 mm	
Velocity	50 mm/s			
Gravitational Acceleration	9.8 m/s^2			
Shear modulus	4×10^7 Pa	2×10^6	2.6×10^6	4×10^6
Static friction Coef.	0.64	0.035	0.046	0.07
Rolling friction Coef.	0.1	0.0025	0.0033	0.005
Number of Particles	$\sim$8500	$\sim$617000	$\sim$1.4 million	$\sim$5 million

This systematic variation in particle size scaling was designed to evaluate the sensitivity of the simulation results to the degree of coarse-graining applied to the sand particles. This validation approach enables a more comprehensive understanding of the capabilities and limitations of the hybrid scaling methodology, providing crucial guidance for future applications in similar geotechnical scenarios.

IV. RESULTS AND DISCUSSIONS

This section presents and analyzes the results from three distinct scaling approaches: exact scaling, coarse grain scaling, and hybrid scaling. Each method's effectiveness is evaluated using penetration resistance and penetration work as key performance indicators.

A. Exact Scaling Performance

The performance of all four exact scaling methods was evaluated against the reference model. Table IX highlights the key differences among other four scaling methods we used in exact scaling. This comparative analysis provides direct visualization of how each scaling approach preserves the essential physics of monopile penetration. Figure 10 shows the results of exact scaling.

TABLE IX: Comparison of Exact Scaling Methods

Parameter	**Method 1**	**Method 2**	**Method 3**	**Method 4**
Gravity (m/s²)	0.392	245.250	9.8	9.8
Velocity (mm/s)	50	1250	50	250
Time (s)	150	6	150	30
Young's Modulus (Pa)	4×10^7	2.5×10^9	4×10^7	1×10^9
Stability	Stable	Unstable	Stable	Stable
Run time (hours)	2.4	-	2.4	1.67

Figure 10a compares the penetration resistance of four scaling methods with the reference model, the results revealed distinct behavioral patterns across the four scaling methods. Method 1, which preserved velocity while reducing gravitational acceleration, demonstrated good agreement with theoretical predictions, showing penetration resistance values that scaled consistently by a factor of 25^2. However, while mathematically sound, this approach's artificial gravity reduction limited its practical relevance. Method 2's attempt to preserve time while scaling velocity and gravity proved computationally unstable, with excessive acceleration values causing particle ejection during the settling phase, preventing meaningful resistance measurements. Method 3, which

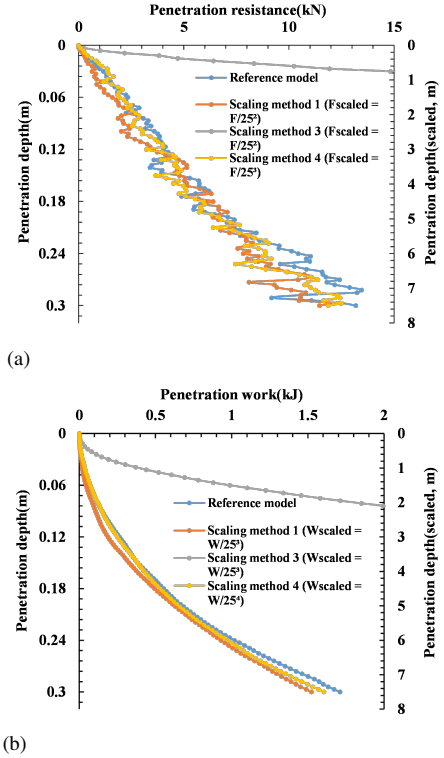

Fig. 10: Results of exact scaling simulations (scale factor = 25) compared to reference model: (a) Penetration resistance versus depth, and (b) Penetration work versus depth.

attempted to maintain real-world gravitational conditions without establishing proper scaling laws, showed inconsistent scaling behavior and produced force magnitudes that deviated significantly from theoretical predictions. Most notably, Method 4 (Froude scaling) emerged as the most effective approach, successfully maintaining both gravitational conditions and dynamic similarity. This method demonstrated consistent penetration resistance scaling by a factor of 25^3, aligning perfectly with theoretical predictions while preserving realistic particle behavior throughout the penetration process.

The penetration work analysis(Figure 10b further reinforced the superiority of the Froude scaling approach (Method 4) among the exact scaling methods. When examining the work done during penetration, Method 1 showed reasonable correlation with scaling predictions but underestimated the energy requirements due to its modified gravitational conditions. Method 2's instability issues made work calculations impossible, as the particle ejection prevented any meaningful energy transfer measurements. Method 3's lack of proper scaling laws led to unpredictable work patterns that couldn't be reliably correlated with the reference model. In contrast, Method 4 demonstrated exceptional agreement with theoretical predictions across the entire penetration depth. The penetration work scaled consistently with depth, maintaining proper energy transfer relationships throughout the process. This method's success in preserving both static and dynamic similarity through Froude number matching resulted in reliable predictions of installation energy requirements, crucial for practical applications in offshore wind turbine installations.

The results highlight Method 4's superiority in maintaining physical similarity while providing stable numerical solutions. This method's success can be attributed to its systematic preservation of both static and dynamic similarity through Froude number matching.

B. Coarse Grain Scaling Analysis

The coarse grain approach was investigated across scale factors ranging from 1 to 30. The initial coarse grain simulations revealed limitations when using larger-scale factors while maintaining the original domain dimensions. With particle diameters increasing from 0.6 mm to 18 mm (scale factor 30), the particle-to-domain width ratio became critically small, leading to artificial boundary effects that compromised result validity. Previous analysis (Domain size optimization) established that a minimum width-to-particle diameter ratio (W/d) of 30 is necessary to avoid these boundary effects.

To maintain this critical ratio while investigating higher scale factors, the domain geometry was scaled up by a factor of 5. This geometric scaling allowed proper evaluation of scale factors from 10 to 30 while ensuring sufficient particles across the domain width. However, this dimensional increase created challenges in directly comparing penetration resistance across different scale factors, as the larger geometry inherently led to higher resistance values. To make this possible we choose stress as KPI (Stress is defined as the force per unit area acting on a material). By comparing the stress values across different scale factors, we can assess whether the coarse grain technique preserves the bulk behavior of the original system. Normalizing results using stress on the geometry as a KPI Results revealed a critical threshold at scale factor 20, beyond which accuracy deteriorated significantly. Using stress on the geometry as a normalized metric, we observed (fig. 11):

The stress-based analysis demonstrated that scale factors up to 20 maintained consistent bulk behavior, while larger factors led to increasingly unrealistic particle interactions. This approach achieved a significant decrease in computation time from 147.5 hours to 0.24 hours while preserving the bulk mechanical response

C. Hybrid Scaling Effectiveness

The hybrid scaling approach combined exact scaling for the scour protection layer with coarse graining for the underlying sand bed. Results showed distinct behavior in two phases:

Analyzing the penetration resistance results from Figure 12a, the hybrid scaling approach demonstrated distinct behavioral characteristics across two critical phases. In the scour protection phase (0-0.15 m depth), all three coarse grain configurations (CG-10, CG-15, and CG-20) showed excellent agreement with the reference model, maintaining

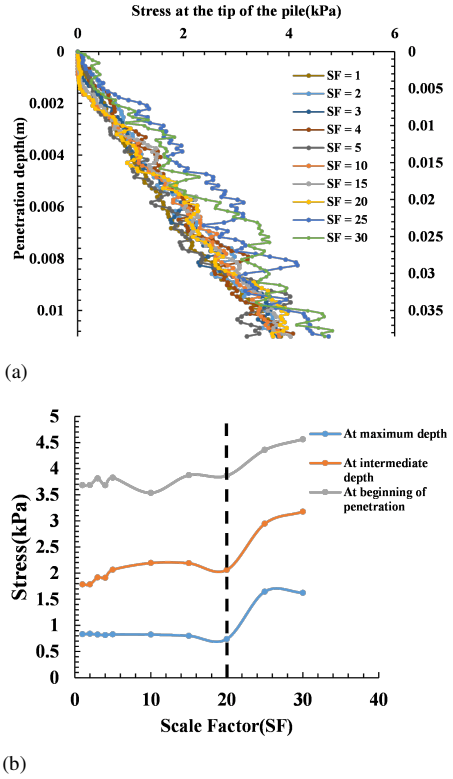

Fig. 11: Results of coarse grain simulations (scale factor = 1-30) : (a) Stress on the geometry versus depth, and (b) Stress at different depth at various scale factors.

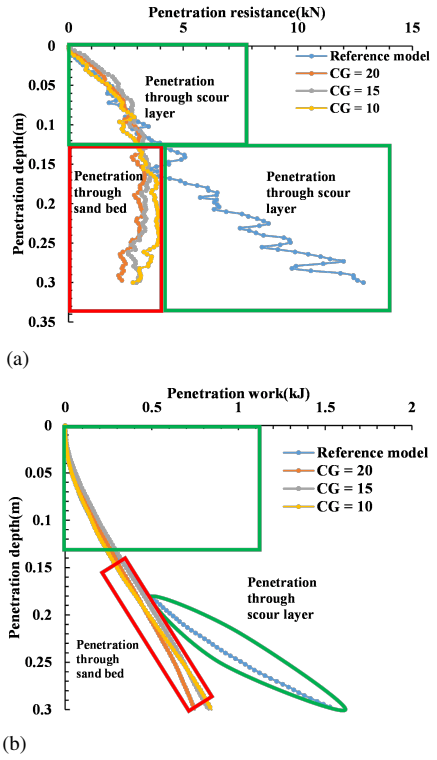

Fig. 12: Results of Hybrid scaling simulations (scale factor = 1-30) : (a) Penetration resistance versus depth, and (b) Penetration work versus depth.

consistent resistance patterns throughout this crucial zone. This agreement is particularly evident in the early penetration stage, where the resistance curves closely follow the reference model's trajectory with minimal deviation as they are penetrating through scour rocks despite the sandbed beneath the scour rocks having different CG values. In the subsequent sand bed phase (>0.15 m), while all configurations maintained similar trends, all the scale factors demonstrated the same behavior deviating from reference model as expected because the reference model is filled with scour rocks instead of sandbed. The transition between the two phases (marked by the clear inflection point at 0.15 m depth) was captured smoothly across all configurations, validating the hybrid approach's ability to handle material interface transitions effectively.

The penetration work analysis, illustrated in Figure 12b, further strengths the findings from penetration resistance. The figure shows a clear distinction between the energy requirements in the scour protection and sand bed phases, with all three configurations closely matching the reference model's work progression in the initial scour protection layer (highlighted by the green box in the figure). This agreement is particularly notable in the steeper gradient of the work curves through the scour protection layer, accurately representing the higher energy demands of penetrating through the rock material. As the penetration progressed into the sand bed region (marked by the transition point at 0.15 m), the work curves maintained consistent slopes across all configurations. The figure demonstrates that while all three configurations (CG-10, CG-15, and CG-20) captured the overall work characteristics, CG-20 achieved the optimal balance between computational efficiency and accuracy, continuous work curve that closely parallels the reference model throughout the entire penetration depth.

D. Comparative Analysis

The three scaling approaches demonstrated complementary strengths:

- Exact scaling (Method 4) excelled in preserving physical similarity for the scour protection layer
- Coarse graining proved effective in reducing computational demands while maintaining bulk behavior
- Hybrid scaling successfully combined these advantages for practical simulation of complete installation scenarios

This comprehensive evaluation establishes a robust framework for selecting appropriate scaling techniques based on specific simulation requirements and computational constraints. The results validate the theoretical foundations developed for each scaling approach while providing practical guidelines for implementation in industrial-scale simulations.

V. CONCLUSIONS AND RECOMMENDATIONS

The most significant finding of this research is the successful development and validation of a hybrid scaling methodology that effectively combines exact scaling with coarse-graining techniques for DEM simulations of monopile penetration. This novel approach bridges the critical gap between laboratory-scale models and industrial applications while maintaining physical accuracy. The hybrid method demonstrated superior performance by preserving essential particle-scale interactions in the scour protection layer through Froude scaling principles, while efficiently handling the underlying sand bed through optimized coarse-graining, ultimately reducing simulation times from 147.5 hours to approximately 15 hours without compromising result quality.

The detailed investigation revealed several important insights across different scaling approaches. The systematic comparison of exact scaling methods established that Froude scaling (Method 4) provided the most reliable results by maintaining both gravitational conditions and dynamic similarity when scaling from 323.9mm to 8097.5mm diameter monopiles. The coarse grain analysis identified a critical scale factor threshold of 20, beyond which particle behavior began deviating significantly from physical expectations. The validation of various domain configurations showed that cylindrical domains with a width-to-particle diameter ratio of 40 effectively minimized boundary effects while optimizing computational resources. The research also demonstrated that using six distinct particle shapes with a smoothing value of 5 provided sufficient geometric complexity to capture realistic granular behavior while maintaining computational efficiency. These findings establish a robust framework for selecting appropriate scaling techniques based on specific simulation requirements and computational constraints, making industrial-scale simulations both feasible and reliable.

A. Future Research Directions

Several promising avenues for future research have been identified:

The research findings open up several promising avenues for future development and application. The most immediate opportunity lies in experimental validation, where physical testing of scaled models could verify the numerical predictions and further refine the scaling relationships established in this study. This experimental work would be particularly valuable in understanding scaling effects on particle crushing and deformation mechanisms during installation. Beyond validation, there is significant potential for enhancing the model's capabilities by using alternate scaling combinations in hybrid scaling like geometric scaling, particle refinement technique and scalping etc. The framework could also be extended to address different seabed conditions and dynamic penetration effects, making it applicable to a broader range of offshore installation scenarios. These advancements would further strengthen the model's utility as a practical tool for the offshore wind energy sector, potentially leading to more efficient and cost-effective installation procedures while maintaining high safety standards.

B. Concluding Remarks

This research demonstrates that appropriate scaling techniques, when carefully selected and implemented, can enable efficient simulation of industrial-scale monopile installations while maintaining physical accuracy. The developed framework provides a foundation for future studies in offshore foundation installation modeling, contributing to the advancement of offshore wind energy infrastructure.

NOMENCLATURE

- DEM = Discrete Element Method
- FEM = Finite Element Method
- MPM = Material Point Method
- CFD = Computational Fluid Dynamics
- 3D = 3 dimensional
- KPI = Key Performance Indicator
- g = gravity
- R_min = Radius of the smallest sphere in a multi-sphere
- W/d_rock = Width of the domain to rock size
- v = velocity
- SF = Scale Factor
- d_g= Scaled particle diameter
- d_g= Original particle diameter
- NPG = Number of Particles per Grain
- GB = Gigabyte

REFERENCES

[1] Negro, Vicente, et al. "Monopiles in offshore wind: Preliminary estimate of main dimensions." Ocean Engineering 133 (2017): 253-261.

[2] Sánchez, Sergio, et al. "Foundations in offshore wind farms: Evolution, characteristics and range of use. Analysis of main dimensional parameters in monopile foundations." Journal of Marine Science and Engineering 7.12 (2019): 441.

[3] Esposito, Ricardo Gurevitz, et al. "Multi-scale sensitivity analysis of pile installation using DEM." Computational Particle Mechanics 5 (2018): 375-386.

[4] Liu, Junwei, et al. "DEM investigation of installation responses of jacked open-ended piles." Acta Geotechnica 14 (2019): 1805-1819.

[5] Li, Lichen, et al. "DEM analysis of the plugging effect of open-ended pile during the installation process." Ocean Engineering 220 (2021): 108375.

[6] Zhou, Jian, et al. "Coupled 3D discrete-continuum numerical modeling of pile penetration in sand." Journal of Zhejiang University SCIENCE A 13.1 (2012): 44-55.

[7] Komodromos, Michail, Gaël Combe, and Gioacchino Viggiani. "Grain-scale DEM study of open-ended pipe pile penetration in granular soils." EPJ Web of Conferences. Vol. 249. EDP Sciences, 2021.

[8] Zhang, Xiangyu, and Behzad Fatahi. "Assessing axial load transfer mechanism of open-ended tubular piles penetrating in weak rocks using three-dimensional discrete element method." Computers and Geotechnics 137 (2021): 104267.

[9] Ciantia, Matteo Oryem, et al. "DEM modelling of cone penetration tests in a double-porosity crushable granular material." Computers and Geotechnics 73 (2016): 109-127.

[10] Lommen, Stef, et al. "DEM particle upscaling for large-scale bulk handling equipment and material interaction." Powder Technology 352 (2019): 273-282.

[11] Tekeste, Mehari Z., et al. "Modeling soil-bulldozer blade interaction using the discrete element method (DEM)." Journal of Terramechanics 88 (2020): 41-52.

[12] Janda, Alvaro, and Jin Y. Ooi. "DEM modeling of cone penetration and unconfined compression in cohesive solids." Powder Technology 293 (2016): 60-68.
[13] Mcdowell, G. R. O. Falagush, and H-S. Yu. "A particle refinement method for simulating DEM of cone penetration testing in granular materials." Géotechnique Letters 2.3 (2012): 141-147.
[14] Falagush, O., G. R. McDowell, and Hai-Sui Yu. "Discrete element modeling of cone penetration tests incorporating particle shape and crushing." International Journal of Geomechanics 15.6 (2015): 04015003.
[15] Hertz, Heinrich. "Ueber die Berührung fester elastischer Körper." Journal für die reine und angewandte Mathematik, vol. 1882, no. 92, 1882, pp. 156-171
[16] Mindlin, R. D. (April 5, 2021). "Compliance of Elastic Bodies in Contact." ASME. J. Appl. Mech. September 1949; 16(3): 259–268
[17] Liu, Run, et al. "Behavior of monopile foundations for offshore wind farms in sand." Journal of Waterway, Port, Coastal, and Ocean Engineering 142.1 (2016): 04015010.
[18] The Engineering ToolBox (2005). Modulus of Rigidity. [online] Available at: https://www.engineeringtoolbox.com/modulus-rigidity-d946.html [13/01/2025]
[19] The Engineering ToolBox (2008). Poisson's Ratio. [online] Available at: https://www.engineeringtoolbox.com/poissons-ratio-d1224.html [Accessed Day Month Year].
[20] Alden, Andrew. "The Density of Common Rocks and Minerals." ThoughtCo, ThoughtCo, 20 July 2024, www.thoughtco.com/densities-of-common-rocks-and-minerals-1439119.
[21] Garcia, M. Combarros, et al. "Segregation in heaps and silos: Comparison between experiment, simulation and continuum model." Powder Technology 293 (2016): 26-36.
[22] Byerlee, James. "Friction of rocks." Rock friction and earthquake prediction (1978): 615-626.
[23] Ucgul, Mustafa, John M. Fielke, and Chris Saunders. "Defining the effect of sweep tillage tool cutting edge geometry on tillage forces using 3D discrete element modelling." Information Processing in Agriculture 2.2 (2015): 130-141.
[24] Pereira, Jorge Paulino. "Rolling friction and shear behaviour of rock discontinuities filled with sand." International Journal of Rock Mechanics and Mining Sciences 34.3-4 (1997): 244-e1.
[25] Washino, Kimiaki, et al. "Time step criteria in DEM simulation of wet particles in viscosity dominant systems." Powder Technology 302 (2016): 100-107.
[26] Albert, R., et al. "Slow drag in a granular medium." Physical review letters 82.1 (1999): 205.
[27] De Vos, Leen, et al. "Empirical design of scour protections around monopile foundations: Part 1: Static approach." Coastal Engineering 58.6 (2011): 540-553.
[28] Whitehouse, Richard JS, et al. "The nature of scour development and scour protection at offshore windfarm foundations." Marine Pollution Bulletin 62.1 (2011): 73-88.
[29] Wu, Minghao, et al. "Large scale experimental study of the scour protection damage around a monopile foundation under combined wave and current conditions." Journal of Marine Science and Engineering 8.6 (2020): 417.
[30] Roessler, Thomas, and André Katterfeld. "Scaling of the angle of repose test and its influence on the calibration of DEM parameters using upscaled particles." Powder technology 330 (2018): 58-66.
[31] Feng, Y. T., and D. R. J. Owen. "Discrete element modelling of large scale particle systems—I: exact scaling laws." Computational Particle Mechanics 1 (2014): 159-168.
[32] Herman, Angga Pratama, Jieqing Gan, and Aibing Yu. "GPU-based DEM simulation for scale-up of bladed mixers." Powder Technology 382 (2021): 300-317.
[33] Mohajeri, M. Javad, et al. "A hybrid particle-geometric scaling approach for elasto-plastic adhesive DEM contact models." Powder technology 369 (2020): 72-87.
[34] Jiang, Xin. "Research on Coarse-Grained Discrete Element Model and Optimization for Fine Particles." Coatings 12.10 (2022): 1483.